Applied Mathematics Body and Soul, Vol. V

Real ThermoDynamics

Claes Johnson
KTH Royal Institute of Technology

Stockholm, Sweden
claesjohnson@gmail.com

Draft, June 12, 2026

Contents

Foreword

The Body and Soul programme, begun three decades ago, has from the start been organised around a single methodological idea: to combine the *Soul* of analytical mathematics with the *Body* of computational mathematics, so that every part of mathematical physics is presented in a form which pairs the underlying analytical structure with a runnable computational realisation. Volumes I–III carried this commitment through *Calculus* and *Linear Algebra*, each subject presented in both its analytical and its computational form. **Volume IV**, on *Turbulent Incompressible Flow* [23], took the programme one step further: the computational form was put forward as the *true mathematical model of physics*, based on the view that physical reality, evolving in time, itself performs an analog computation which the digital computer can parallel or simulate. Turbulence, which had resisted understanding within the purely analytical framework, could then be understood and simulated through a computational form of the Navier–Stokes equations. The **present Volume V** extends the same mathematics from incompressible to compressible flow, where it becomes the essence of *thermodynamics* — with an understandable computational form of the 2nd Law as the inevitable dissipation of finite-precision computation. **Volume VI**, *Real Quantum Mechanics* [1], extends the same mathematics again, from macroscopic compressible flow down to the atomic scale, replacing the classical wave function in $3N$-dimensional configuration space with a multiphase 3D continuum formulation in real three-dimensional space. The two volumes V and VI together complete the Body and Soul programme by carrying the combined analytical/computational point of view across the full scale range from macroscopic flows to atomic structure, with statistical aggregation replaced by deterministic field equations at both ends.

The thesis in one sentence. The 2nd Law of thermodynamics, irreversibility, and the arrow of time are not consequences of statistical aggregation over configurations of atoms. They are consequences of **finite-precision computation** on deterministic continuum field equations: any finite-resolution numerical solution of the Euler equations of compressible flow dissipates kinetic energy into internal energy through the small-scale residual that the resolution cannot represent, and this dissipation is irreversible by the structure of the discretisation, not by any statistical-mechanical assumption. The book argues that this is the right reading of the 2nd Law: a structural consequence of the finite information content of any computable representation of the physical world, including the physical world's own representation of itself as analog computation.

The two central problems: Joule's experiment and the piston-cylinder. The book is organised around two foundational computational problems that together carry the conceptual content of thermodynamics:

- **Joule's 1845 experiment** (Chapter 2) — gas in a high-pressure chamber expands through a channel into a low-pressure chamber. Bulk flow through the channel converts internal energy into kinetic energy during the expansion; turbulent/shock dissipation in the receiving chamber converts it back into heat during the recompression. The two halves are asymmetric in the dynamic dissipation pattern, and the result is a residual temperature gradient between the chambers that classical equilibrium thermodynamics cannot predict. This is the **refrigerator principle**: the same expansion-cooling and compression-heating asymmetry that a refrigeration cycle exploits with external work input, demonstrated in one-shot form by simply releasing a pressure differential between two chambers.

- **The piston-cylinder** (Chapter 14) — gas in a chamber pushes a movable wall (piston) outward against an external load, doing work on the load. With a smooth single-chamber geometry the gas does work quasi-statically and the process approaches reversible efficiency; with a channel constriction between the gas reservoir and the piston (the Joule geometry with a movable far wall), the gas must jet through the constriction and recompress against the piston, with turbulent dissipation pulling the efficiency $\eta = W/\Delta U$ below the reversible limit. This

is the **heat-engine principle**: the conversion of stored internal energy into useful work delivered to an external load, with irreversibility entering through the same turbulent-dissipation channel as in Joule's experiment.

The two problems are duals of each other in the deterministic-continuum reformulation. The Joule experiment shows what happens when the asymmetric expansion-compression cycle is allowed to dissipate freely; the piston-cylinder shows what happens when the same dynamics are channelled into useful work against a load. The 2nd Law in its RealNSE reading — finite-precision dissipation in the discretisation — sets the irreversibility in both cases. Refrigeration cycles run the first problem cyclically with external work input; heat engines run the second problem cyclically with heat input from a reservoir. Vol VI Applications develops both into full cycles (Carnot heat engines, Carnot heat pumps, compressor refrigerators); the present opening chapters establish the foundational single-shot dynamics that the cycles are built from.

Real Thermodynamics in the Body and Soul tradition. The earlier volumes of the programme presented continuum mechanics for macroscopic matter: fluids, elastic solids, plasticity, transport. This volume presents thermodynamics inside the same continuum-mechanics framework, without adding a statistical-mechanical layer. The Euler and Navier–Stokes equations carry the dynamics; the *Real Navier–Stokes* method (RealNSE) — 'Real' here meaning the computational realisation as a least-squares stabilised Galerkin method — supplies the finite-precision computation; the 2nd Law emerges as the entropy condition for weak solutions in the same sense that it does for shocks in classical conservation-law theory. The Boltzmann–Gibbs apparatus — microstates, ensembles, the probabilistic foundation of equilibrium thermodynamics — is not invoked at the foundational level. Where statistical reasoning is the natural framing for a specific regime (large-system equilibrium fluctuations, critical phenomena) it remains available; what is replaced is the claim that statistics is the foundation of the discipline.

The programme as mathematics education, and as it is read today. The Body and Soul mathematics education programme was initiated thirty years ago, around the proposition that a modern undergraduate education in mathematics should be a synthesis of the formal analytical mathematics of

Calculus — the *Soul* of the subject — with the computational mathematics made possible by the computer — the *Body*. The programme was met with resistance from both directions. Established mathematics teachers, trained in formal analysis but not in programming, found the computational half foreign to their craft and slow to incorporate. Computer scientists, comfortable with programming but uncomfortable with the apparatus of Calculus, regarded the analytical half as an obstacle to be routed around. The synthesis languished in the gap between the two cultures it had been designed to bridge. The idea was, however, correct, and with the recent advent of capable AI assistance it acquires a new and stronger sense: the analytical and the computational sides of mathematics no longer have to be carried by the same human in the same head. The mathematician's mind frames the problem, formulates the equations, identifies what must be shown; the AI translates the formulation into running code, executes the calculations, and brings the construction alive on the screen. The synthesis that the Body and Soul programme proposed in education thirty years ago becomes, with AI as collaborator, a practical working method for research.

The Body side and the FEniCS project. The Body side of the programme — the commitment that the computational realisation should be an organic part of the mathematics, not a separate engineering exercise — has its principal historical embodiment in the **FEniCS Project** [2], an open-source platform for the automated solution of partial differential equations by the finite element method. FEniCS was developed by the author's research group over roughly a decade of dedicated work, with the goal that a researcher who could write down a variational form on paper could obtain a running finite-element solver from it directly. The RealNSE method that supplies the computational backbone of this book was developed in that environment, and the original *Computational Thermodynamics* (Hoffman, Johnson and Nazarov, 2012) on which the present volume is based reported numerical results obtained with the FEniCS-Unicorn implementation.

The relevance to the present rewrite is the change of timescale. As Anders Logg, principal developer of FEniCS, has observed, what required a decade of focused effort in the 2000s can today, with the help of capable AI assistance, be carried out in a day. The browser-based interactive simulators that accompany this volume in the public Gallery — compressible flow demonstrations of Joule's 1845 experiment, of bluff-body Mach-2 turbulence, and of

the Burgers equation as the canonical model PDE — were produced on that compressed timescale. The Body side of the programme has not changed; what has changed is how much of it a single mathematical mind, with AI as collaborator, can carry from formulation to running code in a working session.

The GPU revolution: the third enabling condition. The Mind–AI collaboration is one of the enabling conditions for the present volume; the other is the GPU revolution of the past two decades. Graphics Processing Units originated as dedicated accelerators for 3D-graphics rendering in the 1990s and were repurposed for general scientific computation in the mid-2000s (CUDA 2007, OpenCL shortly after). The architectural feature that distinguishes a GPU from a conventional CPU is massive parallelism: thousands of identical compute threads executing the same instruction stream on different data, with memory bandwidth tuned for streaming through large regular arrays. The compressible Euler and Navier–Stokes equations on a regular grid are the canonical workload the GPU is built for. The 2023 finalisation of **WebGPU** — a cross-vendor standard that exposes GPU compute through the browser without driver installation or local compilation — makes it possible to ship a chapter's worth of computational thermodynamics as an HTML page the reader opens and runs on their own hardware at interactive rates, with no install step, no virtual environment, no submission to a remote service. The Joule's-experiment and bluff-body-Mach-2 simulators listed in Appendix A run in this form. The reformulation makes the thermodynamics computable in principle; the GPU makes it computable on a laptop; AI assistance makes the laptop implementation feasible for one author in a working session. The three conditions together are what makes a Body-and-Soul-style thermodynamics volume possible at this moment.

Leibniz's project, realised. The proposition that the labour of calculation should be lifted from the mathematician's shoulders by a suitably constructed machine is, in its modern form, three and a half centuries old. Gottfried Wilhelm Leibniz, in the 1685 explanation of his Stepped Reckoner, wrote that "it is unworthy of excellent men to lose hours like slaves in the labour of calculation which could safely be relegated to anyone else if machines were used." His wider programme — the *calculus ratiocinator*, a mechanical calculus for deriving conclusions from a *characteristica universalis*, a

universal symbolic language for reasoning — proposed not merely arithmetic automation but the automation of mathematical thought as a whole, with the human mind freed to set the scene and the machine to carry the calculation. The intellectual lineage from this proposal through Babbage, Boole, Frege, Hilbert, Gödel, and Turing to modern electronic and AI-assisted computation is the subject of Martin Davis's *The Universal Computer: The Road from Leibniz to Turing* [3]. The collaboration between the human mathematical mind and Claude as AI assistant that produced the present volume is, in this lineage, Leibniz's three-hundred-and-forty-year-old proposal realised — not as a special device for arithmetic, but as a working partnership in which the mind frames the equations and the machine, increasingly fluent in the language of mathematics, brings them alive.

Schrödinger's question, deferred. Schrödinger's *What is Life?* (1944) framed living matter as matter that sustains itself by feeding on *negative entropy*: a question that connects the 2nd Law as developed in this volume to the cell biology taken up at the atomic scale in Volume VI.

The synthesis that the Body and Soul programme completes. The earlier volumes of the programme presented continuum mechanics for macroscopic matter from the calculus side and from the algorithm side simultaneously. This volume does the same for thermodynamics, with the 2nd Law derived from the discretisation rather than postulated from statistical mechanics. Volume VI does it for atomic-scale matter, with the wave function on physical $\mathbb{R}^3$ and the probability interpretation removed. The fluid in a pipe and the electron in an atom are, in the language the programme establishes across its volumes, the same kind of object: a field on $\mathbb{R}^3$ satisfying a partial differential equation, with boundary conditions that close the variational problem, and an algorithm that solves it on a computer. The programme that started with the Navier–Stokes equations and continued through classical elasticity now ends with the atomic Schrödinger equation in its real-3D-space form, with the deterministic continuum reformulation of thermodynamics in this volume as the bridge that connects the macroscopic and the atomic ends in a single methodological commitment.

The book contains no figures or detailed numerical results from the computations. All quantitative output — velocity fields, density slices,

energy-vs-time records, normal-mode animations, Joule expansion trajectories, bluff-body turbulence wakes — is documented in detail in the public Gallery indexed in Appendix A. The decision to keep the printed volume free of static figures is deliberate: static images of interactive simulations omit precisely what makes the framework distinctive. The chapter text describes what is computed and why it agrees with observation; the Gallery shows what it looks like, lets the reader vary parameters, and renders the framework's behaviour live. The two together constitute the book in its intended form.

A Theory of Everything

The new books in the Body and Soul Applied Mathematics series — *Real Thermodynamics* (Vol V) and *Real Quantum Mechanics* (Vol VI) — together form a *Theory of Everything* (ToE): a unified theory for all scales, from the atomic scale geared by Coulomb potentials to the large scale geared by gravitational potentials.

This is a ToE based on just two forces: the Coulomb force between charges of different signs, and the gravitational force between masses of (positive) sign — with both potentials satisfying the same Poisson equation.

It is a ToE based on a continuum model in three space dimensions of one and the same form, using that a continuum harbours all scales.

RealQM shows how a hierarchy of models can be built upon an atomic model, reaching into the mechanics of fluids and solids and beyond into astronomy.

Recall that physicists generally pride themselves on having invented two theories: Quantum Mechanics (QM) for the small scale and General Relativity (GR) for the large scale, both presented as among the highest achievements of the human intellect in all categories. Yet it is generally admitted, after such a declaration, that QM and GR are mutually incompatible, and so together do not offer a Theory of Everything.

The physics community is now confronted with RealQM and Real Thermodynamics as a form of ToE. What I hope for is reading, followed by questions. What I have so far met is anger and rejection without reading.

A note on acknowledgements. The original *Computational Thermodynamics* of 2012 was a joint work of Johan Hoffman, Claes Johnson, and

Murtazo Nazarov; the present volume is its 2026 rewrite as Volume V of the Body and Soul programme, by Claes Johnson in extended collaboration with **Claude**, the large-language-model AI assistant produced by Anthropic. The mathematical reformulation, the architecture, and the writing are the work of the author. The implementation of the browser-based interactive simulators, the systematic translation of the 2012 manuscript into the form the present volume takes, the cross-volume integration with Volume VI, and a substantial fraction of the iterative back-and-forth that produced the rewrite were carried out with Claude. No human colleagues, students, funding agencies, departmental hosts, or institutional sponsors contributed to the rewrite in a way that would warrant the customary form of acknowledgement, beyond the recognition of the original 2012 co-authors recorded on the title page. The pattern of the human–AI collaboration follows the template documented in detail in the corresponding chapter of Volume VI [1]; that chapter is, in effect, the acknowledgements section of the present volume too.

Claes Johnson

Stockholm, 2026

Part I

Physics

Chapter 1

From Classical to Real Thermodynamics

"Thermodynamics is a funny subject. The first time you go through it, you don't understand it at all. The second time you go through it, you think you understand it, except for one or two small points. The third time you go through it, you know you don't understand it, but by that time you are so used to it, it doesn't bother you any more."
— Arnold Sommerfeld

"No one really knows what entropy really is, so in a debate you will always have the advantage."
— John von Neumann, to Claude Shannon

"The law that entropy always increases holds, I think, the supreme position among the laws of Nature. ... if your theory is found to be against the second law of thermodynamics I can give you no hope; there is nothing for it but to collapse in deepest humiliation."
— Arthur Eddington, *The Nature of the Physical World* (1928)

"Were it not for the existence of irreversible processes, the entire edifice of the 2nd Law would crumble."
— Max Planck

This opening chapter states the two laws of classical thermodynamics, identifies the two questions the classical theory leaves unanswered, and then gives the Real ThermoDynamics (RealTD) answer: the same 1st Law, and a

2nd Law in which the entropy product $T\,dS$ is replaced by turbulent dissipation D. A closing section presents the essence of RealTD as a finite-precision computational model of physics.

1.1 Classical 1st and 2nd Laws

Classical Thermodynamics rests on two laws. The *1st Law* is the conservation of total energy, written K for the *kinetic (mechanical) energy* and E for the *internal (heat) energy*. In Clausius' differential form, with dK and dE the changes of these energies from one state to another,

$$dK + dE = 0, \tag{1.1}$$

so mechanical energy lost is gained as heat and vice versa — energy is only converted between its mechanical and thermal forms, never created or destroyed. The *2nd Law*, in Clausius' differential form, is

$$T\,dS = dE + p\,dV, \qquad dS \geq 0, \tag{1.2}$$

with S *entropy*, T absolute *temperature*, V *volume*, and $W = p\,dV$ *work*. The equality is an energy balance; the inequality $dS \geq 0$ is the 2nd Law proper, expressing irreversibility.

Why the form $T\,dS$. The right-hand side $dE+p\,dV$ is the heat supplied in a transition, and by itself it is *not* an exact differential — the heat exchanged depends on the path taken between two states. Dividing by the temperature T repairs this: for a perfect gas $(dE + p\,dV)/T$ *is* an exact differential, so it defines a *state function* S, the entropy, depending on the state alone. With the gas law $p = \gamma\rho T$, specific volume $V = 1/\rho$, and internal energy E satisfying $dE = dT$ per unit mass (a perfect gas), we have $(dE + p\,dV)/T = dT/T - \gamma\,d\rho/\rho$, and integration gives

$$S \;=\; \ln T \;-\; \gamma \ln \rho \;+\; \text{const} \;=\; \ln \frac{T}{\rho^{\gamma}} \;+\; \text{const}, \tag{1.3}$$

a function of the state (ρ, T) alone. This is the reason the 2nd Law is written in the form $T\,dS$: the integrating factor $1/T$ manufactures a state function S whose change ΔS between two equilibrium states is *independent of the path* between them, so that the sign of that change classifies the transition — $\Delta S = 0$ reversible, $\Delta S > 0$ irreversible.

Path-independence as a miracle. That ΔS depends only on the endpoints, and not on the path between them, may appear as a small miracle. It is the same miracle as the Fundamental Theorem of Calculus: an integral need not be evaluated by summing a function over an interval — a computationally intensive process — but is obtained for free as the difference of a *primitive* function between the two endpoints, with no computational work. A state function S is exactly such a primitive for the heat $T\,dS$, and ΔS is read off from the endpoints alone. We shall see this miracle in action in the next chapter, where the entropy increase of Joule's free expansion comes out as $\gamma \ln 2$ from the endpoints — to be compared with the actual turbulent dissipation that RealTD accumulates along the real path.

What it does not give, and where it fails. What the construction does *not* deliver is the *physical meaning* of S or the *reason* $\Delta S \geq 0$. Nor is it general: it depends essentially on the perfect-gas law. For a *non-perfect* gas $(dE + p\,dV)/T$ need not be an exact differential, and the construction then yields no such state function — **the entropy S is a state function for the perfect gas, but not in general**. The clean diagnosis of irreversibility by the sign of ΔS is thus a perfect-gas convenience, not a general fact; outside the perfect gas **the form $T\,dS$ lacks its purpose**, and the 2nd Law must be carried by something else — the turbulent dissipation D of the next section, which is defined and non-negative for *any* gas.

The two unresolved questions. Classical Thermodynamics leaves two questions unanswered, and they are the questions this volume confronts:

- *What is the physical meaning of the entropy S?*
- *Why is $dS \geq 0$ always?*

Boltzmann's statistical mechanics answered the first with "disorder" and the second with an assumption of molecular chaos — shifting the question rather than resolving it. Real ThermoDynamics answers both from the dynamics of slightly viscous flow.

1.2 1st Law and Real 2nd Law

Dissipation in place of entropy. Real ThermoDynamics keeps the *1st Law identical* to the classical one (1.1), $dK+dE = 0$, and replaces the entropy

form (1.2) of the *2nd Law* by a statement about *turbulent dissipation* D — the rate at which coordinated kinetic energy is irreversibly converted to heat in the turbulent cascade. The mysterious product $T\,dS$ is replaced by D:

$$D = dE + p\,dV, \qquad D \geq 0, \tag{1.4}$$

where now $D \geq 0$ holds *by construction* — D is the work done against the small-scale viscous stresses, a sum of squares, non-negative by definition rather than by postulate. In time-dependent (rate) form, with an overdot denoting d/dt, the two laws read

$$\dot{E} + W = D, \qquad \dot{E} + \dot{K} = 0, \qquad D \geq 0. \tag{1.5}$$

This answers the two questions of Section 1.1 at a stroke. The physical meaning of S is *accumulated turbulent dissipation*, and $dS \geq 0$ holds not by assumption but because $D \geq 0$ by construction.

The two energy balances. Writing V for the *volume* and using the 1st Law $dE + dK = 0$, the two laws take the equivalent form of a pair of energy balances,

$$dE + p\,dV = D, \qquad dK - p\,dV = -D, \tag{1.6}$$

which add to the 1st Law $dE + dK = 0$. They show how the pressure work $p\,dV$ shuttles energy between the internal (heat) energy E and the kinetic energy K, while the dissipation $D \geq 0$ runs only one way, into heat. In an *expansion* ($p\,dV > 0$) the internal energy E *decreases* and the kinetic energy K *increases* — the gas cools as it accelerates; in a *compression* ($p\,dV < 0$) the internal energy E *increases* and the kinetic energy K *decreases* — the gas warms as it slows. The dissipation D biases both directions toward heat, adding to E and removing from K irreversibly, whatever the sign of $p\,dV$.

Per unit mass or per unit volume. A word on bookkeeping, because the classical and Real forms differ in *two* independent ways. The first is *normalisation*: the classical quantities are *per unit mass* — specific internal energy $E = T$, specific volume $V = 1/\rho$ — whereas the RealNSE field quantities are *per unit volume* — energy density ρT, dissipation D. The two are related by the single factor ρ. The second is *frame*: the classical relation $T\,dS = dE + p\,dV$ is *Lagrangian*, following a fixed parcel of gas, so the differential d is the change along that parcel's path (the material derivative

D/Dt); the RealNSE equation is *Eulerian*, written at a fixed point in space, with ∂_t and a transport divergence in place of D/Dt, and the pressure work appearing as the expansion rate $p\,\nabla\cdot u$ rather than $p\,\dot{V}$. These two axes are logically independent — one can write a per-mass field, or a per-volume parcel quantity — and they coincide here only because classical thermodynamics is naturally a control-mass (Lagrangian, per-mass) statement and RealNSE a field (Eulerian, per-volume) one.

The two forms are nonetheless the *same* law, and passing between them takes one step on each axis. The *frame* step uses mass conservation: following a parcel,

$$\frac{d}{dt}\Big(\frac{1}{\rho}\Big) \;=\; \frac{\nabla\cdot u}{\rho},$$

so $p\,\dot{V} = p\,(\nabla\cdot u)/\rho$ turns the Lagrangian pressure work into the Eulerian one. The *normalisation* step is just the factor ρ. Applying both, the Eulerian per-volume balance $\rho\,\dot{E} + p\,\nabla\cdot u = D$ (with $E = T$), divided by ρ, returns the Lagrangian per-mass form $dE + p\,dV = D/\rho$ exactly; in particular the D in the per-mass relations (1.4) and (1.6) is the per-volume dissipation D divided by ρ. Both forms say that an expansion ($\nabla\cdot u > 0$, equivalently $dV > 0$) lowers the internal energy. We use whichever is convenient — the per-mass/Lagrangian form to compare with classical thermodynamics, the per-volume/Eulerian field form to compare with the RealNSE equations the simulations actually solve.

$T\,dS$ versus D. The contrast between the two 2nd Laws turns on a single replacement. Classically the irreversible term is the product $T\,dS$, in which *neither* factor is directly accessible: T is measurable, but S is a state function whose physical referent the theory never names, and the inequality $dS \geq 0$ is imposed as a separate postulate. In Real ThermoDynamics the one quantity D carries the whole irreversible content: it is the turbulent dissipation *per unit volume* $D = \mu_{\mathrm{mom}}\,|\nabla u|^2 \geq 0$, where μ_{mom} is the effective (turbulent) viscosity acting in the momentum equation. It is directly computable from the RealNSE velocity field and non-negative *by construction* as a sum of squares. The bridge between the two is the identification

$$\rho\,T\,dS \;=\; D\,dt \;\geq\; 0, \tag{1.7}$$

with D per unit volume (equivalently $T\,dS = (D/\rho)\,dt$ per unit mass). Where the classical theory writes an opaque product $T\,dS$ and *asserts* $dS \geq 0$,

RealTD writes a transparent dissipation D and *derives* $D \geq 0$ from the dynamics. Entropy is not denied; it is identified, after the fact, as $S = \int D\,dt/(\rho T)$.

Equilibrium endpoints versus the real process in time. The two theories also differ in what they describe. Classical thermodynamics relates *equilibrium states* through their state functions. It is not confined to reversible processes: it assigns the irreversible free expansion of a perfect gas to double volume a definite entropy increase $\Delta S = \gamma \ln 2$, obtained by integrating dQ/T along a reference reversible path between the same two equilibrium endpoints — the increase that marks the transition as irreversible. What classical thermodynamics does *not* supply is the *process itself*: the evolution in time, the non-equilibrium states the gas actually passes through, the velocity and turbulence fields, the transient temperature gaps, and where and at what rate the dissipation occurs. **Real ThermoDynamics describes that real transition in time, through the real non-equilibrium states**, resolving the dissipation $D > 0$ accumulated along the actual trajectory; the rate form (1.5) is a statement about that trajectory. Run to full thermal equilibration the two agree on the endpoint — the classical ΔS re-emerges as the integrated dissipation $\int D\,dt/T$ — but only RealTD gives the process that connects them, and short of full equilibration (while a temperature gap remains) it produces less than the classical value (Chapter 2).

1.3 The Essence of Real Thermodynamics

Three models, one science. Real ThermoDynamics rests on a hierarchy of three models:

- The *ideal physical model*: a compressible perfect gas with a small linear (Newtonian) viscosity.
- The *ideal mathematical model*: the compressible *Navier–Stokes Equation* (NSE) for a perfect gas with small linear viscosity — the exact differential equations of that gas.
- The *real physical model*, which is the *computational model*: the **best possible numerical solution** of the NSE at finite precision, which we call **RealNSE**. It is the *real* physical model because Nature itself

realises the gas only as a finite-precision process; RealNSE is what both Nature and the computer actually deliver, the ideal pointwise solution of the NSE being in general unattainable in the presence of turbulence.

Real ThermoDynamics (**RealTD**), the subject of this Volume V, is the science of RealNSE: the macroscopic transformations of energy that survive the finite precision of the computation. It is the sister of **Real Quantum Mechanics** (**RealQM**, Volume VI), which stands in exactly the same relation to the Schrödinger Equation (SE): RealQM is built on **RealSE**, the best finite-precision solution of the SE, just as RealTD is built on RealNSE. The two volumes are one continuum mechanics in three space dimensions across all scales — atomic scales geared by Coulomb potentials (RealSE), large scales geared by gravitational potentials (RealNSE) — with both potentials satisfying the same Poisson equation.

What ThermoDynamics is. ThermoDynamics concerns dynamical transformations between kinetic energy and heat energy in slightly viscous compressible fluids, mediated by pressure work W and turbulent dissipation D, and realised by a computational physical process operating with finite precision.

Turbulent dissipation. Turbulent dissipation transforms *coordinated* bulk kinetic energy at large scales into *uncoordinated* small-scale kinetic energy — which, observed at the macroscopic level, is internal heat energy. The transformation is not optional: it is the mechanism by which the underlying continuum equations of compressible flow avoid the development of infinite velocity gradients in the convective instability characteristic of slightly viscous flow, and to represent the sharp fronts of shock waves, where the smooth-solution branch of the continuum equations loses uniqueness past a critical scale. Without dissipation the flow would crash on its own resolution; with dissipation it does not, and the price paid is that organised motion at large scales is converted to disorganised motion at small scales.

Partial irreversibility from precision deficit. The conversion is *partially irreversible* for a precise reason: to recreate coordinated motion from the resulting uncoordinated small-scale motion would require a precision in the small-scale degrees of freedom that the physical realisation does not, and any finite-precision computation cannot, supply. The irreversibility of the

2nd Law of Thermodynamics is the inevitability of this precision deficit, no more and no less.

Physical computation, digital simulation. Physical ThermoDynamics is, in this reading, an analog computation performed by Nature at finite precision — the precision set by whatever microscopic process limits the resolution at very short length and time scales. The book mimics that physical computation with a digital computation, also at finite precision — the precision set by the resolution of a mesh, the arithmetic of a floating-point number, and the time step of an integrator. The two computations agree on those output quantities that survive the difference in precision: mean values, integrated fluxes, total dissipation D, drag, lift, temperature gaps between chambers. They disagree on point-values of turbulent flow, which neither computation has the precision to predict.

We refer to this formulation, throughout the book, as the **Real 2nd Law** — in distinction to the classical state-function 2nd Law of equilibrium thermodynamics, the statistical-mechanical 2nd Law of Boltzmann, and the information-theoretic 2nd Law of Shannon. The Real 2nd Law subsumes their content in the regimes where they apply and extends to the regimes they do not. The remainder of this volume is an extended demonstration of it: Joule's experiment, the piston-cylinder, refrigeration and heat-engine cycles, chemical bonding, blackbody radiation, the Big Bang and Big Crunch are all instances of the same precision-deficit mechanism, played out in different geometries and at different scales.

Chapter 2

Joule's 1845 Key Experiment

> *The most convincing proof of the conversion of heat into living force [vis viva] has been derived from my experiments with the electro-magnetic engine, a machine composed of magnets and bars of iron set in motion by an electrical battery. I have proved by actual experiment that, in exact proportion to the force with which this machine works, heat is abstracted from the electrical battery. You see, therefore, that living force may be converted into heat, and that heat may be converted into living force, or its equivalent attraction through space.*
> — J. P. Joule, *On Matter, Living Force, and Heat* (Lecture, Manchester, 1847)

How to read this chapter. The chapter is meant to be read with its computational realisation open in a second window — the single self-contained browser page `joule_experiment_cpu.html` (with a higher-resolution companion `joule_experiment_cpu_200.html`) in the RealMolecule GitHub repository, `github.com/Claes542/RealMolecule`, which runs with no installation. Proceed in three steps:

1. *Start reading.* Read Section 2.1 to set up Joule's experiment and what RealNSE computes.

2. *Watch the simulation.* Open the page, press Start, and watch the gas expand: the temperature-coloured particle trace, the cooling left chamber and warming right chamber, and the live read-outs of the dissipation D and the temperature gap ΔT.

3. *Continue reading.* Return to Section 2.2 (Simulation Results) and the Real vs Classical Analysis, which make sense of what you have just watched: why the gap appears, that it measures D, and how the channel-width slider changes D.

The text develops the physics; the code shows it happening in real time.

2.1 The Experiment

We shall now discover the essence of thermodynamics as transformation between heat energy and kinetic energy in a basic experiment performed by the James Prescott Joule (17874-1858), a manager of a brewery and hobby scientist with special interest in electricity. Joule reflected about replacing the brewery's steam engine by the newly invented electrical motor and thus became interested in the efficiency of different forms of energy conversion. *Joule's Law* gives the heat energy Q generated (per unit of time) by an electrical current I through a resistor R as $Q = I^2R$.

In his basic thermodynamics experiment, Joule considered a gas initially at rest, or in equilibrium, at a certain temperature and density in a certain volume immersed into a container of water, see Fig. 2.1. At initial time a valve was opened and the gas was allowed to expand into the double volume while the temperature change in the water was carefully measured by Joule.

To the great surprise of both Joule and the scientific community, no change of the temperature of the water could be detected, in contradiction with the expectation that the gas would cool off under expansion. Moreover, the expansion was impossible to reverse; the gas had no inclination to contract back to the original volume.

We assume that the gas is a *perfect gas* satisfying the gas law

$$p = \gamma\rho T \tag{2.1}$$

where p is pressure, ρ is density and T is absolute temperature and where $0 < \gamma < 1$ is a gas constant. This law come out as a combination of Boyle's law stating that pressure and density under constant temperature are proportional and Charles law stating that absolute temperature and density under constant pressure are inversely proportional.

We simulate Joule's experiment computationally using RealNSE in two space dimensions: at initial time a valve is opened in a channel connecting

two square chambers, a left and a right chamber, filled with gas of the same temperature but different density/pressure with high density/pressure in the left and low in the right chamber. (The simulation is two-dimensional; the chambers are squares, a planar section of the physical box, not cubes.) Figures 2.2 and 2.3 display the time-evolution of the mean temperature, density and kinetic energy in the left and right chambers, while Figure 2.4 gives snapshots of the temperature and density fields at an early and a later instant of the expansion.

We see that temperature drops in the left chamber as the gas expands with heat energy transforming to kinetic energy with a maximal temperature drop in the channel. When the cool expanding gas hits the wall opposite to the channel inlet in the right chamber, it is heated in recompression and turbulent/shock dissipation. The mean temperature thus drops in the left chamber and increases in the right and after a slight rebounce settles to a remaining density/temperature gap as the gas comes to rest with the same pressure in the left and right chambers and the same total heat energy as before expansion. Joule measured the total heat energy of the initial and final equilibrium states and found them to be equal. Joule did not seek to measure the dynamics of the process, nor the remaining temperature/density gap.

From the 1st Law alone there are many different possible end states with varying gaps in density/temperature. It is the 2nd Law which determines the size of the gap, which relates to the amount of turbulent/shock dissipation in the left and right chambers, which is determined by the dynamics of the process including the distribution of turbulence/shock dissipation.

We stay, for now, entirely within the dynamics the simulation computes — the expansion, the dissipation, the gap, and their dependence on the channel width. The comparison with the classical 2nd Law and the entropy S is deferred to the end of the chapter (Section 2.3), once the real process has been seen on its own terms.

The 2nd Law states that reversal of the process with the gas contracting back to the original small volume, is impossible because the only way the gas can be put into motion without external forcing is by expansion: self-expansion is possible, but not self-contraction.

We are thus able to analyze and understand the dynamics of the Joule experiment using the 1st and the new form of the 2nd law. The experiment displays the expansion phase of a compression refrigerator with heat being moved by expansion from the left chamber in contact with the inside of the

refrigerator, into the right chamber in contact with the outside. The cycle is closed by recompression under outside cooling. The efficiency connects to the temperature drop in the left chamber and the gap, with efficiency suffering from rebounce to small gap.

Note that both viscosity and heat conductivity is put to zero in RealNSE and so we do not simulate long time effects from small viscosity and heat conductivity slowly reducing the gap.

Watch the simulation now. This is the point to open `joule_experiment_cpu.html`, press Start, and watch one expansion through to rest: the left chamber cools and the right chamber warms, a temperature gap ΔT remains after the pressure has equalised, and the dissipation read-out D climbs and settles. Try the channel-width slider — a narrower opening produces a larger gap. The next two sections explain exactly what you are seeing.

2.2 Simulation Results

Running the simulation, three physical quantities can be read off the diagnostics and recorded as the expansion proceeds:

- the cumulative turbulent/shock *dissipation* $D = \iint \mu_{\text{mom}} \, |\nabla u|^2 \, dx \, dt \geq 0$;
- the chamber-to-chamber *temperature gap* $\Delta T = T_{\text{right}} - T_{\text{left}}$;
- the *pressure work* $W = \int p \nabla \cdot u \, dx$, which shuttles energy between internal and kinetic form.

The three are connected, and together they exhibit the entire 2nd-Law content of the experiment in measurable physical quantities. We take the connections in turn.

The temperature gap is the window into D. The dissipation D is deposited almost entirely in the right chamber — in the channel jet and the recompression against the far wall — where it appears as a warming of that chamber relative to the left. The dissipation D can therefore be expected to scale with the temperature gap $\Delta T = T_{\text{right}} - T_{\text{left}}$; more precisely, the simulation shows

$$D \;\approx\; m_{\text{right}} \, \Delta T, \tag{2.2}$$

with m_{right} the mass of gas in the right chamber (the box conserves $K + E$ and ends with $K = 0$, so the dissipated kinetic energy reappears as the heat that opens the gap). The temperature gap is the experimentalist's window into D: the quantity Joule would have measured with a sensitive enough calorimeter, and the one the simulation displays alongside the local integral D itself. Joule saw no ΔT only because heat conduction in his water bath erased the transient gap before his thermometer could register it; the simulation isolates the gap before equilibration and so makes it visible.

The work W mobilises the kinetic energy that D dissipates. Although the box does no work on its surroundings, the pressure work $W = p\,\nabla\cdot u$ does not vanish *locally*: the high-pressure left gas expands ($\nabla\cdot u > 0$, $W > 0$), converting internal energy into the kinetic energy of the jet — the gas cools — and in the recompression against the far wall the work reverses ($\nabla\cdot u < 0$, $W < 0$) while the turbulence dissipates that kinetic energy back to heat. In the global budget, with K the kinetic and E the internal energy, this is exactly the pair of balances of Chapter 1,

$$\dot{K} = W - D, \qquad \dot{E} = D - W,$$

which the simulation realises: W shuttles energy reversibly between E and K, while $D \geq 0$ runs only one way, $K \to E$. The kinetic energy first *mobilised* by the work (the simulation's peak K) is what the expansion makes available; the dissipation D is the portion of it the turbulence converts irreversibly into the heat that opens the gap ΔT. So the three recorded quantities lock together: W generates K, D destroys it as heat, and $\Delta T \approx D/m_{\text{right}}$ displays that heat — no entropy anywhere in the account.

The gap is transient; slow conduction preserves it. It is worth being precise about *which* equilibration the gap depends on, because the answer is counter-intuitive. Two processes run on very different timescales. *Mechanical* equilibration is fast: on the acoustic/flow timescale the gas reaches a common pressure in the two chambers — but with *unequal* temperatures, since the dissipation D was deposited asymmetrically (almost all of it in the right chamber). That pressure-balanced, temperature-split state $\rho_l T_l = \rho_r T_r$, $T_l \neq T_r$, is the gap. *Thermal* equilibration — heat conduction carrying the excess heat from the right chamber back to the left — is slow, and it is the process that erases the gap. The gap therefore lives in the window between the two:

fast conduction wipes it out before it can be read (Joule's water bath, hence his null result), while *slow* conduction lets it persist and be measured (what the simulation isolates). Given unlimited time any nonzero conduction drives $\Delta T \to 0$, since $K + E$ is conserved and E redistributes to a uniform T_0 — so the *final* equilibrium always has zero gap, regardless. Slow equilibration thus does not abolish the gap; it *preserves* it. The conduction rate sets the gap's *lifetime*; the dissipation D — controlled by the channel width below — sets its *size*.

The channel width controls the dissipation — read it from the simulation. The size of D — and through (2.2) the size of the temperature gap ΔT — is set by the channel width W. We do not need a closed-form law for this dependence; it is exactly what the simulation makes visible. Sweeping the channel-opening slider and watching the dissipation read-out and the gap, one sees that a *narrower* channel is more dissipative: a tighter opening forces a sharper, more strongly sheared jet, deposits more D in the right chamber, and opens a larger gap ΔT, while a wider channel dissipates less and leaves a smaller gap. *Narrow channels are dissipation-heavy.* The dependence is read *qualitatively*: the simulation here is two-dimensional, so what it establishes is the robust monotone trend — narrower channel, more dissipation, larger gap — not a precise scaling law, which would require a three-dimensional computation. Watching D and ΔT grow as the channel-opening slider is narrowed is the single experiment the reader should run while reading this chapter.

Why this matters later. This control of D by the channel width is the fundamental element of the devices built in Part III. A *narrow* channel concentrates the dissipation into a sharp spatial temperature split that the cold (or hot) side can be tapped from — the throttling principle of the *refrigerator* and *heat pump*. A *wide* channel lets the kinetic energy of the jet survive to be captured as shaft work — the *heat engine*. The single design choice W thus partitions the initial available work between recoverable work and dissipated heat; the quantitative device analysis (efficiencies, COP curves, Carnot ceilings) is deferred to the later chapters.

2.3 Real vs Classical Analysis

Real analysis: what the experiment shows on its own

What can we learn from Joule's experiment *without* invoking classical thermodynamics or any concept of entropy? Three things, in order:

1. **There is a gap.** After the gas expands and comes to rest at a common pressure, the two chambers do not return to a common temperature: a persistent density/temperature gap $\Delta T = T_{\text{right}} - T_{\text{left}}$ remains. The 1st Law alone permits a whole range of end states with different gaps; it does not select one.

2. **The gap is turbulent dissipation made visible.** The gap is the macroscopic projection of the cumulative turbulent/shock dissipation D, by the identity $D \approx \Delta T \cdot m_{\text{right}}$. The expansion converts heat energy to kinetic energy; the jet and its recompression against the far wall convert that kinetic energy *irreversibly* back to heat, deposited mostly in the right chamber. The gap is where that dissipated energy ends up.

3. **Without dissipation there would be no gap.** If the flow could expand and recompress without turbulent/shock dissipation, the kinetic energy would be returned coherently and the chambers would equalise to a common temperature with $\Delta T = 0$. The gap exists *only because* the expansion is dissipative; its size is set by how much D the dynamics generates — which, as the previous section showed, the channel width controls.

We have therefore found no need for any concept of entropy: kinetic energy, heat energy, work and turbulent dissipation — all physical quantities that can be measured — are sufficient to describe what happens. We have also seen the 2nd Law in its dynamic form: expansion from rest proceeds on its own because it generates dissipation $D \geq 0$, while the reverse, compression from rest, would require $D < 0$ and so cannot happen without exterior work.

Classical analysis: the 2nd Law and entropy

The free expansion is the textbook case in which the classical entropy increase is got *without any reference to the dynamics* — the "miracle" of the state

function noted in Chapter 1. The gas expands from volume V to $2V$ at unchanged internal energy ($\Delta E = 0$, hence unchanged temperature for a perfect gas). No heat is exchanged and no work is done, yet the entropy is a state function, so its change is read off from the endpoints by integrating along *any* convenient path — here a reversible isothermal expansion between the same two states:

$$\Delta S \;=\; \int_V^{2V} \frac{p\,dV}{T} \;=\; \gamma \int_V^{2V} \frac{dV}{V} \;=\; \gamma \ln 2, \tag{2.3}$$

using $p = \gamma \rho T$, i.e. $p/T = \gamma/V$ per unit mass. No dynamics and no summing over the process: the difference of the primitive $S = \ln(T/\rho^{\gamma})$ between the endpoints (the density halves, so $\Delta S = -\gamma\,\Delta \ln \rho = \gamma \ln 2$) delivers the answer directly.

What RealTD puts in its place: the dissipation D. Real ThermoDynamics does not need the entropy at all. The real, physically defined quantity is the *turbulent dissipation*

$$D \;=\; \iint \mu_{\mathrm{mom}}\, |\nabla u|^2 \, dx\, dt \;\geq\; 0, \tag{2.4}$$

the kinetic energy irreversibly converted to heat along the *actual* trajectory. D is non-negative by construction (a sum of squares, cell by cell and step by step), is computed directly from the RealNSE velocity field, and carries the whole irreversible content of the 2nd Law. Its *normalised* value $D/(M\,T_{\mathrm{eq}})$ — total dissipation per unit mass and temperature — has the dimensions of a specific entropy and can be set beside the classical ΔS of (2.3) as a sanity check:

$$\frac{D}{M\,T_{\mathrm{eq}}} \;\approx\; \gamma \ln 2, \tag{2.5}$$

the running simulation gives ≈ 0.067 against the ideal $\gamma \ln 2 \approx 0.069$. **The comparison is a check, not a claim that $\gamma \ln 2$ carries any deep truth.** The number $\gamma \ln 2$ is merely what the classical state-function construction returns for the idealised endpoints; D is the real physics.

Why ΔS is the murky quantity and D is not. Three points make the asymmetry concrete. *First*, $\gamma \ln 2$ is the value for the idealised *uniform* end state $(T_0,\ \rho_0/2)$; the real process settles instead to the mechanically

equilibrated *gap* state (uniform pressure, $T_l \neq T_r$), which it never leaves unless slow heat conduction later erases the gap. The classical $\gamma \ln 2$ therefore describes an endpoint the real flow does not actually reach — and a direct entropy evaluation on the settled gap state gives substantially less. *Second*, evaluated as a state function $S = \int \rho(\ln T - \gamma \ln \rho)\, dx$ *directly on the computed solution*, $\Delta S = S(t) - S(0)$ is not even a clean, monotone number: the finite-precision scheme's stabilising diffusion does not respect a discrete entropy inequality for this functional, and ΔS can drift slightly negative during a run — the classical entropy has no robust value on the real flow. *Third*, the dissipation D has none of these troubles: it is ≥ 0 cell by cell and step by step by construction, it is what the solver actually computes, and it is what the temperature gap $\Delta T \approx D/m_{\text{right}}$ of (2.2) makes macroscopically visible. **D is real physics; ΔS is a classical bookkeeping construct of unclear physical meaning.** The agreement (2.5) is reassuring where the classical theory applies, but the operative quantity throughout this volume is D, not S.

Put plainly: the celebrated endpoint "miracle" of Chapter 1 is reduced to a *message about sign* — that the expansion is irreversible, $\Delta S > 0$ — together with, for the idealised endpoints, a reference number. It does *not* deliver the *quantity* the real process actually realises; the sign may be right, the quantity is not. That quantity is the real turbulent dissipation D.

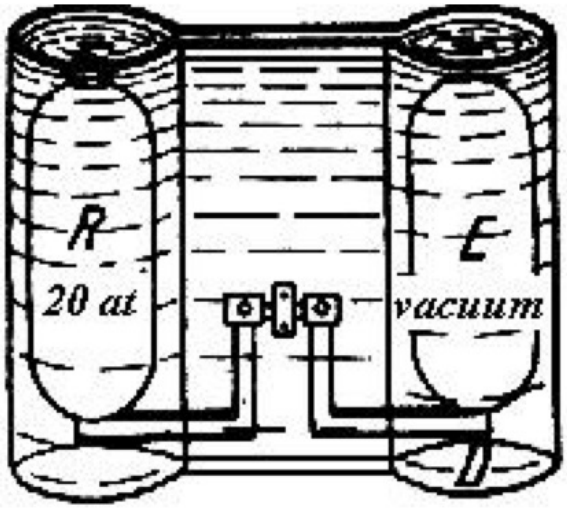

Fig. 358 Concerning overflowing experiment of Joule (Scientific Papers). *R* contains at first air compressed to 20 atm, *E* is initially a vacuum, *D* the tube

Figure 2.1: Joule's 1845 free-expansion apparatus (historical figure from Joule's *Scientific Papers*). Vessel R holds air compressed to 20 atm; vessel E is initially evacuated; the two are connected by the tube D and the assembly is immersed in a water bath. When the stopcock is opened, the gas expands from R into E. Joule's measurement of the water-bath temperature before and after the expansion produced his celebrated null result — which the RealNSE simulation of this chapter resolves by showing that the *transient* dynamic temperature gap $\Delta T \approx D/m_R$ is recovered if heat conduction in the water bath is fast enough to equilibrate the gap before the thermometer can read it.

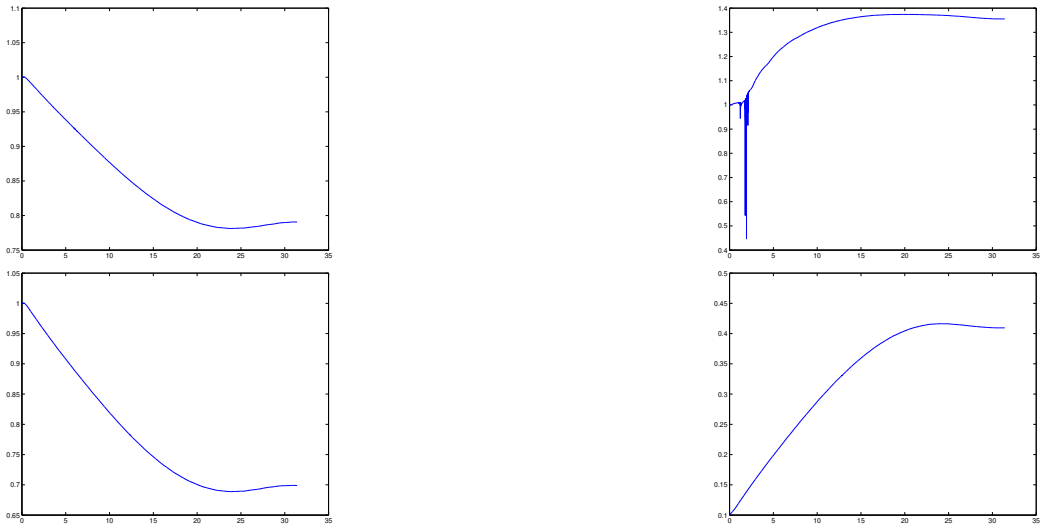

Figure 2.2: Time-evolution of the mean temperature (top) and density (bottom) in the left chamber (left column) and right chamber (right column) during the Joule expansion: the left chamber cools and rarefies, the right chamber warms and densifies, settling to a persistent density/temperature gap.

Figure 2.3: Time-evolution of the mean kinetic energy in the left chamber (left) and right chamber (right): kinetic energy is generated as the gas expands and is dissipated back to heat in the recompression and turbulence against the far wall.

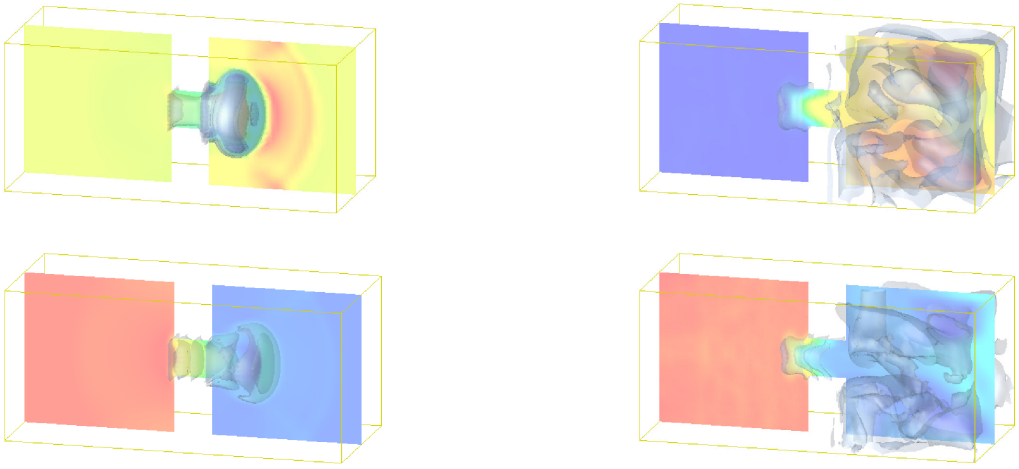

Figure 2.4: Snapshots of the temperature (top) and density (bottom) fields in the two chambers at an early (left) and a later (right) instant of the expansion — the cold expanding jet through the channel and its warming on recompression against the far wall.

Part II

Mathematics

Chapter 3

New Foundation

> Heat, a quantity which functions to animate, derives from an internal fire located in the left ventricle. (Hippocrates, 460 B.C.)

3.1 The Euler and Navier-Stokes Equations

The *Navier-Stokes equations* for a compressible gas express *conservation of mass, momentum and total energy* as a system of partial differential equations with position and time as independent variables, together with *constitutive laws* defining *pressure*, *viscous forces* and *diffusive heat fluxes* in terms of *mass density*, *velocity* and *heat/internal energy*, combined with *initial conditions* and *boundary conditions*. In a *perfect gas* the pressure is proportional to the internal energy. With vanishing viscosity and heat conductivity the Navier-Stokes equations reduce to the *Euler equations*. The Euler/Navier-Stokes equations represent a *fluid mechanics model* of thermodynamics, as compared to a kinetic model with also particle velocity as an independent variable.

Conservation of mass, momentum and total energy in the Euler equations formally arise by averaging over velocities in Boltzmann's kinetic model. However, the constitutive laws of the Navier-Stokes equations including coefficients of *viscosity* and *heat conductivity* show to be solution dependent and thus difficult to determine *ab initio* from a kinetic model, or in experiments. In a *Newtonian fluid* the viscosity is *assumed* to be constant, but this assumption is questionable for slightly viscous fluids with vastly different effects of viscosity in turbulent and laminar flow. The *existence* and

uniqueness (or the converse of *non-existence*) of solutions to the incompressible Navier-Stokes equations for a Newtonian fluid represent one of the open Clay Mathematics Institute Millenium Problems [**?**].

Solutions of the Navier-Stokes equations for a perfect gas *formally* satisfy a 2nd Law expressing that a specific scalar entropy defined in terms of mass density and internal energy is strictly increasing with increasing time, as an expression of a loss of kinetic energy by *positive viscous dissipation* formally obtained by forming the scalar of the momentum equation including viscous stresses with the velocity. The 2nd Law with strictly increasing entropy for solutions of Navier-Stokes equations enforcing irreversibility, is thus formally equivalent to the presence of non-vanishing viscosity. For the Euler equations, the entropy (formally) stays constant as an expression of vanishing viscosity and reversibility.

For the Navier-Stokes equations *with* viscous dissipation, we might thus simply forget the entropy inequality, because it is an automatically satisfied *derived relation*.

This reduces the enigma of the 2nd Law to explaining how effects of viscous dissipation and irreversibility can arise in a formally reversible system such as a system of elasticly colliding particles without viscosity. Simply claiming that viscous effects must come from somewhere is not informative. Neither is to claim that they come from quantum mechanics (or neutrino physics like Feynman), since quantum mechanics is formally reversible. Nor is simply assuming constitutive laws for viscous stresses of some form, e.g. simply assuming the fluid to be Newtonian.

Boltzmann's answer was molecular games of roulette, but it is an answer which poses more questions than it resolves.

3.2 Computational Thermodynamics

In this book we present a *constructive deterministic* fluid mechanics model of the thermodynamics of a slightly viscous gas/fluid based on *finite precision computation* by a *weighted least squares stabilized finite element method* for the *Euler/Navier-Stokes equations* with *slip boundary conditions* at solid boundaries, referred to as *RealNSE*. For definiteness we consider a perfect gas/fluid, but extension to more general state equations for the pressure is possible.

Note that we start from the Euler equations with vanishing viscosity and

heat conductivity and we thus do not need input of constitutive laws for viscous stresses and heat diffision, only a law of state for the pressure.

The least squares stabilization in RealNSE penalizes large Euler residuals by viscosity acting in the streamline direction as a form of *bulk viscosity* of order h, and is complemented by a higher-order residual dependent isotropic *shear viscosity* of order $h^{3/2}$ in turbulent regions, where h is the mesh size, together referred to as *RealNSE viscosity*.

RealNSE is a *constructive model* in the form of the Euler equations *together* with a computational solution procedure including RealNSE viscosity, guaranteeing existence by computational construction, to be distinguished from a *formal model* e.g. in the form of the Navier-Stokes equations without constructive solution procedure and requiring input of viscosity.

RealNSE automatically introduces solution dependent viscosity and thus circumvents the difficult problem of specifying viscosity (and heat conductivity) in a Navier-Stokes model. The only input in this regard is that the flow is *slightly viscous* with *Reynolds number* larger than say 10^6, which covers many important applications in aero- and hydrodynamics.

We discover by computation that RealNSE solutions are *turbulent* and have *shocks*, both phenomena being identified by substantial (positive) *RealNSE turbulent/shock dissipation* from RealNSE viscosity with pointwise large (but weakly small) Euler residuals. Turbulence/shocks are thus identified by substantial RealNSE turbulent/shock dissipation, which reflects pointwise large Euler residuals, which reflects non-existence of pointwise solutions with pointwise vanishing Euler residuals. We observe turbulence in RealNSE solutions with slip boundary conditions, and conclude that turbulence does not (primarily) originate from microscopic boundary layers with no-slip boundary conditions, contrary to state-of-the art boundary layer theory by Prandtl and Schlichting [**?**, **?**], but from macroscopic instability.

We motivate using slip boundary conditions (or more generally a friction boundary condition with small friction) by the computationally and experimentally verified fact that the *skin friction* of a turbulent boundary layer tends to zero with viscosity and thus is (comparatively) small for slightly viscous flow.

We prove that RealNSE solutions satisfy a 2nd Law expressed in terms of kinetic energy, internal energy, work and (positive) turbulent/shock dissipation. We realize that irreversibility is a consequence of substantial turbulent/shock dissipation, which is consequence of pointwise instability of slightly viscous flow, which is reflected by non-existence of pointwise solu-

tions to the Euler equations. We thus justify a 2nd Law without resort to any ad hoc assumption of positive viscous dissipation or molecular chaos.

Existence of RealNSE solutions is guaranteed by construction. Uniqueness relates to *wellposedness* in the sense of Hadamard, which concerns what aspects or *outputs* of RealNSE turbulent/shock solutions are stable under perturbations in the sense that small perturbations have small output effects. We define a RealNSE output to be wellposed if it is insensitive to mesh refinement and thus can be computed with finite mesh size. We show that wellposedness of RealNSE solutions can be tested a posteriori by computationally solving a *dual linearized problem*, through which the output sensitivity of non-zero Euler residuals can be estimated. We find that mean-value outputs such as drag and lift and total turbulent dissipation are wellposed, while point-values of turbulent flow are not. We can thus a posteriori assess the quality of RealNSE solutions as solutions of the Euler equations and identify what outputs are wellposed and converge with decreasing mesh size.

RealNSE solutions can be viewed either as exact Euler solutions subject to perturbations from non-vanishing Euler residuals, or alternatively as approximate Navier-Stokes solutions with specific viscosity given by the mesh-dependent RealNSE viscosity, combined with slip/friction boundary conditions.

We emphasize that RealNSE contributes its own mesh/solution-dependent RealNSE viscosity and thus does not require any input of viscosity (or heat conductivity) coefficients, or turbulence model.

3.3 RealNSE as Automatic Turbulence Model

RealNSE can be viewed as a form of *Large Eddy Simulation LES* for slightly viscous/high Reynolds number flow with an *turbulence model* given by the least squares stabilization for interior turbulence and the slip boundary condition for turbulent boundary layers.

We recall that *Direct Numerical Simulation DNS* by computational solution of Navier-Stokes equations with resolution of all turbulent scales including thin boundary layers, is today possible for Reynolds numbers up to 10^4, while reaching 10^6 is estimated to take another 50 years [**?**, **?**].

Some form of LES with turbulence modeling is therefore needed for high Reynolds number flow, but the design of turbulence models is an open problem since more than hundred years. RealNSE offers an automatic turbulence

model based on computational principles, with automatic assessment of well-posedness by duality.

RealNSE thus gives an answer to the enigma of the origin of viscosity in terms of of finite precision computational simulation of turbulent flow. RealNSE finite precision computation is not statistics, because statistical ensembles of outputs do not appear, only mean-values in space-time of individual trajectories/solutions.

3.4 From Probable to Necessary

The stabilization/viscous dissipation in RealNSE is necessary because without stabilization RealNSE solutions cease to exist in blowup as they inevitably go turbulent, while physical flows continue to exist without blowup even after transition to turbulence. Viscous dissipation thus comes out from an *inevitable* development of turbulence/shocks as a result of an inherent instability of slightly viscous flow, and a *necessity* to avoid blowup into non-existence, because non-existence is not an option: The show must go on, which is not a question of probability. RealNSE viscous dissipation is thus a necessity, and not the result of a game of roulette.

RealNSE viscosity transfers kinetic energy into internal energy by pointwise large but weakly small violation of conservation as the characterstic of turbulence. By necessity, as a characteristic of turbulence, the pointwise violation is large, yet in a sense smallest possible to prevent blowup and thus generic and not ad hoc.

3.5 The Spirit of Dijkstra

We follow the device of the famous computer scientist Dijkstra:

- *Originallly I viewed it as the function of the abstract machine to provide a truthful picture of the physical reality. Later, however, I learned to consider the abstract machine as the* true *one, because that is the only one we can think; it is the physical machine's purpose to supply a working model, a (hopefully) sufficiently accurate physical simulation of the true, abstract machine.*

We thus view RealNSE as a constructive mathematical model (abstract machine) of a physical reality (physical machine). We are then led to interprete

the digital finite precision computation as some form of analog physical computation, and digital RealNSE viscosity as some form of analog physical viscosity.

We compare with a classical formal mathematical model in the form of the Navier-Stokes equations including an ad hoc model of viscosity, e.g. a Newtonian model with constant shear viscosity. We are thus led to turn around the common view of computational viscosity as "artificial" viscosity and Newtonian viscosity as "physical" viscosity, and instead interprete RealNSE viscosity as physical (and then Newtonian viscosity as artificial), following von Neumann who opened compressible flow to computational simulation by introducing artificial viscosity on physical grounds.

RealNSE thus offers a model of fluid flow, which can be inspected, analyzed, understood, utilized and evaluated, while the true physics of turbulent flow may remain inaccessible to inspection and analyzis. Even if the mechanics of turbulent flow in principle can be reduced to quantum mechanics on atomic scales, such a model seems useless for predictions on macroscopic scales. For example, determining the viscosity of water from quantum mechanics is still an open problem.

We remark that the role of viscosity coefficients in classical modeling is to define viscous force in terms of fluid velocity (strain). If now RealNSE automatically supplies viscous forces, without input of viscosity, there is no longer any need to define viscosity coefficients, or the Reynolds stresses of turbulence modeling, and RealNSE thus offers a simplification of fluid mechanics and a way out of a stalemate.

Using RealNSE as a model of thermodynamics changes the questions and answers and opens new possibilities of progress together with new challenges to mathematical analysis and computation. RealNSE solutions are contructed/computed and thus are available to inspection, which means that the analysis of solutions shifts from *a priori* to *a posteriori*; after solutions have been computed they can be inspected, their qualities can be evaluated and interpreted in physical terms.

3.6 The Power of RealNSE

In related work [**?**, **?**, 23] we have demonstrated the new capabilities offered by RealNSE in resolutions of both d'Alembert's paradox from 1752 and the Clay Millenium Problem on existence and uniquenes of the incompressible

Euler/Navier-Stokes equations: In short, existence follow by construction and uniqueness from wellposedness, both being consequences of the basic structure of RealNSE as a midway between the Scylla/Galerkin of weak solution, which is too weak, and the Carybdis/least squares of strong solution, which is too strong. With the proper weighting of the least squares stabilization, RealNSE manages to combine accuracy with wellposedness and thus produce meaningful outputs.

More precisely, we will see below that output variation is bounded by $S\|hR\|_0$, where S is a stability factor, h is the mesh size, R is the Euler residual and $\|\cdot\|_0$ is a space-time L_2-norm. This results from the Galerkin orthogonality of RealNSE, which together with least squares stabilization introducing a bound on $\|\sqrt{h}R\|_0$, enforces control of output variation up to a tolerance $S\sqrt{h}$. We shall find that for mean-value outputs such as drag/lift and total turbulent dissipation, $S << h^{-1/2}$ which implies wellposedness. The unique design of RealNSE with a combination of Galerkin orthogonality and weighted least squares stabilization, thus can be motivated on rational grounds towards the goal of producing wellposed outputs, and can then as such be interpreted in physical terms.

RealNSE shows to be a computationally affordable useful model for slightly viscous (compressible and incompressible) flow, because mean-value outputs can be computed without resolving boundary layers and interior turbulence to physical scales. This reflects that mean-value outputs in slightly viscous turbulent flow, can vary little with the viscosity (beyond the drag crisis), as long as the viscosity is sufficiently small or the Reynolds is number sufficiently large, as observed in both physical experiment and computation.

RealNSE allows accurate prediction of the turbulent losses in a heat engine and the drag/lift of a car and airplane with millions of mesh points [**?**, **?**], instead of the trillions required with DNS according to state-of-the art [**?**]. RealNSE offers automatic turbulence modeling and assessment of wellposedness. Adopting RealNSE as a model of thermodynamics can be seen as a return to Euler's original idea of using inviscid flow as a model of slightly visocus flow, but with new insight and capabilities.

3.7 2nd Law for RealNSE

As already indicated, we formulate a 2nd Law for RealNSE without the concept of entropy, in terms of the basic physical quantities of kinetic energy

K, heat energy E, rate of work W and shock/turbulent dissipation $D > 0$, of the form

$$\dot{K} = W - D, \quad \dot{E} = -W + D, \tag{3.1}$$

where the dot indicates time differentiation. Slightly viscous flow always develops turbulence/shocks with $D > 0$, and the 2nd Law thus expresses an irreversible transfer of kinetic energy into heat energy, while the total energy $E + K$ remains constant because $\dot{E} + \dot{K} = 0$.

3.8 Irreversibility and Finite Precision

The 2nd Law (3.1) with $D > 0$ describes a process which is irreversible with a forward Arrow in time, since the reversed process would correspond to $D < 0$. We can understand the irreversibility as a consequence of finite precision computation combined with a certain form of wellposedness as follows: We have noted that in viscous dissipation with $D > 0$ kinetic energy is transformed into smaller scale kinetic energy in the form of internal/heat energy. This process is wellposed e.g. in the sense that the total viscous dissipation is insensitive to mesh refinement/vanishing viscosity. This can be seen as feature of a process of smashing larger units into smaller pieces with certain mean-value outputs being insensitive to the precision of the smashing procedure.

On the other hand, in the reversed process small pieces would have to be put together into larger units in a precise way, and such a process is very sensitive to the precision of the assembly.

The 2nd Law (**??**) based on finite precision computation thus can be viewed to reflect that smashing into pieces is insensitive to the precision of the smashing, while the reversed process of reassembly is sensitive to the precision of the assembly. The 2nd Law thus expresses a familar phenomenon without any mystery of molecular games of roulette, just finite precision construction/computation.

3.9 Viscosity Solutions

An RealNSE solution can be viewed as particular *viscosity solution* of the Euler equations, which is a solution of *regularized Euler equations* augmented by additive terms modeling viscosity effects with small viscosity coefficients.

The effective viscosity in an RealNSE solution typically may be comparable to the mesh size.

For incompressible flow the existence of viscosity solutions, with suitable solution dependent viscosity coefficients, can be proved a priori using standard techniques of analytical mathematics. Viscosity solutions are pointwise solutions of the regularized equations. But already the most basic problem with constant viscosity, the incompressible Navier-Stokes equations for a Newtonian fluid, presents technical difficulties, and is one of the open Clay Millennium Problems.

For compressible flow the technical complications are even more severe, and it is not clear which viscosities would be required for an analytical proof of the existence of (global smooth) viscosity solutions [35, 36] to the Euler equations. Furthermore, the question of wellposedness is typically left out, as in the formulation of the Navier-Stokes Millennium Problem, with the motivation that first the existence problem has to be settled. Altogether, analytical mathematics seems to have little to offer a priori concerning the existence and wellposedness of solutions of the compressible Euler equations. In contrast, RealNSE computational solutions of the Euler equations seem to offer a wealth of information a posteriori, in particular concerning wellposedness by duality of turbulent/shock solutions.

An RealNSE solution thus can be viewed as a specific viscosity solution with a specific regularization from the least squares stabilization, in particular of the momentum equation, which is necessary because pointwise momentum balance is impossible to achieve in the presence of shocks/turbulence. The RealNSE viscosity can be viewed to be the minimal viscosity required to handle the contradiction behind the non-existence of pointwise solutions. For a shock RealNSE could then be directly interpreted as a certain physical mechanism preventing a shock wave from turning over, and for turbulence as a form of automatic computational turbulence model.

Chapter 4

The Euler Equations

> However sublime are the researches on fluids which we owe to Messrs Bernoulli, Clairaut and d'Alembert, they flow so naturally from my two general formulae that one cannot sufficiently admire this accord of their profound meditations with the simplicity of the principles from which I have drawn my equations ...(Euler 1752)

> I know that most men, including those at ease with problems of the highest complexity, can seldom accept even the simplest and most obvious truth if it be such as would oblige them to admit the falsity of conclusions which they have delighted in explaining to colleagues, which they have proudly taught to others, and which they have woven, thread by thread, into the fabric of their lives. (Tolstoy)

4.1 Conservation of Mass, Momentum and Energy

Computational thermodynamics is based on a 1st Law in the form of the Euler equations for an ideal perfect gas/fluid expressing conservation of mass, momentum and total energy as a system of partial differential equations. We formulate these equations for a gas/fluid enclosed in a fixed (open) domain Ω in three-dimensional space $\mathbb{R}^3$ with boundary Γ over a time interval $[0, T]$ with intial time zero and final time T (from now on T denotes final time and not temperature as above). The Euler equations model a gas/fluid with vanishing (very small) viscosity and heat conductivity. The Euler equations then represent a Hamiltonian system.

We seek the *density* ρ, *momentum* $m = \rho u$ with $u = (u_1, u_2, u_3)$ the *velocity*, and the *total energy* ϵ as functions of $(x, t) \in \Omega \cup \Gamma \times [0, T]$, where $x = (x_1, x_2, x_3)$ denotes the coordinates in $\mathbb{R}^3$ and u_i is the velocity in the x_i-direction. The Euler equations for $\hat{u} \equiv (\rho, u, \epsilon)$ read with $Q = \Omega \times I$ and $I = (0, T]$:

$$\begin{aligned} \dot{\rho} + \nabla \cdot (\rho u) &= 0 && \text{in } Q, \\ \dot{m}_i + \nabla \cdot (m_i u) + p_{,i} &= f_i && \text{in } Q, \quad i = 1, 2, 3, \\ \dot{\epsilon} + \nabla \cdot (\epsilon u + p u) &= g && \text{in } Q, \\ u \cdot n &= 0 && \text{on } \Gamma \times I, \\ \hat{u}(\cdot, 0) &= \hat{u}^0 && \text{in } \Omega, \end{aligned} \tag{4.1}$$

where $p = p(x, t)$ is the *pressure* of the fluid, $v_{,i} = \frac{\partial v}{\partial x_i}$ is the partial derivative with respect to x_i, $\dot{v} = \frac{\partial v}{\partial t}$ is the partial derivative with respect to time t, n denotes the outward unit normal to Γ and $f = (f_1, f_2, f_3)$ is a given *volume force* (like gravity) acting on the fluid, g is a given heat source, and $\hat{u}^0 = \hat{u}^0(x)$ represent initial conditions. Further, the total energy $\epsilon = k + e$, where

$$k = \frac{\rho |u|^2}{2}$$

is the *kinetic energy* with $|u|^2 = \sum_{i=1}^3 u_i^2$, and

$$e = \rho \tau$$

is the *internal energy* or *heat energy* with τ the *temperature*, assuming the heat capacity is equal to one. The boundary condition is a *slip* boundary condition requiring the normal velocity $u \cdot n$ to vanish corresponding to an inpenetrable boundary with zero friction. Below we will consider other boundary conditions including inflow and outflow conditions and non-zero friction. Of course, $\nabla \cdot v = \sum_i v_{i,i}$ denotes the divergence of $v = (v_1, v_2, v_3)$ (and $\nabla w = (w_{,1}, w_{,2}, w_{,3})$ the gradient).

There are five equations in the Euler system (4.1), while the number of unknowns including the pressure is six, and so we need one more equation, which may be a *state equation for a compressible gas* expressing the pressure p as a function of density ρ and temperature τ, e.g. the state equation

$$p = \gamma \rho \tau \tag{4.2}$$

of a *perfect gas*, with here $0 < \gamma < 1$ a *gas constant* (equal to $\frac{c_p}{c_v} - 1$ where c_p the specific heat under constant pressure and c_v that under constant).

For a mono-atomic gas $\gamma = 2/3$. The additional equation may alternatively express that the fluid is *incompressible* in the form $\nabla \cdot u = 0$ in Q. Note that the gas constant γ is here defined as $\gamma = \bar{\gamma} - 1$ with $\bar{\gamma} = \frac{c_p}{c_v}$ the most commonly used gas constant.

The extension of the Euler equations to include viscous forces and heat flow by conduction are referred to as the *Navier–Stokes equations*, which are no longer represent a Hamiltonian system. The Navier–Stokes and Euler equations describe a very rich complex world of fluid dynamics.

The Euler equations (4.1) represents a *one-species* model, which we below will extended to a *many-species* model including chemical reactions with chemical energy adding to the total energy.

The Euler equations represent, up to the gas constant γ, a *parameter-free model*. The determination of parameters such as viscosity and heat conductivity coefficients relevant for complex flows, can be a very difficult (or simply hopeless) task, since the coefficients in general are solution dependent (and the solution depends on the coefficients). In the Euler equations the coefficients are simply put to zero with the motivation that they are small, while their actual values are irrelevant and thus do not have to be determined.

We will find that mean-value outputs are insensitive to the values of viscosity and heat conductivity, once they are small enough, which is reflected in mesh independence in RealNSE. RealNSE thus comes out as an essentially parameter-free model, and we will discover the remarkable (surprising) fact is that RealNSE can accurately predict key outputs such as drag and lift of bluff bodies and and total losses in thermodynamical processes.

4.2 Internal Energy Formulation

We shall below use a formulation of the Euler equations in terms of the internal energy e instead of the total energy ϵ, which reads: Find $\hat{u} = (\rho, m, e)$ such that

$$\begin{aligned} \dot{\rho} + \nabla \cdot (\rho u) &= 0 && \text{in } Q, \\ \dot{m}_i + \nabla \cdot (m_i u) + \gamma e_{,i} &= f_i && \text{in } Q, \quad i = 1, 2, 3, \\ \dot{e} + \nabla \cdot (eu) + \gamma e \nabla \cdot u &= g && \text{in } Q, \\ u \cdot n &= 0 && \text{on } \Gamma \times I, \\ \hat{u}(\cdot, 0) &= \hat{u}^0 && \text{in } \Omega, \end{aligned} \tag{4.3}$$

where we have used that $p = \gamma e$. We will consider (4.3) to express the 1st Law as conservation of mass, momentum and internal energy. Strictly

speaking, here only mass is conserved, because of the presence of f in the momentum equation and $\gamma e \nabla \cdot u$ and g in the equation for internal energy, and so conservation of momentum and internal energy is interpreted modulo the effects of these source terms.

We will below write the Euler equations:

$$\begin{aligned} \dot{\rho} + \nabla \cdot (\rho u) &= 0 && \text{in } Q, \\ \dot{m} + \nabla \cdot (mu) + \gamma \nabla e &= f && \text{in } Q, \\ \dot{e} + \nabla \cdot (eu) + \gamma e \nabla \cdot u &= g && \text{in } Q, \\ u \cdot n &= 0 && \text{on } \Gamma \times I, \\ \hat{u}(\cdot, 0) &= \hat{u}^0 && \text{in } \Omega, \end{aligned} \tag{4.4}$$

with $\dot{m} + \nabla \cdot (mu) + \gamma \nabla e = f$ the same as $\dot{m}_i + \nabla \cdot (m_i u) + \gamma e_{,i} = f_i$ for $i = 1, 2, 3$.

4.3 Derivation of the Euler Equations

We now show that the Euler equations (4.1)/(4.3) express conservation of mass, momentum and total/internal energy in the *conservation variables* (ρ, m, e). To this end consider a fixed small volume V in Ω with boundary S. Mass conservation implies that

$$\int_V \dot{\rho}\, dx = \frac{\partial}{\partial t} \int_V \rho\, dx = -\int_S (\rho v) \cdot n\, ds$$

expressing that the rate of increase of total mass in the fixed volume V is equal to the rate of inflow through the boundary S. The Divergence Theorem (see e.g. B&S Vol 3) states that

$$\int_V \nabla \cdot (\rho v)\, dx = \int_S (\rho v) \cdot n\, ds,$$

and we thus conclude that

$$\int_V \dot{\rho}\, dx + \int_V \nabla \cdot (\rho v)\, dx = 0$$

for all volumes V. Assuming that the integrands are continuous, we thus obtain the equation for mass conservation $\dot{\rho} + \nabla \cdot (\rho v) = 0$.

We obtain the differential equation expressing conservation of each component of the momentum m_i similarly, noting that by Newtons second law

the rate of change of momentum is given by the corresponding component $-p_{,i}$ of the pressure gradient ∇p with increasing pressure retarding the flow, combined with volume force f_i.

Finally, the equation expressing conservation of total energy ϵ is obtained as above using the Divergence Theorem, noting that the rate of change of the total energy over a volume V convected by the flow, is equal to the work $pu \cdot n$ performed on the boundary of V per unit time step. The equation for the internal energy expresses that the work $p\nabla \cdot u$ by compression/expansion is balanced by heat energy.

4.4 Incompressible Flow

In an incompressible fluid the density ρ does not change if we follow the motion of the fluid particles of the flow. We can express this fact in the differential equation form

$$D_u\rho \equiv \dot{\rho} + u \cdot \nabla\rho = 0$$

where $D_u\rho$ is the *convective derivative* of ρ with respect to the velocity u. We obtain the convective derivative by computing the change in time following the *trajectory* $x(t)$ of a fluid particle satisfying the differential equation $\dot{x}(t) = u(x,t)$. Differentiating $\rho(x(t),t)$ with respect to time, we obtain by the chain rule:

$$\frac{d}{dt}\rho(x(t),t) = (\dot{\rho} + \dot{x} \cdot \nabla\rho)(x(t),t) = D_u\rho(x(t),t).$$

Since mass conservation reads $D_u\rho + \rho\nabla \cdot u = 0$, we conclude that the velocity u in incompressible flow is characterized by the equation

$$\nabla \cdot u = 0 \quad \text{in } Q. \tag{4.5}$$

The Euler equations for incompressible flow thus take the form: Find $\hat{u}$ and p such that

$$\begin{array}{rcll} \dot{\rho} + \nabla \cdot (\rho u) & = & 0 & \text{in } Q, \\ \dot{m} + \nabla \cdot (mu) + \nabla p & = & f & \text{in } Q, \\ \nabla \cdot u & = & 0 & \text{in } Q, \\ \dot{\epsilon} + \nabla \cdot (\epsilon u + pu) & = & 0 & \text{in } Q, \\ u \cdot n & = & g & \text{on } \Gamma \times I, \\ \hat{u}(\cdot,0) & = & \hat{u}^0 & \text{in } \Omega, \end{array} \tag{4.6}$$

where the incompressibility condition $\nabla \cdot u = 0$ replaces the equation of state for the pressure p. In this case the energy equation is decoupled from the density and momentum equations; it is possible to solve for (ρ, u, p) from the first three equations and then for the energy ϵ.

If ρ^0 is constant, with $\rho^0 = 1$ say, then the first equation is trivially satisfied with $\rho = 1$, and (u, p) are solvable from the equations

$$\begin{aligned} \dot{u} + \nabla \cdot (uu) + \nabla p &= f && \text{in } Q, \quad i = 1, 2, 3, \\ \nabla \cdot u &= 0 && \text{in } Q, \\ u \cdot n &= 0 && \text{on } \Gamma \times I, \\ u(\cdot, 0) &= u^0 && \text{in } \Omega, \end{aligned} \tag{4.7}$$

which are the usual incompressible Euler equations with constant density and the energy equation left out.

4.5 Continuum and Particle Models

The Euler equations formally represent a *continuum model* with no smallest scale, since there is no smallest scale of the set of real numbers $\mathbb{R}$, and there is no viscosity or heat conduction which could define a smallest scale. It is well known that the Euler equations in general lack exact pointwise solutions, because of the appearance of turbulence and shocks, and our model of thermodynamics is instead RealNSE, where the Euler equations are solved computationally by a finite element method on a mesh of finite precision of *mesh size* h (variable in space and time).

We may think of the finite element computation as a finite precision computation with a fixed number of digits (e.g. single precision with about 7 digits) instead of computing with real numbers with infinitely many digits with infinite precision (which is impossible). Typical meshes have a mesh size of 10^{-2} on the unit cube with 10^6 mesh points. A gas has about 10^{24} molecules per mole, and thus the values of density, momentum and energy at each mesh point represent mean values of about 10^{18} molecules, thus mean values over incredibly many "fluid particles".

A computational *particle model* of a gas accounting for the position and velocity of each of the 10^{24} particles in each mole, is inconceivable on any kind of thinkable computer. Thus, only some form of continuum model can be used for macroscopic phenomena of fluid flow.

With RealNSE we stay within a deterministic framework and only add a restriction of finite precision computation to the formally Hamiltonian Euler equations. A world of thermodynamics governed by Hamiltonian mechanics combined with finite precision computation, follows the laws of mechanics as far as possible taking the finite precision into account, but is not based on any microscopic games of roulette as statistical mechanics. The difference of scientific paradigm is fundamental. We are thus led to a model of the World as a giant *clock with finite precision* as a computer age alternative Laplace's classical clock with infinite precision as well as Boltzmann's micriscopical games of roulette.

In RealNSE the mesh size h enters as a parameter which can be given a physical significance as a smallest scale in space and time. We shall discover that mean values of RealNSE-solutions, or *mean-value outputs*, show little dependence on the mesh size h, and we shall also uncover (some of) the mathematical rationale behind this remarkable feature. This opens the possibility of accurately simulating real phenomena using a coarser mesh size than the physical smallest scale, which is like computing with say 10^6 "super-particles" instead of 10^{24} "real particles", thus making an impossible simulation possible.

4.6 Boltzmann's Equation

Boltzmann starts from a *molecular particle model* of a dilute gas as a very large collection of elastically colliding little spherical particles/molecules according to classical Newtonian mechanics. This model is formally reversible without effects of viscosity, simply because each elastic collision is reversible. From this particle model Boltzmann derives a continuum model from an assumption of *molecular chaos* requiring particles to have statistically independent velocities before collision, in the form of *Boltzmann's equation*:

$$\dot{f} + v \cdot \nabla_x f + F \cdot \nabla_v f = Q(f, f), \tag{4.8}$$

where $f(x, v, t)$ is the number of gas molecules at the position x moving with velocity v per volume $dxdv$, at time t, F is an applied force, and ∇_x is the gradient with respect to x, ∇_v the gradient with respect to v, and $Q(f, f)$ is Boltzmann's *collision operator* representing the rate of change of $f(x, v, t)$ due to (elastic) molecule collisions. Boltzmann's collision term has a certain

dissipative character, from which Boltzmann derived his famous *H-Theorem* stating that $\dot{H} \geq 0$, where

$$H(t) = \int f \log(f) dx dv$$

is Boltzmann's *H-function*. Irreversibility would then be signified by a strictly decreasing H-function, and thus $-H$ could be viewed as a strictly increasing entropy. Boltzmann's equation is deterministic, but it is derived from a statistical assumptiopn of *molecular chaos* requiring the velocities of two molecules about to collide to be statistically independent *before* collision, but not after. The assumption of molecular chaos is what gives the collision term its dissipative character with $H(t)$ strictly decreasing as the gas steadily moves towards its *equilibrium distribution* with minimal H and $Q = 0$.

The motivation of the assumption of molecular chaos is the weak point of Boltzmann's gas kinetics: Statistical independence before collision but not after, obviously introduces a direction of time by direct assumption. The main head-ache of Boltzmann was thus to motivate this assumption, in order not to simply assume what was to be proved, namely time-directionality. To do so he tried various options and finally seemed to converge to the idea that the probability of a macro-state should be related to the number of underlying micro-states, and thus the H-theorem would reflect a tendency of the gas molecules to move from a less probable to a more probable distributions, with the final equilibrium position as the most probable one. To count the number of micro-states underlying a certain macrostate requires (tricky) combinatorics, and this is what makes Boltzmann's statistical mechanics so difficult to understand (for most people). We will come back to this aspect in an account (and resolution) of *Gibb's paradox* exhibiting difficulties of combinatorics in gas kinetics.

We shall below recall that Boltzmann defines the entropy S of a certain macrostate as being proportional to $\log(W)$ where W is the number of corresponding microstates. Boltzmann thus plays with two different definitions of entropy, one statistical in terms of the number of microstates, W and one deterministic in terms of the H-function, which is very confusing to the non-specialist of statistical mechanics.

Did Boltzmann thereby resolve the enigma how irreversibility can arise in a formally reversible Newtonian model like a swarm of elastically colliding particles? Not really, because his basic roulette assumption, also referred to as *molecular chaos*, is asymmetric in time (two particles play roulette *before*

collision), and thus introduces viscosity by assumption. Boltzmann thus *assumed* what was to be proved, namely the occurence of effects of viscosity and time asymmetry, and therefore met strong opposition by in particular Loschmidt [40].

4.7 Euler's Equations from Boltzmann's

The Euler equations of fluid mechanics (4.1) can *formally* be derived from Boltzmann's equation of gas kinetics (4.8), by integration over the velocity variable v and defining with M the mass of a molecule,

$$\begin{aligned} \rho(x,t) &= M\int f(x,t,v)\,dv, \\ m(x,t) &= M\int f(x,t,v)v\,dv \\ e(x,t) &= \frac{M}{2}\int f(x,t,v)|v-u|^2\,dv, \end{aligned} \tag{4.9}$$

where as usual $u = m/\rho$. We note in particular that the internal (heat) energy e is defined as a form of (small scale) kinetic energy measuring the standard deviation from the mean velocity u.

4.8 Navier-Stokes Equations

In the Navier-Stokes equations the momentum equation is augmented by a viscous term of the form

$$-\nabla\cdot(\nu\nabla u) - \nabla(\mu\nabla\cdot u), \tag{4.10}$$

where $\nu > 0$ is a *shear viscosity* coefficient and $\mu > 0$ a *bulk viscosity*. The equation for the heat energy is similarly augmented by a heat conduction term of the form $-\nabla\cdot(\kappa\nabla e)$ with $\kappa > 0$ a *heat conductivity*. The determination of correct values of these coefficients in turbulent flow is very complicated, or more precisely in practice impossible, because the coefficients are solution dependent. We stay away from this complications by assuming the coefficients to be *small* and we then effectively put them to zero in the Euler equations, just as Euler did. The mesh-independence of certain mean-value outputs then reflects that the mean-values are insenistive to the absolute size of viscosities and heat conductivity, as long as they are small.

Figure 4.1: The shock wave of a supersonic airplane made visible by condensation

4.9 Mathematical Literature on Compressible Flow

There is a vast literature on compressibe flow described by Euler's equations [37], but basic questions about existence and wellposedness of solutions are left without answers. The difficulty is that solutions of the Euler equations initiated from smooth initial data, which do exist as unique smooth solutions for some period of time, develop shocks/turbulence and thus can continue only as non-smooth weak solutions with possible lack of physical meaning and uniqueness. To secure physical meaning entropy conditions of different forms are used, but it is now known which conditions will suffice to secure weak solutions to be physical.

With sufficiently strong non-linear viscosities global existence of unique smooth solutions of Navier-Stokes equations can formally be proved by standard mathematical techniques, however without any assessment of wellposedness and physical meaning. For constant viscosities results are lacking. The Navier-Stokes equations are thus as inaccessible to formal mathematical anal-

ysis as the Euler equations.

What remains is computation and we thus make a restart with RealNSE for Euler's equations and we do answer questions about existence and uniqueness related to wellposedness.

One condition proposed in the literature is *maximal dissipation of kinetic energy* [38], but its is not clear that physics follows this principle. In RealNSE as best possible satisfaction of Euler's equations, it is rather a principle of minimal dissipation of kinetic energy as the smallest possible price to pay for non-smoothness.

> A theory is the more impressive the greater the simplicity of its premises, the more different kinds of things it relates, and the more extended its area of applicability. Therefore the deep impression that classical thermodynamics made upon me. It is the only physical theory of universal content which I am convinced will never be overthrown, within the framework of applicability of its basic concepts.(Einstein)

> Nothing in life is certain except death, taxes and the second law of thermodynamics. All three are processes in which useful or accessible forms of some quantity, such as energy or money, are transformed into useless, inaccessible forms of the same quantity. That is not to say that these three processes don't have fringe benefits: taxes pay for roads and schools; the second law of thermodynamics drives cars, computers and metabolism; and death, at the very least, opens up tenured faculty positions. (Seth Lloyd, in *Nature*, 2004)

Chapter 5

Viscosity Solutions to 1d Euler

> The total energy of the universe is constant; the total entropy is continually increasing. (Rudolf Clausius 1865)
>
> You believe in the God who plays dice, and I in complete law and order in a world which objectively exists, and which I, in a wild speculative way, am tryin to capture. Even the great initial success of Quantum Theory does not make me believe in the fundamental dice-game, although I am well aware that younger collegues interpret this as a consequence of senility. No doubt the day will come when we will see those instictive attitude was the correct one. Some physicists. among them myself, cannot believe that we must abandon, actually and forever, the idea of direct representation of physical reality in space and time; or that we must accept then the view that events in nature are analogous to a game of chance...In any case I am convinced that *He* does not throw dice. (Einstein)

5.1 Regularisation of Hamiltonian Systems

We present in this chapter a short-cut to the computational foundation of thermodynamics in the setting of the Euler equations in one space dimension (1d). In particular, we motivate a 2nd Law, which we will below show to be satisfied by RealNSE in the full 3d case.

We use the standard approach of *viscous regularisation* motivated by the fact that the Euler equations do not admit exact pointwise solutions, because of the inevitable appearance of turbulence/shocks. We will view RealNSE solutions as specific regularised solutions, which are computed and

thus exist and can be inspected. We shall below in more detail investigate the precise form of the regularisation in RealNSE, and discover that it has interesting features, not only from mathematical and computational, but also from physical point of view.

The basic idea in viscous regularisation of a Hamiltonian system described by an equation $H(u) = 0$ over a domain $\Omega \times [0, 1]$ in space-time, such as the Euler equations, is to perturb the equation $H(u) = 0$ into

$$H(u_\nu) = \nu\Delta u_\nu \quad \text{in } \Omega \times [0, 1],$$

where $\nu > 0$ is a small parameter representing a small (shear) viscosity, and the Laplacian has a regularising or smoothing effect on the solution.

The presence of the Laplacian (or possibly a higher order regularising differential operator such as the biLaplacian), makes it possible in some cases to prove the existence of a pointwise solution u_ν to the regularised problem, a *viscosity solution*, by standard techniques of mathematical analysis involving Sobolev and Gronwall inequalities, while the original Hamiltonian system is inaccessible to analysis because the equation $H(u) = 0$ lacks pointwise solutions. For the regularised compressible Euler equations, technical difficulties have hitherto prevented a full proof of existence of pointwise solutions. But this is not crucial for the computational foundation since this is based on computed RealNSE-solutions with specific residual-based regularisation and not viscosity solutions, and computed solutions do exist and can be inspected. We here use viscosity solutions to formally illustrate basic features of RealNSE-solutions such as the 2nd Law, which we then verify directly for RealNSE-solutions.

If the regularised solution u_ν is *smooth* in the sense that Δu_ν is of moderates size, then the perturbation $\nu\Delta u_\nu$ will be small, because ν is small, and thus the regularised solution u_ν will be an approximate pointwise solution of the Hamiltonian system with the Hamiltonian residual $H(u_\nu)$ being small in a pointwise sense. In this case the the perturbation can be said to be *regular*, and is inessential in the sense that already the original problem has a pointwise solution and regularisation is not needed.

However, we consider problems where the Hamiltonian residual $H(u_\nu)$ is not small (in fact large) in regions with shocks/turbulence, while $H(u_\nu)$ remains small in a weak norm, so that $\hat{u}_\nu$ still is an approximate solution to the Hamiltonian system, but now only in a weak (but not pointwise) sense. The viscous term $\nu\Delta u$ will thus be pointwise large, which is reflected by the

fact that the total dissipation

$$D(u_\nu) = \int_\Omega \nu |\nabla u_\nu|^2 dx$$

is not small (of moderate size). In particular, the regularised solution u_ν is *non-smooth* in the sense that $|\nabla u_\nu|$ and $|\Delta u_\nu|$ are locally very large (of size ν^{-1} and ν^{-2} at shocks and of size $\nu^{-1/2}$ and $\nu^{-3/2}$ in turbulent regions, respectively). In this case the perturbation is *singular*, and is essential in the sense that only the regularised problem has pointwise solutions. We thus consider a Hamiltonian system with singular perturbation.

We understand that $D(u_\nu)$ results from multiplication of $-\nu\Delta u_\nu$ by u_ν and integration (by parts) over Ω. Typically, $D(u_\nu)$ will have a positive limit as ν tends to zero, which expresses an independence of the specific form of the regularisation, that is the specific value of ν, with always the term $-\nu\Delta u_\nu$ balancing the non-zero Hamiltonian residual $H(u_\nu)$, with Δu_ν getting larger as ν gets smaller.

We will thus view the appearance of the regularisation term as a mathematical formality and we do not seek to connect it to any physical "shear viscosity". This is because the appearance of "shear viscosity" in Hamiltonian systems without viscosity, such as the Euler equations, represents the main mystery of the classical 2nd Law. We thus do not accept the common argument that "there is always some form of (shear) viscosity, which we can model by a Laplacian". The key question is from where such a viscosity comes in a inviscid flow.

We shall see that RealNSE offers a new answer to this key question, where the residual regularisation appears as a loss of kinetic energy because the momentum equation cannot be satisfied pointwise, and not as any form of classical (shear) viscosity. The loss of kinetic energy (which is transformed into heat energy) can be viewed as a "fine" to be paid because the law $H(u) = 0$ is heavily violated pointwise. The fine can take many forms, since there are many possible forms of regularisation, while the violation essentially remains the same. We shall see that RealNSE penalises a large residual $H(\hat{u})$, while classical viscous regularisation penalises all large derivates, not only the particular combination of the residual.

RealNSE thus has "fine-tuned" penalisation with the fine being as close as possible to the violation, like a penicillin with narrow spectrum killing only microbes producing the symptom, which suggests that RealNSE can be given a physical significance. On the ohter hand, classical viscous regularisation, is

more like a broad band penicillin killing both microbes and healthy bacteria, and its physical significance has remained a mystery.

To sum up, we start from a Hamiltonian system without pointwise solutions (the Euler equations), which we replace by a regularised system with pointwise solutions (by viscous regularisation or RealNSE), which can be viewed as approximate solutions to the original system. We find that certain mean-values of the regularised solutions show little dependence on the specific form of the regularisation (the viscosity or the mesh size), and thus can be viewed as stable outputs of approximate solutions to the original system. We first carry out the argument for viscous regularisation and then return below to the real case of RealNSE regularisation.

5.2 1d Euler

We consider an inviscid perfect gas enclosed in a tube represented by the interval $\Omega = (0,1)$ in space over a time interval $I = (0,1]$ and we assume that $f = 0$ and $g = 0$. The 1d Euler equations expressing the 1st Law as conservation of mass, momentum and internal energy, formally take the form: Find $\hat{u} \equiv (\rho, m, e)$ such that with $v' = \frac{\partial v}{\partial x}$

$$\begin{aligned} R_\rho(\hat{u}) \equiv \dot{\rho} + (\rho u)' &= 0 \quad \text{in } Q, \\ R_m(\hat{u}) \equiv \dot{m} + (mu + p)' &= 0 \quad \text{in } Q, \\ R_e(\hat{u}) \equiv \dot{e} + (eu)' + pu' &= 0 \quad \text{in } Q, \\ u(0,t) = u(1,t) &= 0 \quad t \in I, \\ \hat{u}(\cdot, 0) &= \hat{u}^0 \quad \text{in } \Omega, \end{aligned} \tag{5.1}$$

where $p = \gamma e$ with $\gamma > 0$ and $u = \frac{m}{\rho}$, or in short form

$$\begin{aligned} R(\hat{u}) &= 0 \quad \text{in } Q, \\ u(0,t) = u(1,t) &= 0 \quad t \in I, \\ \hat{u}(\cdot, 0) &= \hat{u}^0 \quad \text{in } \Omega, \end{aligned} \tag{5.2}$$

where $R = (R_\rho, R_m, R_e)$.

5.3 Formal Reversiblity

The Euler equations (5.1) without regularization are formally *reversible*: Changing the sign of the velocity u and the direction of time (the sign of the

time-derivative $\dot{u}$), the Euler equations obviously remain unchanged. This means that if $\hat{u}(t)$ is a solution to the Euler equations in forward time on $[0, T]$ taking the initial value $\hat{u}(0)$ to the final value $\hat{u}(T)$, we obtain a solution in backward time taking $\hat{u}(T)$ back to $\hat{u}(0)$ by reversing the velocity at time $\bar{t}$. Of course we can view this solution as proceeding in forward time by just continuing counting time forward after the velocity reversal.

We conclude that if the Euler equations have a pointwise solution then it can be turned into a perpetuum mobile running for ever without consuming any energy, for ever bouncing back and forth by repeated reversal of the velocity at two given time instances.

5.4 Factual Irreversibility

The trouble with the above argument is that the Euler equations lack pointwise solutions and thus the implication is empty. In contrast viscosity solutions to the regularized Euler equations exist, but these solutions are turbulent with substantial turbulent dissipation and thus are irreversible. Therefore a perpetuum mobile is impossible.

We sum up: The exact solutions which would have been reversible if they had existed, do not exist. The viscosity solutions which do exist, are not reversible. This is the main lesson of this book, and resolves the main open problem of classical thermodynamics: *Loschmidt's paradox* asking how irreversibility can arise in a reversible system.

5.5 Energy Estimates for Viscosity Solutions

We shall now prove that a viscosity solutions of the regularized 1d Euler equations (5.1) is a *dissipative weak solution* of the Euler equations in the sense that its Euler residual is small in a weak sense and it satisfies a 2nd Law expressing an irreversible transfer from kinetic to heat energy in the form of turbulent/shock dissipation. In short we prove that viscosity solutions are dissipative weak solutions of the Euler equations.

We thus consider the following regularized version of (5.1): Find $\hat{u}_{\nu,\mu} \equiv \hat{u} = (\rho, m, e)$ such that

$$\begin{aligned} \dot{\rho} + (\rho u)' &= 0 \quad \text{in } Q, \\ \dot{m} + (mu + p)' &= (\nu u')' + (\mu p u')' \quad \text{in } Q, \\ \dot{e} + (eu)' + pu' &= \nu (u')^2 \quad \text{in } Q, \\ u(0,t) = u(1,t) &= 0 \quad t \in I, \\ \hat{u}(\cdot, 0) &= \hat{u}^0 \quad \text{in } \Omega, \end{aligned} \tag{5.3}$$

where $p = \gamma e$, and $\nu > 0$ and $\mu \geq 0$ are small parameters with ν representing *shear viscosity* and μ a form of *bulk viscosity* with $\mu = 0$ if $u' < 0$. For simplicity, we here suppress the subindices ν and μ. We here use the balance equation for the internal energy e, modified to account for the contribution to the internal energy from shear viscosity, but without contribution from bulk viscosity, which we consider as a penalty. We observe that only the velocity u is subject to regularization, which gives (as we will see below) the momentum equation a different quality than the balance equations for mass and internal energy, both involving u as a coefficient.

We shall see that it is natural to choose the regularization parameter ν much smaller than μ, and thus the main effect of the regularization comes from the bulk viscosity μ, rather than from the usual shear viscosity ν. We shall see that the bulk viscosity prevents fluid particles from colliding, or more precisely, prevents faster fluid particles to overtake slower particles (along the same streamline), which thus is the main effect of the regularization and not shear viscosity.

We shall now prove that $\hat{u} = \hat{u}_{\nu,\mu}$ satisfies

$$\|R_m(\hat{u})\|_{-1} \leq \frac{\sqrt{\nu}}{\sqrt{\mu}} + \sqrt{\mu}, \tag{5.4}$$

where $\|\cdot\|_{-1}$ denotes the $L_2(I; H^{-1}(J))$-norm, while obviously $R_\rho(\hat{u}) = 0$ and $R_e(\hat{u}) \geq$ in a pointwise sense in $\Omega \times I$. Further, we shall observe that $\hat{u}$ satisfies the following 2nd Law:

$$\dot{K} \leq W - D, \quad \dot{E} = -W + D,$$

where

$$K = \int_J k dx, \quad E = \int_J e dx, \quad W = \int_J pu' dx, \quad D = \int_J \nu (u')^2 \, dx > 0.$$

Choosing $\mu = \epsilon$ and $\nu = \epsilon^2$, we can assure that $\|R_m(\hat{u}_{\nu,\mu})\|_{-1} \leq 2\sqrt{\epsilon}$ for any positive ϵ. We shall prove the following result on the existence of *dissipative weak approximate solutions* to the 1d Euler equations:

Theorem 1 *A viscosity solution $\hat{u}$ of the regularized Euler equations (5.1) satisfies*

$$R_\rho(\hat{u}) = 0 \quad in\ \Omega \times I, \quad \|R_m(\hat{u})\|_{-1} \leq TOL, \quad R_e(\hat{u}) \geq 0 \quad in\ \Omega \times I,$$

where $TOL = \frac{\sqrt{\nu}}{\sqrt{\mu}} + \sqrt{\mu}$, together with the 2nd Law

$$\dot{K} \leq W - D, \quad \dot{E} = -W + D, \quad D > 0. \tag{5.5}$$

We understand that Theorem 1 states certain properties of the regularised solution $u_{\nu,\mu}$ in terms of its Euler residuals, without explicitly referring to the regularisation, where the 2nd Law compensates for the fact that the momentum residual $R_m(\hat{u})$ is only required to be small in a weak norm, and $R_e(\hat{u})$ is allowed to be pointwise positive. We note that by the 2nd Law (5.5) it follows that

$$\dot{K} + \dot{E} \leq 0 \tag{5.6}$$

stating that the integral (or totality) in space of the total energy ϵ cannot increase.

To make the notion of dissipative weak solution really useful, we have to connect it to *output uniqueness*. We will return to this basic aspect below in the context of RealNSE, using directly the properties of RealNSE without passing through Theorem 1. We can thus view Theorem 1 as a connection to a classical analytical technique of regularized solutions, which we will not pursue in detail, because what we can compute are RealNSE solutions, not classical regularized solutions, and because a RealNSE solution can be viewed as a (new) form of regularized solution.

Since the concept of weak solution can be viewed as expressing a form of approximate solution, with an exact solution being a (strong) pointwise solution, we can condense the notation to *dissipative weak solution*. In short, we will thus prove the existence of dissipative weak solutions to the Euler equations and below see that a RealNSE solution is a dissipative weak solution.

Proof of Theorem 1: The basic technical step is to multiply the momentum equation by u, omitting for simplicity the indices ν and μ, and use the mass balance equation in the form $\frac{u^2}{2}(\dot{\rho} + (\rho u)') = 0$, to get

$$\dot{k} + (ku)' + p'u - \mu(pu')'u - \nu u''u = 0. \tag{5.7}$$

By integration in space it follows that $\dot{K} \leq W - D$, and similarly it follows that $\dot{E} = -W + D$ from the equation for e, which proves the 2nd Law. Adding next (5.7) to the equation for the internal energy e and integrating in space, gives

$$\dot{K} + \dot{E} + \int_0^1 \mu p (u')^2 \, dx = 0,$$

since

$$\int_0^1 (p'u + pu')dx = \int_0^1 (pu)'dx = 0,$$

and thus after integration in time

$$K(1) + E(1) + \int_Q \mu p (u')^2 \, dxdt = K(0) + E(0). \tag{5.8}$$

We now need to show that $E(1) \geq 0$ (or more generally that $E(t) > 0$ for $t \in I$), and to this end we rewrite the equation for the internal energy as follows:

$$\frac{De}{Dt} + (\gamma + 1)eu' = \nu (u')^2,$$

where $\frac{De}{Dt} = \dot{e} + ue'$ is the material derivative of e following the fluid particles with velocity u. Assuming that $e(x, 0) > 0$ for $0 \leq x \leq 1$, it follows that $e(x, 1) > 0$ for $0 \leq x \leq 1$, and thus $E(1) > 0$. Assuming $K(0) + E(0) = 1$ the energy estimate (6.7) thus shows that

$$\int_Q \mu p (u')^2 \, dxdt \leq 1, \tag{5.9}$$

and also that $E(t) \leq 1$ for $t \in I$.

Next, integrating (5.7) in space and time gives

$$K(1) + \int_Q \nu (u')^2 dxdt = \int_Q pu' dxdt - \int_Q \mu p (u')^2 dxdt \leq \frac{1}{\mu} \int_Q p dxdt \leq \frac{1}{\mu},$$

where we used that $\int_Q p dxdt = \gamma \int_Q e dxdt \leq \int_I E(t)dt \leq 1$. It follows that

$$\int_Q \nu (u')^2 dxdt \leq \frac{1}{\mu}. \tag{5.10}$$

By standard estimation it follows from (5.9) and (5.10) that

$$\|R_m(\hat{u})\|_{-1} \leq \sqrt{\mu} + \frac{\sqrt{\nu}}{\sqrt{\mu}},$$

and the proof can be completed in an obvious fashion.

5.6 Irreversibility by the 2nd Law

The 2nd Law (5.5) states an irreversible transfer of kinetic energy to heat energy for in the presence of shocks with $D > 0$, which is the generic case. On the other hand, the sign of W is variable and thus the corresponding energy transfer may go in either direction.

5.7 Compression and Expansion

The 2nd Law (5.5) states that there is a transfer of kinetic energy to heat energy if $W < 0$, that is under compression with $u' < 0$, and a transfer from heat to kinetic energy if $W > 0$, that is under expansion with $u' > 0$. As we just remarked, there is a transfer from kinetic to heat energy for solutions with shocks with $D > 0$.

Returning to Joule's experiment, we see by the 2nd Law that contraction back to the original volume from the final rest state in the double volume, is impossible, because the only way the gas can be set into motion is by expansion.

Chapter 6

Viscosity Solutions to 3d Euler

> Everyone knows that heat can produce motion. That it possesses vast motive power no one can doubt, in these days when the steam engine is everywhere so well known. The study of these engines is of great interest, their importance is enormous, their use is continually increasing, and they seem desined to produce a great revolution in the civilised world. (Carnot [10] 1824).
>
> But maybe that is our mistake: maybe there are no particle positions and velocities, but only waves. It is just that we try to fit the waves to our preconceived ideas of positions and velocities. The resulting mismatch is the cause of the apparent unpredictability.(Stephen Hawking)
>
> What wanted to say was just this: In the present circumstances the only profession I would choose would be one where earning a living had nothing to do with the search for knowledge. (Einstein's last letter to Born Jan 17 1955 shortly before his death on the 18th of April, probably referring to Born's statistical interpretation of quantum mechanics).

6.1 3d Euler

We now show that the above result for the 1d Euler equations directly extends to 3d. We thus consider the 3d Euler equations for an inviscid perfect gas enclosed in a volume Ω in $\mathbb{R}^3$ with boundary Γ over a time interval $I = (0, 1]$,

assuming as above that the applied force $f = 0$: Find $\hat{u} = (\rho, m, e)$ depending on $(x, t) \in Q \equiv \Omega \times I$ such that

$$\begin{aligned} R_\rho(\hat{u}) \equiv \dot{\rho} + \nabla \cdot (\rho u) &= 0 \quad \text{in } Q, \\ R_m(\hat{u}) \equiv \dot{m} + \nabla \cdot (mu) + \nabla p &= 0 \quad \text{in } Q, \\ R_e(\hat{u}) \equiv \dot{e} + \nabla \cdot (eu) + p\nabla \cdot u &= 0 \quad \text{in } Q, \\ u \cdot n &= 0 \quad \text{on } \Gamma \times I \\ \hat{u}(\cdot, 0) &= \hat{u}^0 \quad \text{in } \Omega, \end{aligned} \tag{6.1}$$

where $u = \frac{m}{\rho}$ and $p = \gamma e$ with $\gamma > 0$.

6.2 Energy Estimates for Viscosity Solutions

We consider the following regularized version of (6.1): Find $\hat{u}_{\nu,\mu} \equiv \hat{u} = (\rho, m, e)$ such that

$$\begin{aligned} R_\rho(\hat{u}) &= 0 \quad \text{in } Q, \\ R_m(\hat{u}) &= \nabla \cdot (\nu \nabla u) + \nabla(\mu p \nabla \cdot u) \quad \text{in } Q, \\ R_e(\hat{u}) &= \nu |\nabla u|^2 \quad \text{in } Q, \\ u &= 0 \qquad \text{on } \Gamma \times I, \\ \hat{u}(\cdot, 0) &= \hat{u}^0 \quad \text{in } \Omega, \end{aligned} \tag{6.2}$$

where $\nu > 0$ is a shear viscocity and $\mu \geq 0$ a bulk viscosity with $\mu = 0$ if $\nabla \cdot u < 0$, and $|\nabla u|^2 = \sum_{i=1}^3 |\nabla u_i|^2$.

As already indicated, the existence of a pointwise solution $\hat{u}_{\nu,\mu}$ to the regularised problem is an open problem of mathematical analysis. However, we only use the regularised problem to formally illustrate basic properties of RealNSE-solutions, which we prove directly below.

We shall now prove that $\hat{u} = \hat{u}_{\nu,\mu}$ satisfies

$$\|R_m(\hat{u})\|_{-1} \leq \frac{\sqrt{\nu}}{\sqrt{\mu}} + \sqrt{\mu}, \tag{6.3}$$

where $\|\cdot\|_{-1}$ denotes the $L_2(I; H^{-1}(\Omega))$-norm, while we may assume that $R_\rho(\hat{u}) = 0$ and $R_e(\hat{u}) \geq 0$ in a pointwise sense in Q. We shall also find that $\hat{u}$ satisfies the following 2nd Law:

$$\dot{K} \leq W - D, \quad \dot{E} = -W + D,$$

where

$$K = \int_\Omega k\,dx, \quad E = \int_\Omega e\,dx, \quad W = \int_\Omega p\nabla\cdot u\,dx, \quad D = \int_\Omega \nu|\nabla u|^2\,dx.$$

Choosing $\mu = \epsilon$ and $\nu = \epsilon^2$, we can assure that $\|R_m(\hat{u}_{\nu,\mu})\|_{-1} \leq TOL$ for any positive tolerance TOL. We shall thus show the following formal result on the existence of *dissipative weak approximate solutions* to the 3d Euler equations:

Theorem 2 *A viscosity solution $\hat{u}$ of the regularized Euler equations (6.1) satisfies*

$$R_\rho(\hat{u}) = 0 \quad \text{in } \Omega\times I, \quad \|R_m(\hat{u})\|_{-1} \leq TOL, \quad R_e(\hat{u}) \geq 0 \quad \text{in } \Omega\times I,$$

where $TOL = \frac{\sqrt{\nu}}{\sqrt{\mu}} + \sqrt{\mu}$, together with the 2nd Law

$$\dot{K} \leq W - D, \quad \dot{E} = -W + D, \quad D > 0. \tag{6.4}$$

As above, we note that Theorem 1 states certain properties of the regularized solution $u_{\nu,\mu}$ in terms of its Euler residuals, without explicitely referring to the regularization, where the 2nd Law compensates for the fact that the momentum residual $R_m(\hat{u})$ is only required to be small in a weak norm, and $R_e(\hat{u})$ is allowed to be pointwise positive. We note that by the 2nd Law it follows that

$$\dot{K} + \dot{E} \leq 0 \tag{6.5}$$

stating that the integral (or totality) in space of the total energy ϵ cannot increase. We shall see below that a RealNSE solution is a dissipative weak approximate solution.

Proof of Theorem 2: The basic technical step is to multiply the momentum equation by u, and use the mass balance equation in the form $\frac{|u|^2}{2}(\dot{\rho} + \nabla\cdot(\rho u) = 0$, to get

$$\dot{k} + \nabla\cdot(ku) + \nabla p\cdot u - \nabla(\mu p\nabla\cdot u)\cdot u + \nabla\cdot(\nu\nabla u)\cdot u = 0. \tag{6.6}$$

By integration in space it follows that $\dot{K} \leq W - D$, and similarly it follows that $\dot{E} = -W + D$ from the equation for e, which proves the 2nd Law.

Adding next (6.6) to the equation for the internal energy e and integrating in space, gives

$$\dot{K} + \dot{E} + \int_\Omega \mu p (\nabla \cdot u)^2 \, dx = 0,$$

since

$$\int_\Omega (\nabla p \cdot u + p \nabla \cdot u) dx = \int_\Omega \nabla \cdot (pu) dx = 0,$$

and thus after integration in time

$$K(1) + E(1) + \int_Q \mu p (\nabla \cdot u)^2 \, dxdt = K(0) + E(0). \tag{6.7}$$

We now need to show that $E(1) \geq 0$ (or more generally that $E(t) > 0$ for $t \in I$), and to this end we rewrite the equation for the internal energy as follows:

$$\frac{De}{Dt} + (\gamma + 1) e \nabla \cdot u = \nu |\nabla u|^2,$$

where $\frac{De}{Dt} = \dot{e} + u \cdot \nabla e$ is the material derivative of e following the fluid particles with velocity u. Assuming that $e(x, 0) > 0$ for $x \in \Omega$, it follows that $e(x, 1) > 0$ for $x \in \Omega$, and thus $E(1) > 0$. Assuming $K(0) + E(0) = 1$ the energy estimate (6.7) thus shows that

$$\int_Q \mu p (\nabla \cdot u)^2 \, dxdt \leq 1, \tag{6.8}$$

and also that $E(t) \leq 1$ for $t \in I$.

Next, integrating (6.6) in space and time gives

$$K(1) + \int_Q \nu |\nabla u|^2 dxdt = \int_Q p \nabla \cdot u dxdt - \int_Q \mu p (\nabla \cdot u)^2 dxdt \leq \frac{1}{\mu} \int_Q p dxdt \leq \frac{1}{\mu},$$

where we used that $\int_Q p dxdt = \gamma \int_Q e dxdt \leq \int_I E(t) dt \leq 1$. It follows that

$$\int_Q \nu |\nabla u|^2 dxdt \leq \frac{1}{\mu}. \tag{6.9}$$

By standard estimation it follows from (6.8) and (6.9) that

$$\|R_m(\hat{u})\|_{-1} \leq \sqrt{\mu} + \frac{\sqrt{\nu}}{\sqrt{\mu}},$$

and the proof can be completed in an obvious fashion.

6.3 Irreversibility by the 2nd Law

The 2nd Law (6.4) states an irreversible transfer of kinetic energy to heat energy in the presence of shocks/turbulence with $D > 0$, which is the generic case. On the other hand, the sign of W is variable and thus the corresponding energy transfer may go in either direction.

6.4 Compression and Expansion

The 2nd Law (6.4) states that there is a transfer of kinetic energy to heat energy if $W < 0$, that is under compression with $\nabla \cdot u < 0$, and a transfer from heat to kinetic energy if $W > 0$, that is under expansion with $\nabla \cdot u > 0$.

Returning to Joule's experiment, we see by the 2nd Law that contraction back to the original volume from the final rest state in the double volume, is impossible, because the only way the gas can be set into motion is by expansion.

6.5 A 2nd Law witout Entropy

We note that the 2nd Law (6.4) is expressed in terms of the kinetic energy K, the heat energy E and the work W, and does not involve any concept of entropy S. This relieves us from the task of finding a physical significance of S and a physical justification of a classical 2nd Law of the form $dS \geq 0$. We thus circumvent the main difficulty of classical thermodynamics based on statistical mechanics, while we reach the same goal as statistical mechanics of explaining irreversibility in formally reversible Newtonian mechanics.

Note that since the new 2nd Law is a consequence of the 1st Law and RealNSE computation, we can "forget" the 2nd Law: It is automatically satisfied without special attention. This is like "forgetting" to keep the balance while walking, because is automatically maintained without conscious attention.

Chapter 7

RealNSE

> The 2nd Law cannot be derived from purely mechanical laws. It carries the stamp of the essentially statistical nature of heat. (Bergmann [4])
>
> Therefore I feel that the Heisenberg-Bohr (Copenhagen) statistical interpretation of quantum mechanics is dead. (Zeh [51])
>
> If a scientist says that something is possible he is almost certainly right, but if he says that it is impossible he is probably wrong. (Arthur C. Clarke)

7.1 Introduction

We refer to [23] for a detailed presentation of RealNSE for the incompressible Euler equations. The extension to the compressible Euler equations has the principal form: Find $\hat{u} \in V_h$ such that

$$((R(\hat{u}), \hat{v})) + ((hR(\hat{u}), R'(\hat{u}, \hat{v}))) = 0 \quad \text{for } \hat{v} \in V_h \tag{7.1}$$

where V_h is a space-time finite element space on a mesh with mesh size h, $((\cdot, \cdot))$ denotes space-time L_2 scalar products, and $R'(\hat{u}, \hat{v})$ is a linearization of the Euler residual $R(\hat{u})$ at $\hat{u}$ such that $R'(\hat{u}, \hat{u}) = R(\hat{u})$, which leads to residual least squares stabilization through the positive penalty term $((hR(\hat{u}), R(\hat{u}))$ obtained choosing $\hat{v} = \hat{u}$.

In the actual implementation of RealNSE on cG(1)cG(1)-form stated below, the stabilisation has a reduced form involving only some of the terms

summing to the residual. The rationale is that the stabilisation has an effect when the residual is large pointwise, and then stabilising one term of the residual suffices. A residual-based *shock-capturing* stabilisation with viscosity coefficient $\sim h^2|R(\hat{u})|$ is also used, which eliminates (small) oscillations at shocks, but shock-capturing alone is not sufficient.

The 2nd Law satisfied by RealNSE shows that the stabilisation effectively concerns one term of the momentum equation, and not the mass and energy equations. The motivation is that since the momentum equation will not be pointwise (strongly) small, only weakly small, a stabilisation is required because the the balance of kinetic energy results from multiplication of the momentum equation by the velocity and this operation is not stable under weak convergence to zero of the momentum residual. On the other hand, the mass and energy equations are not similarly multiplied by density and energy, and thus do not need (the same form) of stabilization.

7.2 RealNSE in cG(1)cg(1) Form

RealNSE in cG(1)cG(1)-form for the Euler equations (6.1) is a time-stepping method defined by find $\hat{u} = (\rho, m, e) \in V_h$ such that for all $(\bar{\rho}, \bar{u}, \bar{e}) \in W_h$

$$\begin{aligned} ((R_\rho(\hat{u}), \bar{\rho})) + ((\delta u \cdot \nabla\rho, u \cdot \nabla\bar{\rho})) &= 0, \\ ((R_m(\hat{u}), \bar{u})) + ((\delta\rho u \cdot \nabla u, u \cdot \nabla\bar{u})) &= 0, \\ ((R_e(\hat{u}), \bar{e})) + ((\delta u \cdot \nabla e, u \cdot \nabla\bar{e})) &= ((d_h, \bar{e})), \end{aligned} \tag{7.2}$$

where

$$d_h = \sum_{i=1}^{3} \delta\rho(u \cdot \nabla u_i)^2, \tag{7.3}$$

and V_h is a trial space of continuous piecewise linear functions on a space-time mesh of size h satisfying the initial condition $\hat{u}(0) = \hat{u}^0$ with $u \in V_h$ defined by nodal interpolation of $\frac{m}{\rho}$, and W_h is a corresponding test space of function which are continuous piecewise linear in space and piecewise constant in time, all functions satisfying the boundary condition $u \cdot n = 0$ at the nodes on Γ. The space-time mesh is organised into space-time slabs between discrete time levels, and the velocity in the stabilisation terms is averaged over each time step. Further, $((\cdot, \cdot))$ denotes relevant $L_2(Q)$ scalar products. Finally, the least squares stabilisation weight $\delta = \frac{ch}{|u|}$ with $c \approx 0.5$, and *shock-capturing viscosity* with viscosity coffecient $\nu_i \sim h^2|R_i(\hat{u})|^2$, $i = \rho, m, e$, is also added

to each equation separately, which eliminates the small oscillations occuring at shocks with only least squares stabilisation. For small densities (almost vacuum), the velocity is computed by $u = \frac{m}{\rho+\epsilon}$ with $\epsilon > 0$ suitably small.

RealNSE (7.2) combines a weak satisfaction of the Euler equations with in particular a weighted least squares control of (a part of) the momentum residual $R_m(\hat{u})$ and represents a midway between the Scylla of weak solution and Carybdis of least squares strong solution.

Including all terms of the residual in the stabilisation as indicated in (7.1) improves consistency and thus may improve accuracy. Because test functions are piecewise constant in time the time derivative term will be missing in the residual stabilisation, however without much degrading accuracy in the presence of turbulence and shocks.

The form of the stabilisation terms in the density and energy equations secures exact global conservation since the stabilisation terms vanish with $\bar{\rho} = \bar{e} \equiv 1$. Notice that choosing $\bar{\rho} = \rho$ (mean-value over time step) gives a bound on $\int_Q \delta(u \cdot \nabla\rho)^2 dxdt$ in terms of $\int_Q \rho^2 \nabla \cdot u dxdt$, with a similar control of e.

Notice that RealNSE as expressed in (7.2) has a remarkable simplicity, as compared to finite difference methods based on diagonalization of the full system together with Riemann solvers, and also compared to stabilized finite element methods using diagonalization of the full linearized operator. In (7.2) each scalar convection equation is stabilized separately without diagonalization. In particular, the net numerical dissipation d_h has a contribution from each separate momentum/velocity component, but there is no net numerical dissipation in mass and internal energy.

7.3 The 2nd Law for RealNSE

Choosing $\bar{u}$ in the momentum equation as the time average of u over the time step, and subtracting the mass equation with $\bar{\rho} = I_h(\frac{|u|^2}{2})$, where $I_h(\frac{|u|^2}{2})$ is a nodal interpolant of $\frac{|u|^2}{2}$, we obtain

$$\dot{K} = W - D_h, \tag{7.4}$$

where

$$D_h = \int_Q d_h \, dxdt, \tag{7.5}$$

modulo the additive term

$$I = |((R_\rho, \frac{|u|^2}{2} - I_h(\frac{|u|^2}{2})))|$$

which by super-approximation as in [23] can be estimated as follows,

$$I \leq C\|h^2 R_\rho(\hat{u})|\nabla u|^2\|_0,$$

where $\|\cdot\|_0$ is the $L_2(Q)$-norm and $C \sim 1$ is an interpolation constant. Assuming $|R_\rho(\hat{u})| \sim h^{-1/2}$ and $|\nabla u| \sim h^{-1/2}$, we obtain $I \sim \sqrt{h}$, indicating that I is a small perturbation, which in computation can be checked a posteriori. Finally choosing in the equation for internal energy $\bar{e} = 1$, we obtain

$$\dot{E} = -W + D_h,$$

and we thus obtain the following 2nd Law for RealNSE (modulo a $\sqrt{h}$ correction)

$$\dot{K} = W - D_h, \quad \dot{E} = -W + D_h. \tag{7.6}$$

For solutions with turbulence/shocks, $D_h >> 0$ expressing a substantial irreversible transfer of kinetic energy into heat energy, just as above for regularized solutions. We note that in RealNSE only the momentum equation is subject to viscous regularization, since D_h expresses a penalty on the term $u\cdot\nabla u_i$ appearing in the momentum residual. A turbulent solution is identified by $D_h \sim 1$ under mesh refinement.

7.4 The Stabilization in RealNSE

We have seen that the stabilization in RealNSE is expressed by the dissipative term $D_h \sim 1$ which can be viewed as a weighted least squares control of the term $\rho u \cdot \nabla u_i$ in the momentum residual. The rationale is that least squares control of a part of a residual which is large, effectively may give control of the entire residual, and thus RealNSE gives a least squares control of the momentum residual. But the RealNSE stabilization does not correspond to an ad hoc viscosity, as in classical regularization, but to a form of penalty arising because Euler residuals of turbulent/shock solutions *cannot* be pointwise small.

In particular the dissipative mechanism of RealNSE does not correspond to a shear viscosity acting in all directions, as in standard ad hoc regularization, but rather to a form of bulk viscosity in the form of *streamline diffusion*

preventing fluid particles from colliding while allowing strong shear, connecting to the *streamline diffusion method* presented in [14].

Chapter 8

Output Wellposedness by Duality

> In love all the contradiction of existence merge themselves and are lost. Only in love are unity and duality not at variance. Love must be one and two at the same time. Only love is motion and rest in one. (Rabindranath Tagore, Literature Nobel Prize 1913)
>
> Those who have talked of "chance" are the inheritors of antique superstition and ignorance...whose minds have never been illuminated by a ray of scientific thought. (T. H. Huxley)

8.1 A Posteriori Error Estimation

Consider a mean-value output $M(\hat{u})$ in the form of a space-time integral

$$M(\hat{u}) = ((\hat{u}, \hat{\psi})) \tag{8.1}$$

defined by a smooth (positive) weight function $\hat{\psi}$ with $\|\psi\|_0 = 1$, where as above $\|\cdot\|_0$ is the $L_2(Q)$-norm. Let $\hat{u}$ and $\hat{w}$ be two RealNSE solutions on two meshes with joint maximal meshsize h. By the mean-value theorem their residual difference can be expressed as

$$R(\hat{u}) - R(\hat{w}) = R'(\hat{u}, \hat{w}) \cdot (\hat{u} - \hat{w}),$$

where $R'(\hat{u}, \hat{w})$ is a linearization of $R(\cdot)$. Letting $\hat{\varphi}$ be the solution of the dual linearized equation

$$R'^{\top}\hat{\varphi} = \hat{\psi}, \tag{8.2}$$

where $\top$ denotes transpose, we obtain the following basic *output error representation*:

$$M(\hat{u}) - M(\hat{w}) = ((\hat{u} - \hat{w}, R'^{\top}\hat{\varphi})) = ((R(\hat{u}) - R(\hat{w}), \hat{\varphi})). \tag{8.3}$$

We can thus estimate the output error in terms of the residuals as follows:

$$|M(\hat{u}) - M(\hat{w}| \leq S(\|R(\hat{u})\|_{-1} + (\|R(\hat{w})\|_{-1}) \tag{8.4}$$

or alteratively, using also *Galerkin orthogonality* as in [23]

$$|M(\hat{u}) - M(\hat{w}| \leq S(\|hR(\hat{u})\|_0 + (\|hR(\hat{w})\|_0), \tag{8.5}$$

where

$$S = S(\hat{u}, \hat{w}) = \|\hat{\varphi}\|_1 \tag{8.6}$$

with $\|\cdot\|_1$ the $H^1(Q)$-norm.

For a given output $M(\hat{u})$, we choose an error tolerance TOL and define a RealNSE-solution $\hat{u}$ to be *wellposed* up to the tolerance TOL, if

$$S\|hR(\hat{u})\|_0 \leq TOL/2, \tag{8.7}$$

where $S = S(\hat{u}, \hat{u})$. Given two wellposed RealNSE solutions $\hat{u}$ and $\hat{w}$, we may expect

$$|M(\hat{u}) - M(\hat{w}| \leq TOL, \tag{8.8}$$

up to a variation of the corresponding stability factors, which can be computed a posteriori. A solution which is not wellposed with respect to some tolerance of interest, is said to be *illposed*.

Turbulence is characterized by

$$D_h \sim \|\sqrt{h}R(\hat{u})\|_0 \sim 1 \tag{8.9}$$

under mesh refinement. We may thus expect an output $M(\hat{u})$ to be *wellposed* up to the tolerance TOL if

$$S(\hat{u}, \hat{u}) \lesssim \frac{TOL}{2\sqrt{h}}. \tag{8.10}$$

A wellposed output can be uniquely computed up to a tolerance TOL of interest, but an illposed cannot.

Computational results, some of which is presented below and more on the book web page [**?**], show that indeed $\|hR(\hat{u})\|_0 \sim \sqrt{h}$ conformiing (8.9), and that the corresponding stability factors $S(\hat{u}, \hat{u})$ for global mean-values such as drag, lift and total turbulent dissipation, can satisfy (8.10) for toleralnces TOL of interest. In short, global mean-value outputs can be wellposed, and thus represent stable computable emergent aspects of turbulent flow.

Chapter 9

Linearized Equations and Acoustics

> De Broglie, the creator of wave mechanics, accepted the results of quantum mechanics just as Schrödinger did, but not the statistical interpretation. (Born in the Born-Einstein Letters)

9.1 Linearization

Consider a solution $\hat{u} = (\rho, m, e)$ of the Euler equations:

$$\begin{aligned} \dot{\rho} + \nabla \cdot (\rho u) = \dot{\rho} + \nabla \cdot m &= 0 \quad \text{in } Q, \\ \dot{m} + \nabla \cdot (mu) + \gamma \nabla e &= f \quad \text{in } Q, \\ \dot{e} + \nabla \cdot (eu) + \gamma e \nabla \cdot u &= g \quad \text{in } Q, \\ u \cdot n &= 0 \quad \text{on } \Gamma \times I \\ \hat{u}(\cdot, 0) &= \hat{u}^0 \quad \text{in } \Omega, \end{aligned} \tag{9.1}$$

where $u = \frac{m}{\rho}$. The corresponding *linearized Euler equations*, linearized at $\hat{u}$, take the following form in $\underline{\hat{u}} = (\underline{\rho}, \underline{m}, \underline{e})$ representing a perturbation of $\hat{u}$ with corresponding perturbation of data, with $\underline{u}$ defined by $\underline{m} = \underline{\rho} u + \rho \underline{u}$:

$$\begin{aligned} \dot{\underline{\rho}} + \nabla \cdot (\underline{\rho} u) + \nabla \cdot (\rho \underline{u}) = \dot{\underline{\rho}} + \nabla \cdot \underline{m} &= 0 \quad \text{in } Q, \\ \dot{\underline{m}} + \nabla \cdot (\underline{m} u) + \nabla \cdot (m \underline{u}) + \gamma \nabla \underline{e} &= \underline{f} \quad \text{in } Q, \\ \dot{\underline{e}} + \nabla \cdot (\underline{e} u) + \nabla \cdot (e \underline{u}) + \gamma \underline{e} \nabla \cdot u + \gamma e \nabla \cdot \underline{u} &= \underline{g} \quad \text{in } Q, \\ \underline{u} \cdot n &= 0 \quad \text{on } \Gamma \times I, \\ \underline{\hat{u}}(\cdot, 0) &= \underline{\hat{u}}^0 \quad \text{in } \Omega, \end{aligned} \tag{9.2}$$

or alternatively with $Dw = \dot{w} + u \cdot \nabla w$ the u-convective derivative:

$$\begin{aligned} D\underline{\rho} + \underline{\rho}\nabla \cdot u + \nabla \cdot (\rho \underline{u}) &= 0 \quad \text{in } Q, \\ D\underline{m} + \underline{m}\nabla \cdot u + \nabla \cdot (m\underline{u}) + \gamma \nabla \underline{e} &= \underline{f} \quad \text{in } Q, \\ D\underline{e} + \underline{u} \cdot \nabla e + (\gamma + 1)\underline{e}\nabla \cdot u + (\gamma + 1)e\nabla \cdot \underline{u} &= \underline{g} \quad \text{in } Q, \\ \underline{u} \cdot n &= 0 \quad \text{on } \Gamma \times I \\ \underline{\hat{u}}(\cdot, 0) &= \underline{\hat{u}}^0 \quad \text{in } \Omega. \end{aligned} \tag{9.3}$$

This is a linear convection-reaction system with coefficients depending on the base flow $\hat{u}$ and the stability properties of this system govern the perturbation growth.

9.2 Wave Equation

Let $\hat{u}$ be a constant ground state with velocity $u = 0$ and temperature $\tau = 1$. If τ is not subject to perturbation, so that $\underline{e} = \underline{\rho}$, then (9.2) reduces to (leaving out initial and boundary conditions):

$$\begin{aligned} \dot{\underline{\rho}} + \nabla \cdot \underline{m} &= 0 \quad \text{in } Q, \\ \dot{\underline{m}} + \gamma \nabla \underline{\rho} &= \underline{f} \quad \text{in } Q, \end{aligned} \tag{9.4}$$

which leads to the *wave equation* for the density perturbation, assuming $\nabla \cdot \underline{f} = 0$:

$$\ddot{\underline{\rho}} - \gamma \Delta \underline{\rho} = 0 \quad \text{in } Q. \tag{9.5}$$

Small density-pressure variations at constant temperature around a constant ground state thus obeys the linear wave equation with wave speed $c = \sqrt{\gamma}$.

Allowing a non-zero velocity of the ground state, but still constant unit temperaure, the linearized equations reduce to (assuming $\underline{e} = 0$):

$$\begin{aligned} \dot{\underline{\rho}} + \nabla \cdot \underline{m} &= 0 \quad \text{in } Q, \\ \dot{\underline{m}} + 2\nabla \cdot (\underline{m}u) - \nabla \cdot (\underline{\rho} uu) + \gamma \nabla \underline{\rho} &= \underline{f} \quad \text{in } Q, \end{aligned} \tag{9.6}$$

which is a generalized wave equation with contributions from convection with velocity u.

9.3 Acoustics

Acoustics concerns propagation of (usually small) density-pressure variations in a fluid. Acoustics simulation can be based on (i) directly solving the Euler

equations for the full state (ground state plus perturbation), or (ii) solving the Euler equations for the ground state followed by solution of the linearized Euler equations for the perturbation with the ground state given. We just saw that the simplest model for acoustics is the wave equation (9.5) as a basic case of (b). In general, (ii) may be expected to give higher accuracy at the expense of solving both the Euler and linearized Euler equations.

The wave equation can be used for progagation of sound waves in in a fluid at rest, but for the generation of sound in e.g. human speech or musical instruments, fluid-structure interaction is used, which requires the Euler equations for the (usually turbulent) flow and an elasticity model for the structure (e.g, vocal chords).

9.4 Linearized Stability

The nature of the linearized system (9.2) depends on the ground state and ranges from its simplest incarnation in the form of the wave equation (9.5) for a constant ground state, to a highly complex problem for a turbulent ground state. Below we analyze the linearized problem for a shocks and rarefaction waves in a model case, and in [23] we discuss the case of turbulent incompressible flow. For now, we only observe that the equation for $\underline{\rho}$ contains the term $\underline{\rho}\nabla\cdot u$, and the same for $\underline{m}$ and $\underline{e}$, which indicates exponential perturbation growth along particle paths under compression with $\nabla\cdot u<0$, which occurs when a compression shock is forming.

Chapter 10

Dual Linearized Problem

> Those who do not understand the nature of sin and virtue are attached to duality; they wander around deluded. (Sri Guru Granth Sahib)

Formally multiplying the linearized equation (9.2) by the dual variable $\hat{\varphi} = (\rho_d, \varphi, e_d)$ and integrating by parts and varying $\underline{\hat{u}}$, we obtain the following dual problem

$$\begin{array}{rcl} -\dot{\rho}_d + \sum_j (u \cdot \nabla \varphi_j)\, u_j + \frac{e}{\rho} u \cdot \nabla e_d + \frac{\gamma}{\rho} u \cdot \nabla (e e_d) & = & \psi_\rho, \\ -\dot{\varphi} - u \cdot \nabla \varphi - \sum_i u_i \nabla \varphi_i - \nabla \rho_d - \frac{e}{\rho} \nabla e_d - \frac{\gamma}{\rho} \nabla (e e_d) & = & \psi, \\ -\dot{e}_d - u \cdot \nabla e_d + \gamma \nabla \cdot u e_d - \gamma \nabla \cdot \varphi & = & \psi_e, \end{array} \tag{10.1}$$

where the data $\hat{\psi} = (\psi_\rho, \psi, \psi_e)$ defines the output. We check by writing the Euler equations alternatively in the variables $\hat{u} = (\rho, u, e)$:

$$\begin{array}{rcl} \dot{\rho} + \nabla \cdot (\rho u) & = & 0, \\ \dot{\rho} u + \rho \dot{u} + \nabla \cdot (\rho u u) + \gamma \nabla e & = & f, \\ \dot{e} + \nabla \cdot (e u) + \gamma e \nabla \cdot u & = & g, \end{array} \tag{10.2}$$

with corresponding dual linearized problem in $\hat{\varphi} = (\rho_d, \varphi, e_d)$:

$$\begin{array}{rcl} -\dot{\rho}_d - u \cdot \nabla \rho_d - u \cdot \dot{\varphi} - \sum_i u_i u \cdot \nabla \varphi_i & = & \psi_\rho, \\ -\rho \dot{\varphi} - \rho u \cdot \nabla \varphi - \rho \nabla \rho_d - e \nabla e_d - \gamma \nabla (e e_d) - \rho \sum_i u_i \nabla \varphi_i & = & \psi, \\ -\dot{e}_d - u \cdot \nabla e_d + \gamma \nabla \cdot u e_d - \gamma \nabla \cdot \varphi & = & \psi_e, \end{array}$$

which by eliminating $\dot{\varphi}$ from the first equation using the second gives

$$\begin{array}{rcl} -\dot{\rho}_d + \sum_j (u \cdot \nabla \varphi_j)\, u_j + \frac{e}{\rho} u \cdot \nabla e_d + \frac{\gamma}{\rho} u \cdot \nabla (e e_d) & = & \psi_\rho, \\ -\dot{\varphi} - u \cdot \nabla \varphi - \sum_i u_i \nabla \varphi_i - \nabla \rho_d - \frac{e}{\rho} \nabla e_d - \frac{\gamma}{\rho} \nabla (e e_d) & = & \psi, \\ -\dot{e}_d - u \cdot \nabla e_d + \gamma \nabla \cdot u e_d - \gamma \nabla \cdot \varphi & = & \psi_e, \end{array}$$

which is the same as (10.1) with a properly modified right hand side: the elimination divides the second equation by ρ (so that $\psi \to \psi/\rho$), and substituting $\dot{\varphi}$ into the first equation absorbs the data contribution $\psi_\rho \to \psi_\rho - \frac{1}{\rho} u \cdot \psi$, while the three quadratic terms in u combine to the single term $\sum_j (u \cdot \nabla \varphi_j)\, u_j$.

The dual problem (10.1) is solved backward in time on $[0, T]$ with e.g. $\hat{\varphi}(\cdot, T) = 0$, for simplicity with stabilization by artificial diffusion of size h in each equation instead of least squares stabilization. The crucial stability factor is defined by $S = \|\varphi\|_{H^1(Q)}/\|\psi\|_{L_2(Q)}$, which bounds the error in the output $(\hat{u}, \psi)_Q$ by $S\|hR(\hat{u})\|_{L_2(Q)}$.

Chapter 11

Burgers Equation

> Some physicists. among them myself, cannot believe that we must abandon, actually and forever, the idea of direct representation of physical reality in space and time; or that we must accept then the view that events in nature are analogous to a game of chance. (Einstein 1954)

11.1 A Model of the Euler Equations

As an instructive model of the Euler equations exhibiting basic aspects of *shock waves* and *rarefaction waves*, we consider the following *scalar conservation law*, referred to as *Burgers equation*: Find the scalar function $u = u(x,t)$ such that

$$\begin{aligned} \dot{u} + (f(u))' &= 0 \quad \text{in } Q, \\ u(\cdot,0) &= u^0, \end{aligned} \tag{11.1}$$

where $f(u) = u^2/2$, $Q \equiv \mathbb{R} \times I$ with $I = (0,T]$, and we assume that the initial data $u^0(x)$ vanishes for large $|x|$.

Burgers equation takes the pointwise form $\dot{u} + uu' = 0$ for a differentiable pointwise solution u, which expresses that $u(x,t)$ is constant with values $u^0(\bar{x})$ along straight lines $x = st + \bar{x}$ with slope $s = u^0(\bar{x})$), that is, along *characteristics* defined by $\frac{dx}{dt} = u(x,t)$ with $x(0) = \bar{x}$.

If $u^0(x)$ is increasing with increasing x and is smooth, then there is a pointwise solution $u(t,x)$ for all time given by the simple recipe

$$u(x,t) = u^0(\bar{x}) \quad \text{for } x = u^0(\bar{x})t + \bar{x}. \tag{11.2}$$

However, if the initial data $u^0(x)$ somewhere is strictly decreasing, which of course will always be the case if $u^0(x)$ vanishes for large $|x|$, then characteristics will cross in finite time with different values and the solution formula gives conflicting function values, which can be interpreted as *breakdown* of the pointwise solution. The result is that there is no differentiable function $u(x,t)$ satisfying Burger's equation $\dot{u} + uu' = 0$ pointwise. We shall see that this corresponds to the occurence of *shocks*, which are represented by *discontinuous* functions, which satisfy the differential equation in a weak sense, and in a pointwise sense only away from discontinuities or jumps.

What to do with an equation without pointwise solution? Of course, we regularize and consider instead the *viscous/regularized Burgers equation*:

$$\begin{aligned} \dot{u} + uu' - \nu u'' &= 0 \quad \text{in } Q, \\ u(\cdot, 0) &= u^0, \end{aligned} \tag{11.3}$$

with $\nu > 0$ a small viscosity. This problem can be solved uniquely in a pointwise sense for all initial data, and as above the solution can be viewed as an approximate weak solution to the original inviscid Burgers equation satisfying a 2nd Law of the form

$$\dot{K}(u;t) = -D_\nu(u;t) \quad \text{for } t \in I, \tag{11.4}$$

where

$$K(u;t) = \int_{\mathbb{R}} \frac{u(x,t)^2}{2}\,dx, \quad D_\nu(u;t) = \int_{\mathbb{R}} \nu(u'(x,t))^2\,dx. \tag{11.5}$$

The 2nd Law follows by multiplication of the viscous Burgers' equation by u and integration (by parts) with respect to x.

To give a perspective we now briefly recall the basics of the mathematical theory for conservation laws developed in the 1950s motivated by the Euler equations of compressible flow, in the model setting of Burgers equation. The basic idea is to introduce the concept of *weak solution* allowing discontinuous solutions, and complement by a 2nd Law. We shall see that the 2nd Law singles out *physical shocks*, which are discontinuous weak solutions satisfying the 2nd Law, from *non-physical shocks* which are discontinuous weak solutions violating the 2nd Law.

We also present an alternative approach to single out physical shocks based on a stability analysis showing that a a physical shock is stable and represents a an observable physical phenomenon (like the "bang" from a

supersonic airplane), while a non-physical shock is unstable and thus does not represent any observable physical phenomenon.

Burgers equation is formally reversible: If $u(x,t)$ is a pointwise solution in forward time on $[0,T]$, so is $-u(x,T-t)$ in reverse time. Burgers equation thus is formally reversible system, but in reality is irreversible, as a consequence of the non-existence of stable pointwise solutions. We thus use Burgers equation to illustrate that a World governed by the formally reversible Euler equations, is an irreversible World, that is a world with an Arrow of time.

11.2 Weak Solutions

A possibly discontinuous function $u(x,t)$ is said to be a *weak solution to Burgers' equation* if

$$\int_{\mathbb{R}\times\mathbb{R}_+} (-u\dot{\varphi} - f(u)\varphi')dx\,dt - \int_{\mathbb{R}} u^0(x)\varphi(x,0)\,dx = 0 \tag{11.6}$$

for all differentiable test functions φ such that $\varphi(x,t)$ vanishes for large (x,t), assuming here $I = (0,\infty)$. This equation is obtained from (11.1) by multiplication by φ and integration by parts, shifting the derivatives onto φ, thus allowing u to be discontinuous.

11.3 The Rankine-Huginiot Condition

A discontinuous function $u(x,t)$ defined by $u(x,t) = u_+$ if $x > st$ and $u(x,t) = u_-$ if $x < st$, where u_+ and u_- are two constant states and s is a constant, corresponding to a discontinuity propagating with speed s, is a weak solution to Burgers' equation if the shock speed satisfies the *Rankine-Hugoniot condition*

$$s = \frac{[f(u)]}{[u]}, \tag{11.7}$$

where $[u] = u_+ - u_-$ and $[f(u)] = f(u_+) - f(u_-)$. With $f(u) = u^2/2$ as in Burgers' equation, we have

$$s = (u_+ + u_-)/2. \tag{11.8}$$

The Rankine-Hugoniot condition expresses the conservation law (Burgers' equation) in weak form for a piecewise constant discontinuous solution candidate u.

11.4 Rarefaction wave

The solution to Burgers equation with the *increasing* discontinuous initial data $u^0(x) = 0$ for $x < 0$, and $u^0(x) = 1$ for $x > 0$, is a *rarefaction wave* given by

$$\begin{array}{rcl} u(x,t) & = & 0 \quad \text{for} \quad x < 0, \\ u(x,t) & = & \frac{x}{t} \quad \text{for} \quad 0 \leq \frac{x}{t} \leq 1, \\ u(x,t) & = & 1 \quad \text{for} \quad 1 < \frac{x}{t}. \end{array} \tag{11.9}$$

This is a continuous function for $t > 0$ which satisfies (11.1) pointwise for $t > 0$ off the lines $x = 0$ and $x = t$ and can be viewed as a pointwise solution (since it is continuous and piecewise differentiable). In a rarefaction wave, an initial discontinuity separating two constant states develops into a continuous linear transition from one state to the other of width t in space, corresponding to "fan-like" level curves in space-time as shown in Fig. 11.1.

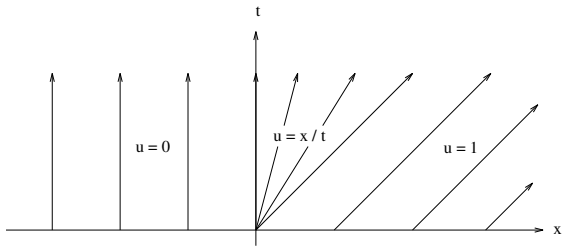

Figure 11.1: Characteristics of a rarefaction wave.

11.5 Shock

The solution with decreasing discontinuous initial data $u^0(x) = 1$ for $x < 0$, and $u^0(x) = 0$ for $x > 0$, is a discontinuous *shock wave* moving with speed $\frac{1}{2}$:

$$\begin{array}{rcll} u(x,t) & = & 1 & \text{for} \quad x < \frac{t}{2}, \\ u(x,t) & = & 0 & \text{for} \quad x > \frac{t}{2}, \end{array} \tag{11.10}$$

as shown in Fig 11.2. We shall motivate that this is a *physical shock* satifying a 2nd Law.

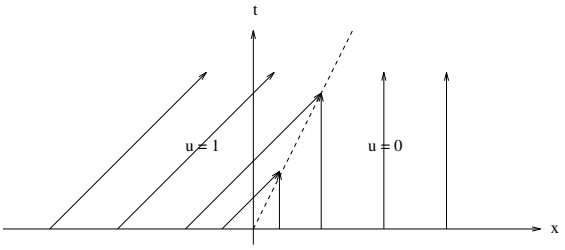

Figure 11.2: Characteristics of a shock

11.6 Weak solutions may be non-unique

The rarefaction wave initial data $u^0(x) = 0$ for $x < 0$ and $u^0(x) = 1$ for $x > 0$, also admits the alternative discontinuous weak solution

$$\begin{array}{rcll} u(x,t) & = & 0 & \text{for} \quad x < \frac{t}{2}, \\ u(x,t) & = & 1 & \text{for} \quad x > \frac{t}{2}, \end{array} \tag{11.11}$$

corresponding to a discontinuity $\{x,t) : x = st\}$ moving with speed $s = \frac{1}{2}$. This solution is obviously different from the rarefaction wave solution (11.9), which since it is a pointwise solution, also is a weak solution. Thus, we have in this case two different weak solutions, and thus we have an example of *non-uniqueness of weak solutions.* We shall see that the discontinuos solution (11.11) violates the 2nd Law and thus is a *non-physical shock solution.* The physical solution in this case is the rarefaction wave (which satisfies the 2nd Law with equality).

11.7 The 2nd Law for Burgers Equation

We now check if (11.11) satisfies the appropriate form of the 2nd Law (11.4) restricting space to $-1 \leq x \leq 1$ and time to $0 \leq t \leq 1$ assuming the boundary conditions $u(-1,t) = 0$ and $u(1,t) = 1$. In this setting, we obtain by multiplication of the viscous Burgers equation with u and integrating by parts and using the sign of the viscous term, the following form of the 2nd Law

$$-D_\nu(u;t) = \dot{K}(u;t) + \int_{-1}^{1} (\frac{u^3}{3})' = \dot{K}(u;t) + \frac{1}{3} \tag{11.12}$$

But for (11.11) we have $\dot{K} = -\frac{1}{2}\frac{d}{dt}\frac{t}{2} = -\frac{1}{4}$, which violates (11.12).

Changing to the boundary conditions to $u(-1,t) = 1$ and $u(1,t) = 0$, the 2nd Law changes to

$$-D_\nu(u;t) = \dot{K}(u;t) + \int_{-1}^{1} (\frac{u^3}{3})' = \dot{K}(u,t) - \frac{1}{3}, \tag{11.13}$$

which is satisfied by (11.10) since now $\dot{K} = \frac{1}{2}\frac{d}{dt}\frac{t}{2} = \frac{1}{4} < \frac{1}{3}$.

We conclude that a discontinuous function $u(x,t)$ with the constant states u_- for $x < st$ and u_+ for $x > st$ corresponds to a physical shock solution with shock speed $(u_- + u_+)/2$ if $u_- > u_+$, and to a non-physical shock if $u_- < u_+$.

We furher see that a shock dissipates substantial kinetic energy into heat since for a viscous profile of width ν joining two states u_- and u_+

$$D_\nu(u;t) \equiv \int_{\mathbb{R}} \nu(u')^2\,dx \approx (u_- - u_+)^2 \tag{11.14}$$

for small ν.

11.8 Burning Books

The 2nd Law states that the characteristics of a physical shock "converge into" the shock, corresponding to $u_- > u_+$. For the unphysical shock solutin corresponding to the rarefaction initial data with $u_- < u_+$, the characteristics appear to "emerge from" the discontinuity. The 2nd Law thus allows information (features of the solution) to be "destroyed" (in a shock with converging characteristics), but not "created out of nothing" (in an unphysical

rarefaction with diverging characteristics). This connects to the essence of irreversibility: Burning books can readily be done without any sophistication, while recovering the original text from the ashes is impossible.

11.9 Stability of a Rarefaction Wave

We shall now see that the 2nd Law can be replaced by a stability analysis in its main mission to distingush physical shocks from unphysical shocks. This reflects the fact that a stable process can be physically realized and observed, while an unstable process will have no permanence and thus will be very difficult (or impossible) to realize.

The stability of a solution $u(x,t)$ is governed by the linearized equation

$$\dot{w} + (uw)' = 0 \quad \text{in } \mathbb{R} \times \mathbb{R}_+ \tag{11.15}$$

where w represents a (small) perturbation (tending to zero for $|x|$ tending to infinity), and the solution u acts as a given coefficient. The growth properties of the solution w of the linearized equation determines the stability: If w grows quickly in time, then the solution u is unstable, and if w stays bounded, then u is stable. Of course, stability connects to finite precision: the level of the perturbation represents the precision.

We first consider the case of a rarefaction wave given by (11.9). Multiplying by w and integrating in space, we obtain by a simple computation using the fact that $u'(x,t) = 1/t$ for $0 \le x \le t$ and $u'(x,t) = 0$ else,

$$\frac{d}{dt}\int_{\mathbb{R}} w^2(x,t)\,dx + \int_0^t w^2(x,t)\frac{1}{t}\,dx = 0, \quad \text{for } t > 0,$$

from which follows that

$$\int_{\mathbb{R}} w^2(x,t)\,dx \le \int_{\mathbb{R}} w^2(x,0)\,dx \quad \text{for } t > 0. \tag{11.16}$$

This inequality shows that the L_2-norm in space of a perturbation from initial data does not grow with time, which proves stability of a rarefaction wave. Note that this argument builds on the fact that the rarefaction wave $u(x,t)$ is increasing in x so that u' is non-negative.

11.10 Stability of Shock

The stability proof used above to prove stability of a rarefaction wave, does not work the same way for a shock, since in this case $u(x,t)$ is decreasing with x. In fact a shock does not satisfy an L_2 stability estimate of the form (11.16). However, one can prove instead an L_1-bound of the form

$$\int_{\mathbb{R}} |w(x,t)|\,dx \leq \int_{\mathbb{R}} |w(x,0)|\,dx \quad \text{for } t > 0. \tag{11.17}$$

This follows by multiplying (11.15) by $sgn(w) = +1$ if $w > 0$ and -1 if $w < 0$, to get by integration by parts:

$$\frac{d}{dt}\int_{\mathbb{R}} |w(x,t)|\,dx + (u_- - u_+)|w(\frac{t}{2},t)| = 0, \tag{11.18}$$

and using the fact that for a shock $u_+ < u_-$. Moreover, we will below with a different type of stability estimate show that a shock is stable from computational RealNSE point of view, Thus, a shock is a stable phenomenon from both physical and computational point of view.

11.11 Instability of Non-Physical Shock

We saw above that the rarefaction wave solution is stable, and we now study the stability of the alternative weak solution (11.11). By the same argument as used to prove (11.18) we obtain

$$\frac{d}{dt}\int_{\mathbb{R}} |w(x,t)|\,dx = (u_+ - u_-)|w(\frac{t}{2},t)|, \tag{11.19}$$

where now $u_+ > u_-$. In this case, $\int_{\mathbb{R}} |w(x,t)|\,dx$ can grow arbitrarily fast, since the positive right hand side in (11.19) in no way can be controled by the left hand side. We thus conclude that an unphysical shock is unstable.

11.12 2nd Law = Stability + Finite Precision

We thus have two methods to single out physical shocks, one based on stability, and the other based on the 2nd Law. This shows that ultimately the 2nd Law expresses a stability condition, reflecting that Nature only can realize

phenomena which are properly stable, in its analog finite precision computation. We thus may view the 2nd Law to express a combination of stability and finite precision.

11.13 A Traffic Model

The equation (11.1) with $f(u) = u(1-u)$ models the flow of cars along a highway represented by the x-axis with $0 \leq u \leq 1$ the car density and $0 \leq v = (1-u) \leq 1$ the car velocity as a function of density: Sparse cars ($u \approx 0$) move fast ($v \approx 1$) and packed cars ($u = 1$) stand still ($v = 0$). The equation (11.1) then expresses conservation of mass in the sense that there are no side roads through which cars can enter or exit (and they cannot simply disappear into the sky).

We understand that if $u(x,t)$ is increasing in x so that the car density increases in the direction of motion, then the car velocity will be decreasing in the direction of motion which means that faster cars behind will approach slower cars ahead. But the x-axis is a one-lane street and does not allow a faster car to overtake a slower car, and so eventually faster cars will have to break in order to not run into slower cars ahead, that is, the law $v = (1-u)$ will have to be violated and thus the conservation law (11.1) cannot be satisfied pointwise. In the inviscid equation (11.1) this will correspond to the appearence of a shock. The corresponding regularized equation takes the form

$$\dot{u} + ((u(1-u))' - \nu u'' = 0,$$

which we formally can write as

$$\dot{u} + (uv)' = 0$$

with the modified velocity law

$$v = (1 - u - \frac{\nu}{u}u'),$$

with the effect that in the dangerous case of increasing density ($u' > 0$), faster cars will be slowed down more than slower cars and collisions from behind will thus be avoided.

In this model the shock corresponds to the well-known situation when an inexperienced driver suddenly steps on the brake to avoid collision into a

cue, which in the regularized problem corresponds to the smoother action of an experienced driver slowing down because the car density is larger ahead than behind.

11.14 Non-Existence Exact Euler Solutions

We have seen that the inviscid Burgers equation has discontinuous shock solutions, which can be viewed as weak solutions satisfying a 2nd Law. One can thus speak about a shock solution as an exact weak solution of Burgers equation satisfying a 2nd Law, and this solution is the limit of regularized solutions as the viscosity tends to zero. The goal of the classical mathematical analysis of conservation laws based on regularization, is to establish a corresponding result for the Euler equations: The goal is thus to prove the existence of a function satisfying the Euler equations in a weak sense together with a 2nd Law, as a limit of regularized solutions.

However, this goal has not been reached, and we have good reasons to believe that it cannot be reached. This is because of the appearence of turbulent solutions to the regularized Euler equations which do not seem have a limit in the form of a function. It is thus not meaningful to speak about exact solutions to the Euler equations, because such objects do not exist, but we may speak about regularized solutions because they do exist and we may view such solutions as approximate solutions to the Euler equations.

With this perspective it is reasonable to view a shock solution not as is usual as an exact weak solution to the Euler equations, but rather to view a viscous shock solution, an exact solution to the regularized Euler equations, as an approximate solution to the Euler equations. Thus only strong pointwise solutions could deserve the title of "exact solution"; a weak solution which is not a strong solution like a shock, could only be an approximate solution. This may seem to differ from the common way of looking at weak solutions of differential equations, as functions satisfying the differential equation "weakly exactly", but this is not completely natural since the notion of "weakly" has an element of "inexactly" built in. Only a strong pointwise solution can be an exact solution. I somebody offers you to buy an unknown painting by van Gogh, which you are only allowed to inspect from a distance of 10 meters, you may get suspicious and refrain from a deal.

Chapter 12

RealBurgers

> But maybe that is our mistake: maybe there are no particle positions and velocities, but only waves. It is just that we try to fit the waves to our preconceived ideas of positions and velocities. The resulting mismatch is the cause of the apparent unpredictability. (Stephen Hawking 1988)

12.1 Introduction

We will now consider RealNSE applied to Burgers' equation as a simple version of RealNSE. We recall that RealNSE is Galerkin's finite element method combined with a weighted least-squares control of the residual. RealNSE is based on piecewise polynomial approximation in space-time and offers spectrum of computational methods depending on the choice of the space-time mesh, as presented in detail in [14, 23]. RealNSE uses piecewise polynomials which are continuous in space and possibly discontinuous in time. These variants are referred to as cG(p)cG(q) or cG(p)dG(q) with cG(p) referring to continuous piecewise approximation of degree p in space, and cG(q)/dG(q) referring to continuous/discontinuous approxiamtion in time of degree q. RealNSE is *Eulerian* if the space-time mesh oriented along the space and time coordinate axis, is *Lagrangean* if the space-time mesh is oriented along particle paths in space-time, and *Arbitrary Lagrangean-Eulerian* or *ALE* if the space-time mesh is oriented according to some other feature such as space-time gradients of the solution. Lagrangean variants are also referred to as *characteristic Galerkin*, and Eulerian variants as *streamline diffusion methods*.

In all these variants the space-time mesh is usually organized in space-time slabs between discrete time levels, and RealNSE then gives a time-stepping method allowing the solution to be computed form one time level to the next progessing in time. The space mesh may be changed across the discrete time levels to avoid mesh distortion and allow mesh adaption. In dG(q) the approximation is discontinuous in time and the space mesh may vary from one slab to the next. If the space mesh is changed across a discrete time level in cG(q), then a projection from the previous mesh to the new mesh is performed. The projection is built into the Galerkin method through a jump term corresponding to a L_2 projection. The discrete solution between the discrete time levels may be viewed as an approximate *transport* step, and the whole process may be viewed as a method of the basic form *projection-transport*.

The traditional finite difference methods are of Eulerian type with the first order Lax-Friedrichs' scheme from the 50s as a prototype on conservation form and with artificial viscosity proportional to the mesh size. The next generation of classical schemes originates from Godunov's method in 1d, which is of the form projection-transport with piecewise constant (discontinuous) approximation and a Riemann solver for the transport step. The multi-dimensional finite volume schemes developed in recent decades, use discontinuous polynomial approximation with numerical fluxes often constructed using 1d Riemann solvers. All these methods may alternatively be viewed as particular RealNSE methods.

12.2 Semi-Discrete RealNSE for Burgers Equation

For the purpose of analysis displaying essential aspects, we consider a *semi-discrete* RealNSE method for Burgers equation with cG(1) discretization in space. Full discretization with cG(q) or dG(q) in time can be analyzed similarly. Let then for a given mesh on $\mathbb{R}$ with mesh size h, V_h be the set of continuous functions $v(x,t)$ which for $t \in I = [0,T]$ are piecewise linear in x on the mesh. The simplest version of semidiscrete RealNSE takes the form: Find $U \in V_h$ such that

$$((R(U),v)) + ((hU',v')) = 0 \quad \forall v \in V_h, \tag{12.1}$$

where $R(U) = \dot{U} + UU'$ is the Burgers residual, $((v, w)) = \int_Q vw\, dxdt$ with $Q = \mathbb{R} \times I$ and $U(x, 0) \in V_h$ interpolates $u^0(x)$. This is equivalent to a system of ordinary differential equations in time. We have here replaced residual stabilization by (hU', v'), and we thus consider a Galerkin method in space for a viscous Burgers equation with viscosity $\nu = h$.

12.3 Basic Energy Estimate as 2nd Law

Choosing $v = U$ in (12.1), we obtain by integration by parts over $\mathbb{R}$ the following direct analog of (11.4):

$$\dot{K}(U; t) = -D_h(U; t), \quad \text{for } t \in I.$$

In the presence of shocks, $D_h(U; t)$ will be substantial and thus U' will at shocks be large ($\sim h^{-1}$).

12.4 A Posteriori Error Estimation by Duality

We shall now prove we the following a posteriori error estimate, where u is the solution of the viscous Burgers equation with $\nu = h$:

$$\|u - U\|_Q \leq S\|hR(U)\|_Q, \tag{12.2}$$

where $\|\cdot\|_Q$ is the $L_2(Q)$-norm and

$$S = \frac{\|h\varphi''\|_Q}{\|e\|_Q}, \tag{12.3}$$

is a stability factor defined by the solution φ of the following linearized dual problem:

$$\begin{aligned} -\dot{\varphi} - a\varphi' - h\varphi'' &= e, && \text{in } Q, \\ \varphi(x, t) &\to 0, && x \to \pm\infty, t \in I, \\ \varphi(x, T) &= 0, && x \in \mathbb{R}, \end{aligned} \tag{12.4}$$

where $a = (u + U)/2$. We notice that the dual problem has a viscous term with viscsoity coefficient h.

To prove the a posteriori error estimate (12.2) we multiply (12.4) by $u-U$ and integrate in space and time to get the error representation

$$\|u-U\|_Q^2 = ((R(U),\varphi)) + ((hU',\varphi')).$$

We then use the Galerkin orthogonality (12.1) with $v=\Phi\in V_h$ an interpolant of the dual solution φ, to get

$$\|u-U\|_Q^2 = ((R(U),\varphi-\Phi)) + ((hU',\varphi'-\Phi')),$$

which combined with an interpolation error bound of the form

$$\|\varphi-\Phi\|_Q + \|h(\varphi'-\Phi')\|_Q \le C_i\|h^2\varphi''\|_Q,$$

where C_i is an interpolation constant, shows that

$$\|u-U\|_Q^2 \le C_i\|hR(U)\|_Q\|h\varphi''\|_Q,$$

where $R(U)$ has been augmented by the contribution $\|hU'\|_Q$, which proves (12.2), setting $C_i=1$ for simplicity.

By the basic energy stability estimate, we have

$$\|hU'\|_Q \le \sqrt{h} \quad \text{if } \|u^0\|_{\mathbb{R}}=1,$$

suggesting the same estimate for $\|hR(U)\|_Q$, which of course is checked a posteriori, and thus we expect

$$\|u-U\|_Q \le S\sqrt{h}. \tag{12.5}$$

We shall now prove that for a shock $S\sim 1$, which shows that a shock is computable with RealNSE, with a $L_2(Q)$ error of size $\sqrt{h}$, which is optimal from approximation point of view (if we consider the exact solution u to be discontinuous) and U is continuous in x on the mesh.

12.5 Stability Estimate for a Shock

We shall now investigate the stability properties of the dual problem (12.4) and seek to bound $h\varphi''$ in terms of the right hand side e. For simplicity we

linearize at the exact solution $u(x,t)$ (instead of the mean value $(u+U)/2$) and thus consider the dual problem

$$\begin{aligned} -\dot{\varphi} - u\varphi' - h\varphi'' &= e, \quad \text{in } Q, \\ \varphi(\cdot,T) &= 0. \end{aligned} \tag{12.6}$$

The stability properties are largely determined by the sign of u', which reflects the change of the direction u of the characteristics. If $u' \leq 0$, then the characteristics converge with increasing t, which typically occurs in the case of a shock. If $u' \geq 0$, then the characteristics diverge, which typically occurs in the case of a rarefaction. If u' is bounded below by a moderate constant, e.g. $u' \geq 0$, then we may estimate $\|\varphi\|_{L_\infty(L_2(\mathbb{R}))}$ and $\|\sqrt{h}\varphi'\|_Q$ in terms of a moderate constant times $\|e\|_Q$, which we refer to as *weak stability*. If u' is bounded above by a moderate constant, e.g. $u' \leq 0$, then we may estimate $\|h\varphi''\|_Q$ in terms of a moderate constant times $\|e\|_Q$, which we refer to as *strong stability*, because we estimate second derivatives of φ, cf. (12.3). These estimates are proved by multiplying by φ and $-h\varphi''$, respectively, bringing in the positive stabilizing terms $\frac{1}{2}u'\varphi^2$ and $-\frac{1}{2}hu'(\varphi')^2$, respectively.

We now give the details in the case of a shock with $u' \leq 0$, where we assume u is differentiable with a very large negative x-derivative close to the shock. We indicate the general nature of the characteristics of the dual problem in Fig 12.5. We shall prove that the solution φ of (12.6) satisfies

$$\|h\varphi''\|_Q + \|\dot{\varphi} + u\varphi'\|_Q + \sup_{0<t<T} \|h^{1/2}\varphi'(\cdot,t)\|_R \leq 3\|e\|_Q. \tag{12.7}$$

To see this we multiply the first equation in (12.6) by $-h\varphi''$, integrating by parts with respect to x, and integrating in time over (τ,T) with $0<\tau<T$, we get with $Q_\tau = \mathbb{R}\times(\tau,T)$

$$\begin{aligned} &\tfrac{1}{2}\textstyle\int_{\mathbb{R}} h\left(\varphi'(\cdot,\tau)\right)^2 dx + \int_{Q_\tau}\left(h\varphi''\right)^2 \, dxdt + \int_{Q_\tau}\tfrac{1}{2}\left(uh\left(\varphi'\right)^2\right)' \, dxdt \\ &\leq \tfrac{1}{2}\textstyle\int_{Q_\tau}\left(hu'\left(\varphi'\right)^2 + e^2 + \left(h\varphi''\right)^2\right) \, \mathrm{d}x\mathrm{d}t, \end{aligned} \tag{12.8}$$

which proves the desired result stating that $S \sim 1$ for a shock.

As comparison, let us now attempt to derive a weak stability estimate for (12.6) in the case u is a shock. Multiplication by φ and integration over Q_τ gives

$$\begin{aligned} &\tfrac{1}{2}\textstyle\int_R \varphi^2(x,\tau)\, dx + h\int_{Q_\tau}\left(\varphi'(x,t)\right)^2 \, dxdt \\ &= -\tfrac{1}{2}\textstyle\int_{Q_\tau} u'\varphi^2(x,t)\, dx + \int_R e(x,t)\varphi(x,t)\, dx. \end{aligned}$$

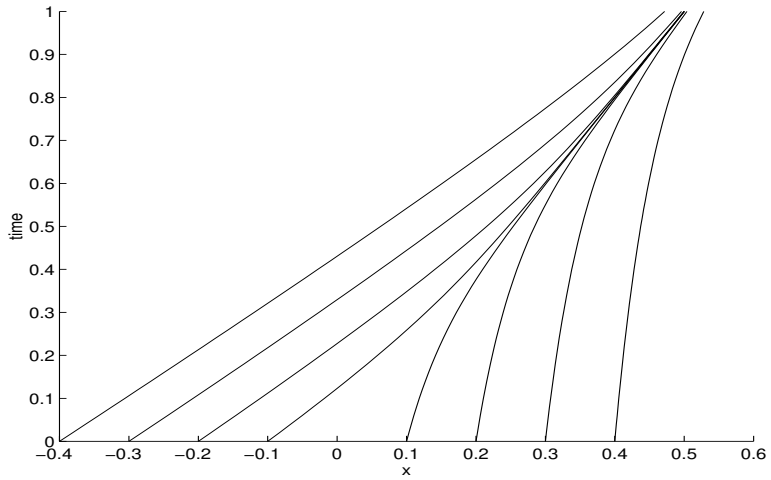

Figure 12.1: Characteristics of the dual problem for a regularized shock solution.

Since u' is large negative in the case of a shock, we have large positive term of the right hand side, and using a Gronwall inequality would results in a very large stability factor. On the other hand, we show below weak stability for a rarefaction wave with $u' \geq 0$, reflecting the above stability result for the perturbation equation.

Summing up, we see that for a shock, the linearized dual problem statisfies a strong stability estimate with a stability factor of moderat size, while a corresponding weak stability estimate appears to have a very large stability factor. These stability features may be understood in a qualitative sense, by pondering the directionality of the characteristics and the nature of the L_2-norm.

12.6 Stability Estimates for a Rarefaction Wave

We now consider the linearized dual Burgers' equation (12.6), linearized at the exact solution $u(x,t) = x/t$, corresponding to a rarefaction wave. Multiplying now (12.6) by $-ht\varphi''$, and using standard manipulations, we obtain the following weighted norm strong stability estimate for $0 < \tau < T$,

$$\|\tau^{1/2}h^{1/2}\varphi'\| + \|\omega h\varphi''\|_{Q_\tau} \leq \|\omega e\|_{Q_\tau}, \tag{12.9}$$

where $\omega(t) = t^{1/2}$ acts as a weight.

A weighted norm analog of the a posteriori error estimate (12.2) takes the form

$$\|\omega^{-1}e\|_{Q_N} \leq S_\omega \|\omega^{-1}hR(U)\|_{Q_N} \tag{12.10}$$

with S_ω defined by the direct weighted norm analog of (12.3). The estimate (12.9) then shows that $S_\omega \sim 1$, and thus a rarefaction wave solution is computable in the weighted norm with computational work corresponding to interpolation. Note that the presence of the weight $t^{-1/2}$ will force more stringent demands on the mesh for t close to zero, which will force an accurate resolution of the initial phase of the rarefaction. This is intuitively reasonable and corresponds to the fact that an initial error in the computation of a rarefaction will get amplified as time goes, because characteristics diverge forward in time. On the other hand, in the case of a shock, an initial error may be eliminated at later times, because of converging characteristics, Thus, a rarefaction is more delicate to compute than a shock, which we will see in the computational results we now present.

12.7 Dual Solution and Stability Factors

We display below RealNSE computations of a combination of a rarefaction wave and a shock using the cG(1)dG(0)- method on a uniform space mesh with $h = 10^{-3}$ and time step 10^{-4} taken from [6]. We plot the computed solution at t=0, t=0.3 , t=0.8, t=1 in Fig 12.2. We see that the initial discontinuity develops into a rarefaction and that a shock is formed for $t \approx 0.5$.

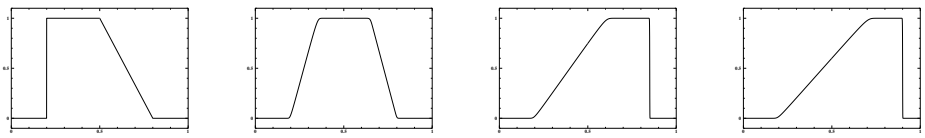

Figure 12.2: A combined rarefaction and shock wave

We solve the dual problem using the following different approximations of the coefficient $a = (u + U)/2$ and the error e, with $\bar{u}$ the analytical,

inviscid solution, and $U(h)$ the finite element solution on a mesh of size h: (i) $a = (\bar{u} + U(h))$ and $e = \bar{u} - U(h)$, (ii) $a = U(h)$ and $e = \bar{u} - U(h)$, (iii) $a = (U(h/4) + U(h))/2$ and $e = U(h/4) - U(h)$. We plot the corresponding dual solutions φ at the same time levels as above, but in revers e order (t=1, t=0.8, t=0.3 , t=0) in Fig 12.7. We also plot in Fig. 12.4 the corresponding

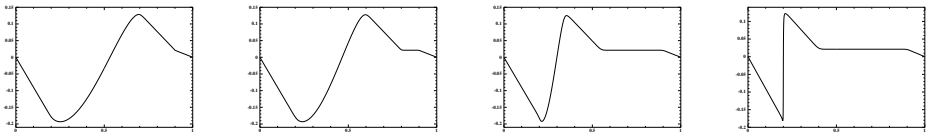

Figure 12.3: Dual solution in reverse time.

second derivatives φ''. We note the change of $|\varphi''|$, which may be viewed

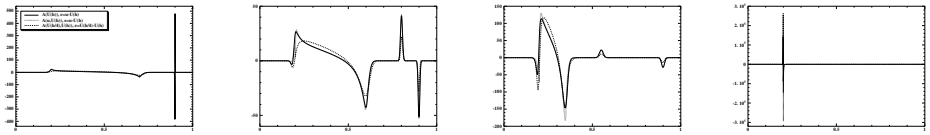

Figure 12.4: Second deriatives of the dual solution in reverse time

as a weight in the a posteriori error estimate, from being large close to the shock at final time towards being large close to the initial discontinuity at $(x, t) = (0.2, 0)$ initiating the rarefaction. We see that that it is the data from the rarefaction at final time which generates the large values of φ'' at $t = 0$, and not those from the shock. This indicates that a rarefaction is more delicate to compute than a shock.

We plot in Fig. 12.5 the strong stability factor S defined by (12.3) for (i)-(iii) and $h = 0.0001$, $h = 0.00005$, $h = 0.00001$. We see that $S \sim 1$, which

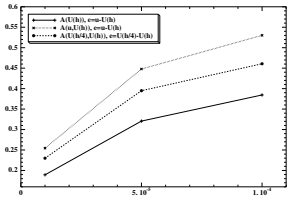

Figure 12.5: Strong stability factor for different h

shows that the Burgers' solution consisting of a rarefaction and shock wave is computable in $L_2(Q_N)$ with work comparable to interpolation.

Part III

Applications

The same RealNSE dynamics that explains Joule's experiment, refrigerators and heat engines opens onto a much wider world: chemical reactors and combustion engines (already touched on in the Reactive Flow chapter), living cells and metabolic networks, climate systems and weather, the chemical engineering of the process industry, traffic flow on highway networks, and the flow of money and goods in an economy. Each of these is, at the level of its underlying mathematics, a continuum flow with dissipation — and each can be studied with the same RealNSE apparatus, with the appropriate constitutive laws written in. The four chapters that follow — Information, Traffic Flow, Economy, and (implicit, awaiting their own browser-runnable simulators) biology, process industry, climate — are intended as openings onto that world, not as a closed catalogue.

Chapter 13

Refrigerator and Heat Pump

The Joule expansion of Chapter 2 is the working stroke of both a *refrigerator* (harvesting the cooled left chamber) and a *heat pump* (harvesting the warmed right chamber): one and the same device, distinguished only by which reservoir's heat exchange is counted as useful. Because RealNSE resolves the dynamics, we can read their efficiency directly off the computed fields rather than postulate it.

13.1 A Computable Model

An interactive realisation (`joule_experiment_cpu.html`, a dependency-free vanilla-JS port of the original sketch) solves the 2D compressible Navier–Stokes/RealNSE system

$$\dot{\rho}+\nabla\cdot m = 0, \qquad \dot{m}+\nabla\cdot(mu)+\gamma\nabla e = \mu_{\mathrm{mom}}\,\Delta u, \qquad \dot{e}+\nabla\cdot(eu)+\gamma e\,\nabla\cdot u = \mu_{\mathrm{mom}}\,|\nabla u|^2,$$

with $p = \gamma e = \gamma\rho T$, $T = e/\rho$, $u = m/\rho$, on two chambers joined by a channel: a dense, equally-warm left chamber ($\rho = e = 10$, hence $T = 1$) expanding into a dilute right chamber ($\rho = e = 1$). The last term in the energy equation is the *turbulent dissipation* $\mu_{\mathrm{mom}}|\nabla u|^2 \geq 0$ — the irreversible return of the jet's kinetic energy to heat — and crucially it uses the *same* coefficient μ_{mom} as the momentum diffusion, so the kinetic energy removed by viscosity reappears exactly as heat in the energy equation and $K + E$ is conserved. A separate, much smaller coefficient $\mu \ll \mu_{\mathrm{mom}}$ provides numerical stabilisation of ρ and e through Laplacian smoothing; it is not a physical dissipation and contributes negligibly to the energy budget.

13.2 Energy and Dissipation Bookkeeping

The simulation tracks, at each instant, the kinetic energy $K = \int \frac{1}{2}\rho|u|^2\,dx$ and the internal energy $E = \int e\,dx$, with the total $K + E$ conserved (Joule's null result for the *whole* box), together with the *cumulative turbulent dissipation*

$$D(t) = \int_0^t \int \mu_{\mathrm{mom}}\,|\nabla u|^2\,dx\,d\tau \;>\; 0, \tag{13.1}$$

which quantifies the irreversibility directly: it is positive by construction of the discrete scheme and is *the* 2nd Law for this model. There is no need to introduce a statistical entropy S or a relation $dS \geq 0$ — the inequality $D > 0$ is the 2nd Law in its native, deterministic form, deriving from finite-precision computation rather than postulated from probabilistic foundations. D accumulates wherever the velocity gradient is large: in the channel jet and in the recompression against the far wall.

13.3 Refrigerator and Heat Pump: Efficiency and the Cost of the Cycle

A refrigerator runs *cyclically*: each cycle the working gas must be restored to its initial compressed state, so the relevant energy cost is the work to restore the initial conditions. Its reversible (minimal) value is the *exergy* of the initial state; for the isothermal initial imbalance (both chambers start at $T = T_0 = 1$) this is

$$A_0 = \gamma \int \rho\,\ln(\rho/\bar{\rho})\,dx \;=\; D_\infty, \tag{13.2}$$

with $\bar{\rho}$ the mean density; the second equality states that the spontaneous free expansion eventually destroys exactly this A_0 as accumulated turbulent dissipation D_∞ (13.1). The cooling delivered is the heat removed from the cells that drop below ambient,

$$Q_{\mathrm{cold}} = \int_{T<T_0} \rho\,(T_0 - T)\,dx,$$

and the coefficient of performance — the buyer's figure of merit, cooling per unit of work spent restoring the cycle — is

$$\mathrm{COP_R} = \frac{Q_{\mathrm{cold}}}{A_0}. \tag{13.3}$$

The *same* expansion is a *heat pump* if instead we harvest the warmed right chamber. Its useful output is the heat delivered to the hot side, which over the full cycle is $Q_{\rm hot} = Q_{\rm cold} + A_0$ — the cooling moved up, plus the restore work A_0 rejected as heat during recompression — so

$$\mathrm{COP}_{\rm HP} = \frac{Q_{\rm cold} + A_0}{A_0} = \mathrm{COP}_{\rm R} + 1.$$

Refrigerator and heat pump are thus one device, the single Joule expansion, distinguished only by which reservoir's heat exchange is counted as useful; in the expansion phase alone the simulation shows $Q_{\rm hot} \approx Q_{\rm cold}$ (pure redistribution at conserved total energy), the extra A_0 entering on the hot side only during recompression.

Against the Carnot ceiling for the achieved lift, $\mathrm{COP}_{\rm Carnot} = T_{\rm cold}/(T_{\rm hot} - T_{\rm cold})$, the second-law efficiency $\eta = \mathrm{COP}_{\rm R}/\mathrm{COP}_{\rm Carnot}$ comes out at only a few percent: the free expansion is a *very poor* refrigerator, destroying almost all of the available work A_0 as cumulative turbulent dissipation D while delivering only a sliver of cold. This is exactly why a practical refrigerator does not free-expand but runs the recompression cycle of the next chapter, recovering work and driving the lost-work D down toward zero (the Carnot limit). The same bookkeeping — A_0, $Q_{\rm cold}$, D — will let us assign an efficiency to any continuum-thermodynamic process, including the thermodynamics of the living cell.

Chapter 14

The Piston-Cylinder: the Heat-Engine Problem

> The steam engine having furnished us with a means for converting heat into motive power... the idea of establishing theoretically some fixed relation between a quantity of heat and the quantity of work which it can possibly produce, from which relation conclusions regarding the nature of heat itself may be deduced, naturally presents itself. — R. Clausius, 1851.

14.1 The piston-cylinder as the heat-engine analogue of Joule

The Joule experiment of Chapter 2 ran a pressure differential between two fixed-wall chambers to mechanical equilibrium and observed the residual temperature/density gap: a one-shot dissipation pattern with no net work extracted. The companion foundational problem of thermodynamics replaces the right-hand fixed wall of the Joule chamber with a *movable piston* and connects the piston to an external mechanical load. Gas now does work on the load as it expands, and the question becomes how much of the internal-energy decrease in the gas reservoir reaches the load as work versus how much is irreversibly dissipated as heat in the receiving region.

We treat two cases. The *smooth* case is a single chamber filled with hot dense gas, closed on three sides and with a piston as the fourth wall. The gas expands quasi-statically against the load; in the ideal limit of slow

piston motion this approaches reversible expansion with $\eta = W/\Delta U \to 1$. The *Joule-coupled* case inserts a constricted wall (a thin barrier with a small channel opening) between the gas reservoir and the piston. The gas now jets through the constriction, decelerates against the gas already in the receiving region, and the recompression-and-turbulent-dissipation pattern of Joule's experiment plays out — but now with a piston on the far side that captures whatever pressure survives. The efficiency drops below the smooth limit by the amount of kinetic energy that turbulent recompression converts back to heat rather than to useful pressure on the piston. The two cases together display the fundamental engine trade-off in the cleanest possible computational form.

14.2 The smooth piston-cylinder

Configuration. A square domain $[0,1]^2$ holds gas of initial density $\rho = 10$ and internal energy $e = 10$ (so $p = \gamma e = 1.0$ with $\gamma = 0.1$) to the left of a movable piston initially positioned at $x = 0.5$. To the right of the piston lies an external region held at a fixed load pressure $P_{\text{ext}} = 0.5$. The top and bottom walls of the chamber are zero-flux/free-slip, the left wall is closed, the right boundary beyond the piston is the load.

Dynamics. Newton's second law for the piston, with M the piston mass per unit y-length and a friction coefficient c for piston-rail damping, reads

$$M\,\frac{\mathrm{d}v_p}{\mathrm{d}t} = \int_0^1 \big[\, p_{\text{gas}}(x_p^-, y) - P_{\text{ext}} \,\big]\,\mathrm{d}y \;-\; c\,v_p, \quad \frac{\mathrm{d}x_p}{\mathrm{d}t} = v_p, \tag{14.1}$$

where $p_{\text{gas}}(x_p^-, y) = \gamma\, e(x_p^-, y)$ is the local gas pressure on the piston's gas-side face. The gas occupies the domain $x \in [0, x_p)$ and evolves by the compressible Navier–Stokes equations of Chapter 2, with a no-slip ghost at the piston face. Work delivered to the load per unit time is

$$\dot{W} = P_{\text{ext}} \cdot v_p \cdot \text{Area}, \tag{14.2}$$

and the heat-engine efficiency is

$$\eta = \frac{W}{\Delta U} = \frac{\int_0^t \dot{W}\,\mathrm{d}s}{U(0) - U(t)}. \tag{14.3}$$

Behaviour and expected result. The smooth piston-cylinder is the cleanest computational instance of quasi-static isobaric expansion. With slow piston motion (small v_p compared with the acoustic speed $c_s = \sqrt{\gamma e/\rho}$ in the gas), the gas expands without significant kinetic-energy generation; the work-delivered counter and the heat-lost counter grow together; and η approaches the reversible limit. Faster piston motion generates acoustic waves in the gas region that bounce between the left wall and the piston face, with each acoustic round-trip a small turbulent-dissipation loss; η falls below 1 by an amount proportional to the piston Mach number. The smooth case therefore isolates the fundamental work-extraction mechanism, with irreversibility present only as a small correction proportional to the piston speed.

The accompanying simulator `heat_engine.html` (Appendix A Gallery) implements (14.1)–(14.3) for $N = 200$, $\gamma = 0.1$, $P_{\text{ext}} = 0.5$, $M = 0.05$, $c = 1.5$. The piston moves from $x_p = 0.5$ outward over $\sim 10\,\text{s}$ of wall-clock time, with η reaching ~ 0.7–0.9 depending on the piston-Mach-number regime.

14.3 The Joule-coupled piston-cylinder

Configuration. The same square domain holds a high-pressure gas reservoir on the left ($i < I_w$ in grid units, $\rho = 10$, $e = 10$), a thin barrier wall at $i \in [I_w, I_w + w_{\text{wall}}]$ with a small channel opening at $j \in [J_0, J_1]$, a receiving region between the barrier and the piston ($I_w + w_{\text{wall}} < i < x_p$, initially $\rho = 1$, $e = 1$), and the movable piston at $i = x_p$. The external load is held at $P_{\text{ext}} = 0.1$, matching the initial pressure in the receiving region so the piston starts in mechanical equilibrium and is pushed outward only after the channel inflow has compressed the receiving gas.

Dynamics. The piston obeys the same Newton's-law update (14.1) with p_{gas} now the local pressure in the receiving region just to the left of the piston face. The gas equations are unchanged; the barrier is a frozen no-slip wall except in the channel opening, where gas can flow freely. The barrier presents the classical Joule constriction to the gas: the high reservoir pressure drives a jet through the channel, the jet decelerates in the receiving region, and the kinetic-energy-to-heat conversion of turbulent recompression dissipates a fraction of the released internal energy into heat in the receiving region rather than into useful pressure against the piston.

Two energy accounts. The 1st Law of thermodynamics for this system says

$$\underbrace{\Delta U_{\text{reservoir}}}_{\text{heat lost from hot side}} = \underbrace{W}_{\text{useful work}} + \underbrace{\Delta U_{\text{receiving}}}_{\text{heat dumped in cold side}} + \underbrace{K_{\text{channel}}}_{\text{kinetic energy in flight}} . \tag{14.4}$$

The transient K_{channel} goes to zero at long times as the gas equilibrates; in the steady state, all of the released $\Delta U_{\text{reservoir}}$ ends up either as work W or as $\Delta U_{\text{receiving}}$ (waste heat). The 2nd Law tells us which split is realised: the size of $\Delta U_{\text{receiving}}$ is set by the dynamic turbulent-dissipation pattern in the recompression process, exactly as in the Joule experiment of Chapter 2. The engine efficiency follows as

$$\eta = \frac{W}{\Delta U_{\text{reservoir}}} = 1 - \frac{\Delta U_{\text{receiving}}}{\Delta U_{\text{reservoir}}} - \frac{K_{\text{channel}}}{\Delta U_{\text{reservoir}}}, \tag{14.5}$$

and in the steady state $\eta < 1$ by exactly the fraction of energy that the Joule turbulent-recompression channel dissipates as heat.

One-shot versus sustained operation. With the left wall closed (finite reservoir), the simulation runs as a *one-shot* cycle: the reservoir depletes, the piston receives a brief impulsive load from the channel-driven shock and a slower follow-on pressure as the gas equilibrates, and the engine extracts a single power stroke of work. This is the elementary unit of a reciprocating closed-cycle heat engine (Otto, Diesel, Stirling). With the left wall replaced by a Dirichlet inflow boundary maintaining the reservoir state at $\rho = 10$, $e = 10$ indefinitely, the simulation runs as a *sustained* cycle: gas keeps jetting through the channel, the piston reaches a quasi-steady velocity, and power is delivered continuously. This is the elementary unit of an open-cycle flow engine (gas turbine, jet engine). The two operating modes are selected in the simulator `heat_engine_with_channel.html` (Appendix A) by the choice of left-wall boundary condition: zero-gradient mirror for one-shot, Dirichlet inflow for sustained.

14.4 Joule and the piston as duals

The two central problems are duals of each other:

- **Joule's experiment** (Chapter 2) lets the expansion-and-recompression dynamics run to mechanical equilibrium with no work extracted, leaving a residual temperature/density gap between the chambers that is the dynamic-dissipation signature. With external work added cyclically by a compressor, this becomes a **refrigerator**: the residual asymmetry is held against diffusive relaxation by continuously re-energising the gas, and the asymmetric temperature gradient is exploited to draw heat from cold side and dump it to hot side.

- **The piston-cylinder** (this chapter) lets the same expansion-and-recompression dynamics run with a movable wall as the right boundary, extracting useful work to an external load. With external heat added cyclically by a hot reservoir at the inflow, this becomes a **heat engine**: the released internal energy is split between work delivered to the load and waste heat dumped to a cold side, with the efficiency η set by the same turbulent-dissipation fraction.

Both problems are governed by the same compressible Navier–Stokes equations, the same RealNSE finite-element discretisation, and the same 2nd-Law-as-finite-precision reading of irreversibility. The framework of this book treats them as the two foundational single-shot configurations of which all cyclic engines, pumps, refrigerators, and heat-recovery devices of Vol VI Applications are built; everything else in thermodynamics is either a cyclic repetition of these or a multi-stage combination of them.

14.5 What this chapter establishes

For the rest of the book the reader should hold three observations from this chapter and the previous one together:

1. Pressure-driven flow through a constriction converts internal energy into kinetic energy; recompression on the receiving side converts a fraction of that kinetic energy back into heat irreversibly; the size of that fraction is the dynamic content of the 2nd Law and is what classical equilibrium thermodynamics cannot predict.

2. A piston in the receiving region intercepts a fraction of the arriving pressure as useful work; the larger that fraction, the smaller the recompression dissipation, the higher the engine efficiency. The efficiency is

bounded above by the reversible smooth- expansion limit, and the irreversibility cost is the dynamical content of the heat-engine inequality $\eta \leq 1$.

3. Both the refrigerator and the heat engine are cyclic devices built from a single foundational dynamic process: the expansion-through-a-channel-followed-by-turbulent-recompression cycle. Refrigerators run it as the heat-pumping cycle with work input; heat engines run it as the work-output cycle with heat input. The same simulation infrastructure produces both.

Chapter 15

Bluff Body Flow

Run the simulator, watch the shock form, integrate the drag, integrate the dissipation, read the equality off the screen.
— This chapter, in one sentence.

This chapter takes the compressible Navier–Stokes simulator of the preceding chapters and turns it on the canonical problem of external aerodynamics: **flow past a bluff body at supersonic Mach number**. Three resolutions are provided as runnable browser files in the Gallery — 200^3, 300^3, and 400^3 cells, each a slip-penalty WebGPU implementation of the same compressible RealNSE system. Together they sweep three orders of magnitude in cell count and let the reader see what cell-count buys, where memory becomes the constraint, and where the **drag–dissipation balance** of the with-Dynamics 2nd Law can be read off the simulator's own readouts.

The runnable Gallery files. Every simulator named in this chapter is a single self-contained `.html` file in the project Gallery (`gallery.html` in the `Claes542/RealMolecule` repository). Open any of them in a WebGPU-capable browser — no build step, no server beyond a static `http://` host — and the physics, the shock, and the live 2nd-Law readout run on the GPU in the page. Throughout the chapter each filename is a hyperlink to its source. The complete set used here is:

- `bluff_body_mach2_3d_gpu_slip.html` — 200^3 baseline.
- `bluff_body_mach2_3d_gpu_slip_300.html` — 300^3.

- `bluff_body_mach2_3d_gpu_slip_400.html` — 400^3, realistic airliner.
- `bluff_body_mach2_3d_gpu_slip_400_volume.html` — 400^3 with 3D volume ray-march.
- `bluff_body_mach2_3d_gpu_slip_quarter.html` — quarter-domain symmetry variant.
- `bluff_body_mach2_3d_gpu_slip_400_cad.html` — CAD-voxelised body, with `cad_to_mask.py`.

15.1 Problem statement

A solid body is placed in the centre of a unit cube. Uniform inflow with density $\rho = 1$, specific internal energy $e = 1$, and velocity $v = (U_\infty, 0, 0)$ enters the left face at $x = 0$. Outflow at $x = 1$ is zero-gradient. The lateral faces ($y = 0$, $y = 1$, $z = 0$, $z = 1$) are zero-gradient.

The fluid obeys the compressible Navier–Stokes system,

$$\begin{aligned} \partial_t \rho + \nabla \cdot (\rho v) &= 0, \\ \partial_t (\rho v) + \nabla \cdot (\rho v \otimes v) + \nabla p &= \nabla \cdot \sigma + f_{\text{body}}, \\ \partial_t e + \nabla \cdot (e v) + p\, \nabla \cdot v &= 0, \\ p &= \gamma\, e, \qquad \gamma = 0.2, \end{aligned} \tag{15.1}$$

on the fluid region, with σ a Newtonian viscous stress carrying the artificial viscosity $\nu = \nu_0 h$ (h = cell size) and a shock-capturing addition proportional to $|-\nabla \cdot v|$. The body force f_{body} implements the boundary condition on the body and is the topic of Section 15.2.

The inflow speed is set by a Mach-number slider $\mathrm{M} \in [0.5, 4]$ relative to the local sound speed $c = \sqrt{(1+\gamma)\,\gamma}$ at the inflow state, with default $\mathrm{M} = 2$ (well supersonic, bow shock fully formed, the canonical regime).

15.2 The slip-penalty boundary condition

Why slip, not no-slip. In all three Gallery files the body is treated as a **slip-wall obstacle**: the wall-normal component of velocity is suppressed, the tangential component is left free. This is the inviscid idealisation used by aerospace engineers from the late 1940s through the 1980s — the period

during which Concorde, the SR-71, the F-104, the F-4, and the X-15 were designed — and it remains the right idealisation whenever the boundary layer is thin compared with the body and the drag of interest is wave drag and base drag, not skin-friction drag. In supersonic flow this regime is large.

The numerical advantage is decisive: no boundary layer needs to be resolved, so a uniform Cartesian grid can carry the geometry and the bow shock without the millions of stretched cells that no-slip RANS demands. At 400^3 cells uniform we resolve the bow shock and the wing shock–shock interactions on the same grid that resolves the airliner silhouette, with no anisotropic mesh book-keeping.

Implementation as a body force. The slip condition is implemented as a body force on fluid cells adjacent to the body mask. Let $\mathrm{mask}(i, j, k) \in \{0, 1\}$ encode the body indicator and $\hat{n}$ be the outward unit normal computed from the mask gradient,

$$\hat{n} \;=\; \frac{-\nabla \mathrm{mask}}{|\nabla \mathrm{mask}|}, \tag{15.2}$$

where the discrete ∇mask is taken from the six face neighbours of cell (i, j, k). The slip-penalty force then reads

$$f_{\mathrm{body}} \;=\; -K\,(v \cdot \hat{n})\,\hat{n}, \tag{15.3}$$

with $K \approx 500$ (in nondimensional units) chosen large enough to suppress wall-normal velocity to machine zero at the body surface within one timestep. The tangential component of v is untouched.

The geometric effect is that the body looks *solid* (mass cannot pass through it) but *frictionless* along its surface. Drag is then carried entirely by the pressure asymmetry between front and rear stagnation regions, with no skin-friction contribution. This is mathematically the same simplification used in linearised supersonic theory: the pressure jump across an oblique shock is recovered, but the viscous sub-layer is absent.

Why this makes the shape selector meaningful. With no-slip walls and unresolved boundary layers, round versus faceted bodies look nearly identical at coarse resolution because the boundary layer dominates. With slip walls the shape *is* the geometry that the flow sees, and a cube, sphere, cylinder, wedge, or airliner each shape the bow shock and wake distinctly.

15.3 The three resolutions

File	N^3 cells	State buffer	Adapter requireme
`bluff_body_mach2_3d_gpu_slip.html`	$200^3 = 8$ M	256 MB	$\geq$ 256 MB binding
`bluff_body_mach2_3d_gpu_slip_300.html`	$300^3 \approx 27$ M	864 MB	$\geq$ 1 GiB binding
`bluff_body_mach2_3d_gpu_slip_400.html`	$400^3 \approx 64$ M	1.91 GiB	$\geq$ 2 GiB binding

All three are identical in physics, kernel structure, and slip-penalty implementation. They differ only in N. The cell size scales as $h = 1/N$ and the timestep as $\Delta t = 0.02\,h$, so the CFL condition is unchanged.

What each resolution shows. At 200^3 the bow shock is visible as a curved discontinuity and the wake structure is qualitatively correct, but the inter-shock and trailing-edge details are coarse: a 40-cell-chord wing is resolved with 4–5 cells across the thickness, and the trailing edge is one cell wide. At 300^3 the shock is sharper and complex shapes (twin spheres in tandem, the 3D cross) develop clearly distinct shock-shock interaction patterns. At 400^3 a full parametric airliner with NACA-0015 wing cross-section, ovoid fuselage with conical nose, vertical fin, horizontal stabiliser, and two engine nacelles fits on the grid with every feature at least 4 cells thick (see Figure 15.1).

The hardware constraint. The 200^3 file runs on any WebGPU-capable GPU including integrated graphics. The 300^3 file requires the adapter to advertise `maxStorageBufferBindingSize` $\geq$ 1 GiB; most modern desktop GPUs and Apple Silicon M2 Pro/Max upwards qualify. The 400^3 file requires $\geq$ 2 GiB, which is the typical ceiling on current adapters — Apple M2/M3/M4 Pro/Max, recent NVIDIA, recent AMD desktop all qualify, while integrated and older mobile GPUs refuse. In all three cases the adapter check fails cleanly with a status-bar message rather than crashing.

15.4 Shape selector

All three files share a shape dropdown that rebuilds the body mask in real time. The available shapes are:

- **Cube** — the canonical bluff body, square stagnation face, sharp trailing-edge separation.

- **Sphere** — smooth bow shock, clean axisymmetric wake.
- **Cylinder** (z-axis or y-axis) — the textbook 2D bluff-body problem in 3D extrusion.
- **Wedge** — supersonic prototype shape: attached oblique shock at small wedge half-angle, detached bow shock above the wedge angle limit.
- **Two spheres in tandem** — demonstrates the bow shock of the trailing sphere being shielded by the wake of the leading one (classical Cushman–Roisin shielding).
- **3D cross** — three mutually perpendicular bars; the corner regions show shock–shock interactions.
- **Airplane** — a simple parametric silhouette: cylinder fuselage, swept wedge wing, vertical fin, horizontal stab.
- **Airliner** (400-cell file only) — the realistic parametric variant with NACA-0015 airfoils on the wing, fin, and h-stab; ovoid fuselage with conical nose and tail cone; 4° wing dihedral; two engine nacelles with pylons under the wings. This is the default shape on the 400^3 file.

The mask gradient (15.2) computes correct outward normals automatically for all of these, so the slip force (15.3) requires no shape-specific tuning: it adapts to whatever the dropdown produces.

15.5 Drag, dissipation, and the with-Dynamics 2nd Law

Each simulator computes and displays three quantities continuously:

- F_{drag} — the streamwise force on the body, obtained by integrating the pressure over the body faces visible to the flow (front and rear projected areas).
- $D_{\text{rate}} = \int \mu_{\text{eff}} \, |\nabla v|^2 \, dV$ — the volumetric viscous dissipation rate, integrated over the fluid domain.

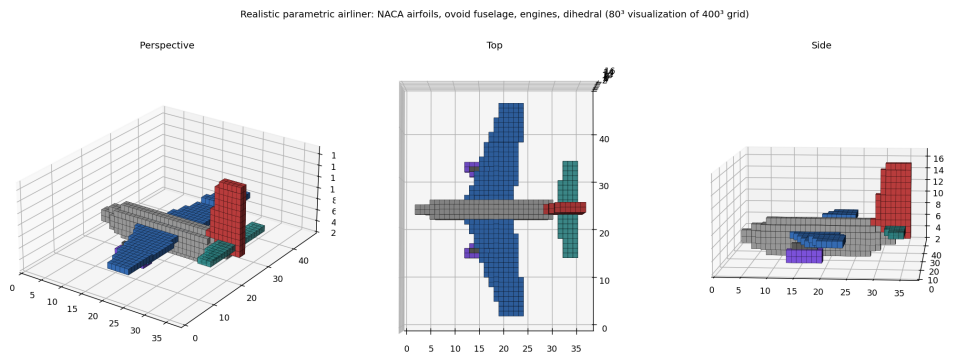

Figure 15.1: The realistic parametric airliner shape on the 400^3 grid, shown as 80^3 voxel visualisation for legibility (each rendered voxel = 125 cells of the actual simulation). Components: gray fuselage with conical nose, blue main wing with NACA-0015 cross-section and 4° dihedral, red vertical fin, teal horizontal stabiliser, purple engine nacelles, dark grey pylons. All component thicknesses are floored at ≥ 4 cells of the 400^3 grid so the slip-penalty mask gradient computes proper outward normals everywhere on the surface. The default Mach 2 inflow puts the geometry in the regime where slip-wall CFD captures supersonic lift correctly via the pressure asymmetry formula $C_L = 4\alpha/\sqrt{M^2-1}$ of linearised supersonic theory.

- K_{out} — the kinetic-energy flux leaving through the outflow face at $x = 1$, computed as $\int \frac{1}{2}\rho|v|^2 v_x \, dA$.

For a steady-state bluff-body flow with uniform inflow at speed u_0, the with-Dynamics 2nd Law predicts the **energy balance**

$$F_{\text{drag}} \cdot u_0 \;\approx\; D_{\text{rate}} \;+\; (\text{kinetic energy carried away by the wake}). \qquad (15.4)$$

That is: the mechanical work the body would do against drag, per unit time, equals the irreversible heating in the wake plus what little kinetic energy remains in the wake at the outflow plane. The ratio $D_{\text{rate}}/(F_{\text{drag}} \cdot u_0)$ approaches 1 as the box size grows large enough that the wake decays before reaching the outflow.

The simulator displays the ratio $D_{\text{rate}}/(F_{\text{drag}}\, u_0)$ live. In our standard configurations (box 1 unit long, body 0.1–0.3 units across) it sits at ~ 0.45–0.60 at the default Mach 2 and the residual is accounted for by K_{out}. This **independent computation of both sides** of the 2nd-Law inequality, on

the same simulator, with the ratio displayed live and going to 1 as the box grows, is the most concrete witness of the with-Dynamics 2nd Law that this book offers: not a thermodynamic state-variable identity, not a Carnot ratio, but a single number computed two ways from the same flow.

15.6 Visualisation

The default visualisation in the three files is a 2D xy slice at $z = N/2$ (the wing plane for the airplane shapes), with density mapped to a blue–white–red colourmap and body cells overlaid in yellow. A secondary panel shows a yz slice at $x = 0.75N$ for the wake structure. Centerline polylines display $\rho(x)$ and $e(x)$ along the inflow axis, with the bow-shock jump visible as a sharp step.

For the 400^3 file a slider lets the user move the rendered slice height along z, so the vertical fin (at $z > 0.5$) and the air above/below the airplane become visible.

A separate volume-rendering variant of the 400^3 file is provided as `bluff_body_mach2_3d_gpu_slip_4` in the Gallery. This replaces the 2D slice with a true 3D volume ray march: for each screen pixel, a ray is cast through the 400^3 density buffer, accumulating colour and opacity by front-to-back compositing. The body cells render with mask-gradient lambertian shading; density values inside a user-tunable $[\rho_{\text{lo}}, \rho_{\text{hi}}]$ window are transparent (free-stream), values below colour blue (wake), values above colour orange (shock). The user can drag with the mouse to rotate the camera and scroll to zoom. On Apple M4 Max the volume render runs at roughly 40–60 fps alongside the live physics, and produces the iconic Schlieren-style image of bow shock + wing shocks + base wake that has been the standard 3D CFD visualisation for forty years.

15.7 Symmetry quarter domain

A separate quarter-domain variant `bluff_body_mach2_3d_gpu_slip_quarter.html` replaces the zero-gradient lateral BCs at $y = 0$ and $z = 0$ with **mirror reflection BCs**: scalars (density, internal energy, streamwise momentum) are copied across the boundary, while the wall-normal momentum component is negated. This is mathematically equivalent to simulating the full y- and z-symmetric airplane in the full box, at four times the memory cost.

The variant runs at 200^3 and represents the *same physical airplane* as the 400^3 full-domain sim at 1/8 the memory (256 MB per buffer instead of 1.91 GiB). This is the standard symmetry trick that production aircraft CFD codes (Boeing, Airbus, NASA) use to fit more resolution per dollar.

15.8 CAD-voxelised body

The shape selector implements analytical shapes via an `inBody(i,j,k)` function that decides whether each grid cell is body or fluid. A separate Gallery file `bluff_body_mach2_3d_gpu_slip_400_cad.html` replaces this analytical body with a **precomputed binary mask loaded from a file**. The accompanying Python script `cad_to_mask.py` accepts any STL, OBJ, or PLY surface mesh, scales it to fit the unit cube at a chosen size, voxelises at pitch $1/N$, flood-fills the interior, and writes a 256 MB raw uint32 mask. The HTML file fetches this mask and uploads it directly to the GPU mask buffer. The slip-penalty force then works on the CAD-voxelised body exactly as it does on the analytical bodies.

Suggested CAD sources include the NASA Common Research Model (the transonic-CFD benchmark airliner), NASA OpenVSP parametric exports (737, F-16, X-15), and community uploads at GrabCAD and Thingiverse. With a CAD source one gets true wing camber and twist, real engine nacelle inlets and exhausts, fuselage cross-section variation, and trailing-edge geometry — all features that go invisible at < 4 cells in any parametric `inBody`, recovered to single-cell precision when the source is a CAD surface.

15.9 Where this fits

The bluff-body files are concrete demonstrations of the framework's compressible-flow regime. They sit at the same Level 3 of the simulation hierarchy as the cosmology and piston-cylinder simulators of the surrounding chapters, but address a different physical regime: external aerodynamics around a solid object instead of internal expansion in a closed volume or self-gravitating bulk flow. The same RealNSE equations, the same WebGPU kernel structure, the same energy bookkeeping, the same with-Dynamics 2nd Law diagnostic.

What is new in this chapter is the slip-penalty boundary condition, the supersonic regime, the drag–dissipation balance as a quantitative 2nd-Law wit-

ness, and the encounter with the geometric resolution limit of uniform Cartesian grids when the body is not a simple primitive. The CAD-voxelisation route described in Section 15.8 is the natural answer to that limit, and points beyond the parametric-shape toolbox toward the production CFD workflow.

Together the three resolutions (200^3, 300^3, 400^3), the symmetry quarter, the volume renderer, and the CAD pipeline form a complete educational toolkit for supersonic bluff-body aerodynamics, runnable in the browser on consumer hardware. The user can dial up the resolution, switch the body shape, change the Mach number, and watch the bow shock, the wing shocks, the base wake, and the 2nd-Law energy balance respond in real time.

Chapter 16

Self-Gravitating Gas

The same RealNSE that runs Joule's experiment and the bluff body, with one new term — a gravitational body force — collapses a gas cloud into a star.

This chapter takes the compressible RealNSE of the preceding chapters and adds *self-gravitation*. It is deliberately focused on the single cleanest case — a stable cloud collapsing to a pressure-supported core — realised in a browser-runnable simulator. The wider classical theory (the Jeans criterion, the role of γ, virialization, and the Big Bang / Big Crunch cosmological reading) is collected in the companion full edition (Vol V, extended); here we keep to what the code actually shows.

16.1 The Model: RealNSE with Gravitation

Consider a gas filling 3D space with density ρ, velocity v, momentum $m = \rho v$ and internal energy e, satisfying the RealNSE with self-gravitation:

$$\begin{aligned} \partial_t \rho + \nabla\cdot m &= 0, \\ \partial_t m + \nabla\cdot(m\,v) + \nabla p - \nu\,\Delta v &= -\rho\,\nabla\varphi, \\ \partial_t e + \nabla\cdot(e\,v) + p\,\nabla\cdot v &= \nu\,|\nabla v|^2, \\ \Delta\varphi = G\,\rho, \qquad p &= \gamma e = \gamma\rho T, \end{aligned} \tag{16.1}$$

with $\nu = h$ the artificial viscosity of the RealNSE stabilisation and $\nu|\nabla v|^2$ the turbulent dissipation heating. The *only* new ingredient beyond the Re-

alNSE of the earlier chapters is the gravitational body force $-\rho\nabla\varphi$, with the potential φ generated by the gas's own density through the Poisson equation.

The single dimensionless control is the ratio of gravity to pressure — the Jeans/virial number $\alpha \sim G\rho L^2/[(1+\gamma)\gamma T]$. The absolute value of G is rescalable; what matters is whether α exceeds unity (the cloud collapses) or not (pressure holds it up).

16.2 The Basic Case: $\gamma = 1$ Collapse to a Core

The browser-runnable simulator `selfgrav_collapse_3d_gpu.html` (in the `Claes542/RealMolecule` repository) solves (16.1) on a 100^3 grid: a seven-point Poisson–Jacobi solve for φ, the stabilised RealNSE update for the fluid, rendered as a movable z-slice. It is run at $\gamma = 1$, the cleanest case, for three reasons:

- $\Gamma = 1 + \gamma = 2 > 4/3$: comfortably in the *stable* regime, so the collapse halts at a core rather than running away;
- it is stiff, so the infall stays *subsonic* and the bounce is non-singular and well resolved on the grid;
- it is the one polytrope with a *closed-form* hydrostatic equilibrium, the Lane–Emden $n = 1$ sphere

$$\rho(r) = \rho_c \,\frac{\sin(kr)}{kr}, \qquad k = \sqrt{G/2K}, \quad R = \pi/k, \tag{16.2}$$

  (for $p = K\rho^2$), an exact reference for the settled state.

Started as a *warm, mildly super-Jeans* over-density at rest, the cloud runs through the canonical sequence:

1. **Collapse** — gravity exceeds the pressure gradient; the centre runs up in density and, by compression and dissipation, in temperature.
2. **Bounce** — the rising central pressure halts the infall, which overshoots hydrostatic balance, so the core rebounds.
3. **Ring-down** — the overshoot oscillates and is damped by the dissipation (violent relaxation in miniature).
4. **Pressure-supported core** — the cloud settles into a quasi-hydrostatic core, a Newtonian "star", approaching the equilibrium (16.2).

16.3 Reading the Force Balance and the Real 2nd Law

Among the centre-row line plots the simulator draws the two terms of the momentum equation directly: *white* $|\nabla p|$ (pressure) and *red* $\rho|\nabla\varphi|$ (gravity). During collapse the red curve runs above the white — gravity winning. Once the core settles the two curves *lie on top of each other*: hydrostatic balance $\nabla p = -\rho\nabla\varphi$ recovered. In the settled state the white curve sits a hair *below* red, a small net inward force — the slow quasi-static contraction of the core — so the gap is a live measure of how close the discrete solution is to exact balance. White particle tracers on the slice show the velocity field: sweeping inward during infall, reversing at the bounce, and coming to rest when the core forms.

This is the **Real 2nd Law** (Chapter 1) in the self-gravitating setting. Where the flow drives gradients sharper than the mesh can hold, the smooth solution *breaks down*; the dissipation thermalises the broken-down small-scale energy and a smoother mean solution *re-emerges*. The pointwise fine structure is lost irreversibly, but the outputs — the density profile, the temperature, the force balance — recover and carry on, and the simulator finds the equilibrium (16.2) dynamically as the attractor of the damped collapse.

Two honest limits. A *cold* (near-pressureless) start makes the infall supersonic and the bounce near-singular — a core a few cells wide that no fixed grid resolves; that is the correct statement that the continuum is heading for a singularity where new physics must enter. For $\gamma < 1/3$ ($\Gamma < 4/3$) no stable core exists and the collapse runs away regardless of dissipation. And the cubic box (with $\varphi = 0$ on flat faces) and the Cartesian grid break spherical symmetry, so the sloshing of the ring-down carries a faint cubic imprint rather than staying perfectly spherical. None of these change the basic, clean result: a warm, super-critical self-gravitating gas collapses, bounces, rings down, and settles into a pressure-supported core — a star, in the Newtonian RealNSE model where General Relativity has not yet been reached.

Chapter 17

ThermoDynamics of Blackbody Radiation

The high-frequency cut-off of blackbody radiation is, in the reading of this book, the radiative twin of turbulent dissipation: energy fed into frequencies that finite precision cannot resolve is not radiated but turned into heat.

This is a deliberately short chapter. The full quantitative account — the derivation of the Planck law from finite precision, and the connection to atomic emission and absorption in RealQM — is given in *Real Quantum Mechanics*, Body and Soul Vol VI [1], and in the companion *Computational Blackbody Radiation* notes. Here we only place blackbody radiation inside the with-Dynamics 2nd Law of the present volume.

17.1 The ultraviolet catastrophe

Classical statistical mechanics assigns, by equipartition, the same mean energy to every electromagnetic mode of a cavity in equilibrium at temperature T. Since the number of modes grows like $\nu^2\,d\nu$, the radiated energy density is predicted to grow without bound as the frequency ν increases:

$$dE \;\propto\; \nu^2\,T\,d\nu \quad\Longrightarrow\quad \int_0^\infty dE = \infty. \tag{17.1}$$

This is the *ultraviolet catastrophe*: equilibrium statistics with an unbounded spectrum gives infinite energy. Historically it was removed by Planck's quantum of action, with the energy quantum $h\nu$ suppressing the high-frequency modes.

17.2 Finite precision as the high-frequency cut-off

The present volume never works with an unbounded spectrum. Every continuum flow here is resolved at *finite precision* — a finite mesh size h, the same h that sets the artificial viscosity $\nu = h$ and the dissipation scale of the turbulence model. A finite precision carries a *smallest resolvable wavelength* and hence a *highest resolvable frequency* ν_{c}, with ν_{c} growing with temperature (Wien's displacement law is the statement that the cut-off scales with T).

Below the cut-off the spectrum follows the classical Rayleigh–Jeans form (17.1). *Above* the cut-off the relevant oscillations cannot be coherently sustained or radiated by the finite-precision medium: the energy pumped into those frequencies is instead *dissipated as heat*. The result is a spectrum that rises like ν^2, peaks near $\nu_{\mathrm{c}} \propto T$, and is exponentially cut off beyond it — the Planck spectrum — obtained here not by postulating energy quanta but as a finite-resolution effect, with the quantum of action appearing as the threshold of coherent radiation.

17.3 The parallel to turbulent dissipation

This is exactly the dissipation mechanism that runs through the whole of this volume. In turbulent flow, kinetic energy cascades down to scales below the mesh, and at that finite-precision scale it is dissipated irreversibly into heat at a positive rate $D > 0$; the with-Dynamics 2nd Law reads

$$\dot{K} \;\le\; W - D, \qquad D = \int_{\Omega} \nu\, |\nabla u|^2 \, dx \;>\; 0.$$

Blackbody radiation is the same statement for the electromagnetic field: radiative energy "cascades" towards ever higher frequencies, and at the finite-precision cut-off ν_{c} it is thermalised — heating above the cut-off. The high-frequency cut-off plays the role of the turbulent dissipation scale, and the

heating of unresolvable high-frequency modes is the radiative analogue of viscous dissipation. In both cases irreversibility is not a statistical postulate but the unavoidable consequence of feeding energy into degrees of freedom that finite precision cannot resolve.

The quantitative spectrum, the temperature dependence of ν_{c}, and the emission/absorption picture from atomic RealQM are developed in Vol VI [1].

Chapter 18

Climate: Convection in a Gas under Gravity

This closing chapter takes the simplest model that already contains the essential physics of climate and makes it the theme: a compressible gas held under gravity, heated from below and cooled from above. Run as RealNSE it convects, and the convection — not radiation — sets the vertical temperature structure of the atmosphere. *The companion simulations* `climate_convection_2d_gpu.html`, *its CPU twin* `climate_convection_2d_cpu.html`, *and the three-dimensional version* `climate_convection_3d_gpu.html` are *the chapter; the text only explains what they show. The full Earth atmosphere adds rotation, moisture and radiative transfer on top of this core — but the lapse rate, the overturning that carries heat upward, and the irreversible dissipation that is the climate's 2nd Law are all already present in the bare heated-gas-under-gravity model.*

18.1 The atmosphere as a compressible gas under gravity

The starting point is the simplest model that already contains the essential climate physics: a perfect gas filling an extended two-dimensional rectangle, held in the gravitational field of the planet, *heated from below* and *cooled from above*. The lower boundary is the ground (or ocean surface) warmed by

absorbed sunlight; the upper boundary is the top of the atmosphere, which loses heat to space by longwave radiation. The side walls are periodic — a horizontal slice of atmosphere with no special edges. This is RealNSE with a constant downward body force $\mathbf{g} = (0, -g)$,

$$\rho_t + \nabla\cdot m = 0, \quad m_t + \nabla\cdot(m\otimes v) + \nabla p - \nu\Delta v = \rho\,\mathbf{g}, \quad e_t + \nabla\cdot(ev) + p\,\nabla\cdot v = \nu|\nabla v|^2, \tag{18.1}$$

with $p = \gamma\rho T$ and the thermal forcing entering only as the boundary temperatures T_{hot} at the ground and T_{cold} at the top.

18.2 Convection sets the lapse rate

The decisive question is what fixes the vertical temperature profile. Heated gas at the ground expands, becomes less dense than the gas above it, and is buoyant; it rises. Cooled gas at the top is denser and sinks. The deterministic continuum equations (18.1) organise this into *convection cells* — rising warm plumes and sinking cold ones — the same overturning seen in a cumulus field or a pot of heated water. The convection does not run away: it carries heat upward until the vertical gradient is reduced to the *adiabatic lapse rate*

$$\frac{dT}{dz} \;\approx\; -\frac{g}{c_p}, \tag{18.2}$$

the gradient at which a rising parcel, expanding and cooling as the pressure falls, stays neutrally buoyant. **The lapse rate is set by gravity and convection, not by radiation.** A profile steeper than (18.2) is convectively unstable and is wiped out by overturning within a few buoyancy times; a shallower profile is stable and convection shuts off. The atmosphere sits at the convectively adjusted state in between, and the surface temperature follows as the temperature of the radiating top level plus the lapse rate times its height — a gravitational–thermodynamic result in which radiation sets only the *top* boundary condition, not the gradient beneath it.

This is the RealTD 2nd Law again: the overturning is an irreversible process generating cumulative dissipation $D = \iint \nu|\nabla v|^2 \geq 0$, the turbulent heat transport that moves energy from the warm ground to the cold radiating top. Radiative heat transfer itself is one-way, hot to cold, by the Stefan–Boltzmann analysis of the Blackbody Radiation chapter — there is no "back-radiation" by which a cold atmosphere warms a warmer ground. The upward

energy flow through the troposphere is carried by convection and latent heat, with longwave radiation taking over only above the convective layer where the gas is thin.

18.3 The companion simulation

The model is realised in `climate_convection_2d_gpu.html` (WebGPU, 512× 144) and its CPU twin `climate_convection_2d_cpu.html`. A perfect gas fills a wide rectangle in approximate hydrostatic balance; the lower wall is held at T_{hot}, the upper at T_{cold}, the sides periodic. Pressing Start shows the gas organise into convection cells within a few buoyancy times: warm plumes (red) rise from the heated floor, cold plumes (blue) sink from the cooled top, and tracer particles follow the overturning rolls. Sliders sweep the gravity g, the two wall temperatures and the viscosity; raising the temperature contrast or the gravity makes the convection more vigorous, while the time-averaged profile relaxes toward the lapse rate (18.2). The simulation is the dynamic content of the climate's vertical structure that classical equilibrium thermodynamics — seeing only the gross radiative balance between absorbed sunlight and outgoing longwave — leaves out. (The model uses $\gamma = 1$, the simplest compressible gas that still convects and stratifies; the same mechanism with the air value $\gamma = 7/5$ gives the observed tropospheric lapse rate of about 6–10 K/km.)

Vertical profiles. Alongside the temperature field the code plots the horizontally-averaged vertical profiles of temperature, density and turbulent dissipation D against height. The temperature profile relaxes toward the lapse rate (18.2); the density falls off hydrostatically with height; and the dissipation profile shows where the convective shear is strongest. These three curves are the chapter's central diagnostic: the temperature profile *is* the climate's vertical structure, and the dissipation profile is the visible, measurable form of the 2nd-Law quantity D that replaces entropy throughout this volume.

Three dimensions. `climate_convection_3d_gpu.html` runs the same model in a $128 \times 128 \times 64$ box, periodic in both horizontal directions, displaying a vertical temperature slice through the mid-plane together with the layer-averaged profiles. The convection cells become fully three-dimensional

plumes, but the lapse-rate result is unchanged — confirming that the gravitational–convective adjustment is not an artefact of the two-dimensional geometry. The same fifteen-minute, library-free code that runs Joule's experiment and the bluff-body wake, scaled up, is enough to exhibit the load-bearing physics of climate.

Bibliography

[1] C. Johnson, *Real Quantum Mechanics: A Multiphase 3D Continuum Formulation Realised through Mind–AI Cooperation*, Applied Mathematics Body and Soul, Vol. VI, 2026.

[2] A. Logg, K.-A. Mardal and G. N. Wells (eds.), *Automated Solution of Differential Equations by the Finite Element Method: The FEniCS Book*, Lecture Notes in Computational Science and Engineering, Vol. 84, Springer, 2012.

[3] M. Davis, *The Universal Computer: The Road from Leibniz to Turing*, W. W. Norton, New York, 2000.

[4] P. Bergmann, *Basic Theories of Physics*, Prentice-Hall, 1950.

[5] http://www.bodysoulmath.org.

[6] E. Burman, Adaptive finite element methods for compressible two-phase flow, Ph D Thesis, Chalmers University of Technology, 1998.

[7] L. Boltzmann, *Lectures on Gas Theory*, Dover, 1964.

[8] Stephen Brush, *The Kind of Motion We Call Heat: Physics and the Atomists*, Elsevier Science, 1986.

[9] S. Brush, *The Kind of Motion we call Heat. A History of the Kinetic Theories of Gases in the 19th century*, Volumes I and II, Studies in Statistical Mechanics, Vol. VI, E.W. Montroll and J.L. Lebowitz (eds.), North-Holland Publishing Company, Oxford, 1976.

[10] Sadi Carnot, in Reflections of the motive power of fire and on machines fitted to develop that power, 1824.

[11] Rudolph Clausius, *Abhandlungen über die Mechanische Wäremtheorie*, Band 1-2, 1864.

[12] R. Clausius, Über die Wärmeleitung gasförmiger Körper, Annalen der Physik 125: 353-400, 1865.

[13] Paul Davies, *The Cosmic Blueprint, New Discoveries in Nature's Creative Ability to Order the Universe*, Templeton Foundation Press.

[14] K. Eriksson, D. Estep and C. Johnson, *Computational Differential Equations*, Cambridge University Press, 1996.

[15] L. Euler, Principes généraux du mouvement des fluides (General laws of the motion of fluids), Archives of the French Academy of Sciences, 1755.

[16] Richard Feynman, *The Feynman Lectures on Physics*, Caltech, 1963.

[17] The FEniCS Project, http://www.fenics.org.

[18] Michel Foucault, Discipline and Punishment, The Birth of the Prison, Vintage books, 1991.

[19] V. Guillemin, *The Story of Quantum Mechanics*, Scribner, 1968.

[20] J. Hoffman, A general Galerkin finite element method for turbulent compressible flow, Finite Element Center Preprint 2006-13.

[21] J. Hoffman, C. Johnson and A. Logg, *Dreams of Calculus: Perspectives on Mathematics Education*, Springer, 2006.

[22] J. Hoffman and C. Johnson, Finally, Resolution of d'Alembert's Paradox, to appear in Journal of Mathematical Fluid Mechanics, 2008.

[23] J. Hoffman and C. Johnson, *Computational Turbulent Incompressible Flow*, Applied Mathematics Body and Soul Vol 4, Springer, 2007.

[24] J. Hoffman and C. Johnson *Computational Quantum Mechanics*, to appear.

[25] C. Johnson, Adaptive finite element methods for conservation laws, Advanced Numerical Approximation of Nonlinear Hyperbolic Equations, Springer Lecture Notes in Mathematics 1697 (1998), 269-323.

[26] C. Johnson, *The Clock and the Arrow: A Brief Theory of Time*, Computational Technology Laboratory Preprint, 2008.

[27] C. Johnson, *Computational Black-Body Radiation*, Computational Technology Laboratory Preprint, 2008.

[28] W. Thomson (Lord Kelvin), On the dynamical theory of heat; with numerical results deduced from Mr. Joule's equivalent of a thermal unit and M. Regnault's observations on steam, Math. and Phys. Papers vol.1, p 179, 1851.

[29] Robert Laughlin, *A Different Universe*, 2005.

[30] Elliot Lieb and Jakob Yngvason, The Physics and Mathematics of the Second Law of Thermodynamics, Physics Reports 310, 1-96 (1999).

[31] Leff, H.S. and Rex, A.F. (eds), Maxwell's Demon: Entropy, Information, Computing. Bristol: Adam-Hilger, 1990.

[32] Lindsay and Margenau, *Foundations of Physics*, 1936.

[33] Thomas Kuhn, *Black-Body Theory and the Quantum Discontinuity*, 1894-1912, Oxford Univ Press 1978.

[34] M. Laurendau, *Statistical Thermodynamics, Fundamentals and Applications*, Cambridge University Press, 2005.

[35] Measure-vaued solutions to the complete Euler system revisited, Zeitschrift für angewandte Mathematik und Physik, June 2018. 69:57.

[36] The Cauchy Problem for the Euler Equations Compressible Fluids, Handbook of Mathematical Fluid Dynamics (eds S.J Friedlander and D. Serre), Volume I, Chapter 5, Elsevier 2012.

[37] Handbook of Mathematical Fluid Dynamics Vol I and II, S.J. Friedlander and D. Serre (eds), Elsevier 2002.

[38] C.M Dafermos, Maximal dissipation in equations of evolution, J. Differential Equations 252, 2012, 567-587.

[39] E. Lieb and J. Yngavason, The Physics and Mathematics of the Second Law of Thermodynamics, 1997.

[40] J. Loschmidt, Sitzungsber. Kais. Akad. Wiss. Wien, Math. Naturwiss. Classe 73, 128-142, (1876).

[41] William Ockham (1285-1349): "Entia non sunt multiplicanda praeter necessitatem" (Entities should not be multiplied unnecessarily).

[42] Max Planck, Über den zweiten Hauptsatz der mechanischen Wärmetheorie, Dissertation, Berlin, 1879.

[43] Max Planck, *Vorlesungen über Thermodynamik*, 1897.

[44] Max Planck, Acht Vorlesungen über Theoretische Physik, Fünfte Vorlesung: Wärmestrahlung und Elektrodynamische Theorie, Leipzig, 1910.

[45] Karl Popper, The Logic of Scientific Discovery, 1949.

[46] E. Schrödinger, *The Interpretation of Quantum Physics*, Ox Bow Press, Woodbridge, CN, 1995.

[47] C. E. Shannon, A mathematical theory of communication, The Bell System Technical Journal, Vol. 27, pp 379-423, 623-656, July, Oct, 1948.

[48] C. Truesdell, *The Tragicomial History of Thermodynamics 1822-54*, Springer, 1980.

[49] Max Tegmark, The Interpretation of Quantum Mechanics: Many Worlds or Many Words?, in Fundamental Problems in Quantum Theory, eds. Rubin and Shih.

[50] J. Uffink, Bluff your way in the Second Law of Thermodynamics, Department of History and Foundation of Science, University of Utrecht, 2001.

[51] H.D. Zeh, in The problem of conscious observation in quantum mechanical description, ArXiv Quant-Phy June 2000.

Index